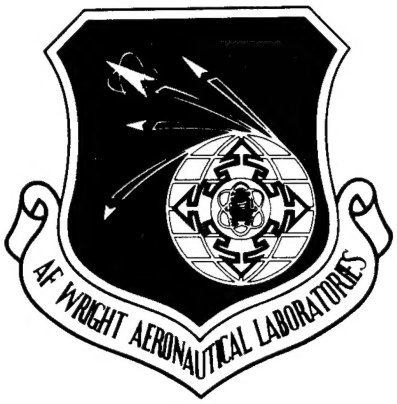

AFWAL-TR-88-4115

MANUFACTURING THERMOPLASTIC MATRIX COMPOSITES

George S. Springer

Department of Aeronautics and Astronautics

Stanford University, Stanford, California 94305

July 1988

Final Report for Period October 1985--April 1988

MATERIALS LABORATORY
AIR FORCE WRIGHT AERONAUTICAL LABORATORIES
AIR FORCE SYSTEMS COMMAND
WRIGHT-PATTERSON AIR FORCE BASE, OHIO 45433-6533

NOTICE

When government drawings, specifications, or other data are used for any purpose other than in connnection with a definitely related government procurement operation, the United States government thereby incurs no responsibility nor any obligation whatsoever; and the fact that the government may have formulated, furnished, or in any way supplied the said drawings, specifications, or other data, is not to be regarded by implication or otherwise as in any manner licensing the holder or any other person or corporation, or conveying any rights or permission to manufacture, use, or sell any patented invention that may in any way be related thereto.

This report has been reviewed by the Office of Public Affairs (ASD/PA) and is releasable to the National Technical Information Service (NTIS). At NTIS, it will be available to the general public, including foreign nations.

This technical report has been reviewed and is approved for publication.

FOR THE COMMANDER

S.W. Tsai

STEPHEN W. TSAI, Chief
Mechanics & Surface Interactions Br
Nonmetallic Materials Division

M. L. Minges

MERRILL L. MINGES, SES, Director
Nonmetallic Materials Division

"If your address has changed, if you wish to be removed from our mailing list, or if the addressee is no longer employed by your organization, please notify **AFWAL/MLBM**, Wright-Patterson AFB, OH 45433-6533 to help us maintain a current mailing list."

Copies of this report should not be returned unless return is required by security considerations, contractual obligations, or notice on a specific document.

SECURITY CLASSIFICATION OF THIS PAGE

REPORT DOCUMENTATION PAGE

1a REPORT SECURITY CLASSIFICATION Unclassified	1b. RESTRICTIVE MARKINGS
2a SECURITY CLASSIFICATION AUTHORITY	3 DISTRIBUTION/AVAILABILITY OF REPORT Approved for public release; distribution is unlimited.
2b DECLASSIFICATION/DOWNGRADING SCHEDULE	
4 PERFORMING ORGANIZATION REPORT NUMBER(S)	5. MONITORING ORGANIZATION REPORT NUMBER(S) AFWAL-TR-88-4115
6a NAME OF PERFORMING ORGANIZATION Stanford University 6b. OFFICE SYMBOL (If applicable)	7a. NAME OF MONITORING ORGANIZATION Materials Laboratory (AFWAL/MLBM) Air Force Wright Aeronautical Laboratories
6c ADDRESS (City, State and ZIP Code) Stanford, California 94305	7b. ADDRESS (City, State and ZIP Code) Wright-Patterson AFB, Ohio 45433-6533
8a NAME OF FUNDING/SPONSORING ORGANIZATION 8b. OFFICE SYMBOL (If applicable)	9. PROCUREMENT INSTRUMENT IDENTIFICATION NUMBER F33615-84-C-5049
8c ADDRESS (City, State and ZIP Code)	10 SOURCE OF FUNDING NOS.

PROGRAM ELEMENT NO.	PROJECT NO.	TASK NO.	WORK UNIT NO
62102F	2419	01	67

11 TITLE (Include Security Classification)
Manufacturing Thermoplastic Matrix Composites

12. PERSONAL AUTHOR(S)
George S. Springer

13a TYPE OF REPORT	13b TIME COVERED	14. DATE OF REPORT (Yr., Mo., Day)	15. PAGE COUNT
Final	FROM 10/1985 TO 4/1988	July 1988	112

16 SUPPLEMENTARY NOTATION

17 COSATI CODES			18 SUBJECT TERMS (Continue on reverse if necessary and identify by block number)
FIELD	GROUP	SUB GR	composite materials, thermoplastics, processing, properties
11	04		

19 ABSTRACT (Continue on reverse if necessary and identify by block number)

A model is presented of the steps involved in the manufacturing process of semicrystalline thermoplastic matrix composites. The model relates the temperature and pressure applied during processing to a) the flow of the matrix into the fiber tow, b) the formation of contact and bond between adjacent plies, and c) the crystallinity. The results of the model were verified by tests performed with PEEK 150P polymer and APC-2 graphite/PEEK composite. In addition the mechanical properties of PEEK 150P polymer and APC-2 graphite/PEEK composite were measured at different crystallinities, from 0 to 40 weight percent. For PEEK 150P the tensile, compressive, and shear properties and the fracture toughness were measured. For APC-2 the Mode I and Mode II fracture toughnesses and fracture energies as well as the mixed mode stress intensity factors were determined. Expressions are presented relating the mechanical properties to crystallinity. Finally, data are given which compare the mechanical properties of materials in which the same crystallinity was established by different thermal processes.

20 DISTRIBUTION/AVAILABILITY OF ABSTRACT	21. ABSTRACT SECURITY CLASSIFICATION
UNCLASSIFIED/UNLIMITED ☒ SAME AS RPT. ☐ DTIC USERS ☒	Unclassified

22a NAME OF RESPONSIBLE INDIVIDUAL	22b TELEPHONE NUMBER (Include Area Code)	22c OFFICE SYMBOL
Dr. S. Tsai	(513) 255-3068	AFWAL/MLBM

DD FORM 1473, 83 APR EDITION OF 1 JAN 73 IS OBSOLETE

unclassified
SECURITY CLASSIFICATION OF THIS PAGE

FOREWORD

This work was performed in the Department of Aeronautics and Astronautics, Stanford University, under the support of the Mechanics and Surface Interactions Branch (AFWAL/MLBM), Nonmetallic Materials Division, Materials Laboratory, Air Force Wright Aeronautical Laboratories, Wright-Patterson Air Force Base, Ohio; Project Number 2419, "Nonmetallic Structural Materials," Task Number 241901, "Composite Materials and Mechanics Technology," Contract Number F33615-84-C-5049.

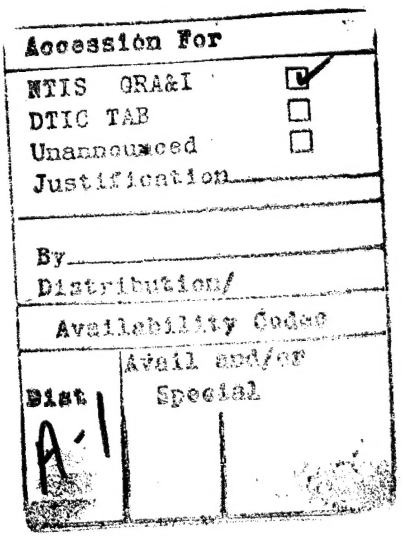

TABLE OF CONTENTS

LIST OF FIGURES

LIST OF FIGURES (continued)

LIST OF FIGURES (continued)

LIST OF TABLES

Section I

INTRODUCTION

It is well recognized that the procedures employed during the manufacture of composite materials have a significant effect on the quality and cost of the finished product. Therefore, the procedures used during manufacture must carefully be selected for each application. In particular, attention must be paid to the processing variables, such as the temperature and pressure, applied during fabrication. The processing variables can best be chosen by the use of analytic models. For this reason, process models applicable to thermoset matrix composites have been developed in recent years [1–4]. However, a complete model of the manufacture of thermoplastic matrix composites has not yet been reported. Hence, the objective of this investigation was to develop a model simulating the major steps involved in the processing of semicrystalline thermoplastic matrix composites.

Processing of thermoplastic matrix composites consists of three major steps:

1) Matrix is introduced into the space between the fibers in each tow, "impregnating" the tow.

2) Individual plies are "consolidated" such that there is good contact as well as good bond between adjacent plies.

3) The composite is heated and then cooled at a rate which provides the desired "crystallinity" in the matrix.

In this paper a model is presented describing each of the above three steps. The model is divided into the three submodels designated as "impregnation", "consolidation", and "crystallinity". Each of these submodels is developed separately. The three submodels are then combined, so as to be applicable in situations where some or all of the phenomena described by the different submodels occur simultaneously.

The submodels were verified by data obtained with PEEK 150P polymer, with T300

fiber, and with APC-2 graphite/PEEK composite. It is recognized that the grade of PEEK used in APC-2 may differ from PEEK 150P in molecular weight distribution and in additive content. PEEK 150P was chosen on the recommendation of Fiberite Corporation, an ICI subsidiary. According to the information provided by Fiberite Corporation, 150P is the closest commercial grade of PEEK to the APC-2 material.

Section II

IMPREGNATION SUBMODEL

The first step in the manufacture of thermoplastic composites is impregnation. During this step a polymeric matrix is introduced into the fiber tow. Impregnation is done either by the material supplier (manufacturer) during preparation of prepreg fibers, plies, or laminates, or by the user during "in situ" fabrication of laminates and parts. Impregnation is accomplished by surrounding the tow with the matrix and heating the tow-matrix system to a temperature T_m at which the matrix becomes "soft", capable of penetrating into the space between the fibers (Figure 1). Our objective is to determine a) the depth to which the matrix penetrates in a given time, and b) the time required to completely fill (impregnate) the tow with the matrix.

Here we postulate that the impregnation process takes place by the following mechanism. The fibers in the tow are not perfectly straight. Therefore, the distance between fibers varies along the fiber length (Figure 2). At a point where two fibers are sufficiently close the matrix around one of the fibers comes into contact with the adjacent fiber, bridging the gap between the two fibers. Driven by surface tension, the matrix then moves lengthwise along the fibers until another bridging point is reached. The lengthwise flow along the fibers is accompanied by radial flow across the fibers. The lengthwise flow is modeled as laminar flow in an annular channel of length L, height h, and inside radius r (Figure 3). The radial flow is modeled as flow through a porous medium.

By assuming a linear pressure drop along the channel, the mass flow rate $\dot{m}_a$ lengthwise along the channel may be expressed as [5]

$$\dot{m}_a = \rho\,(2\pi h)\,\left(\frac{h^2}{12\mu}\frac{P_{co} - P_c}{x_m}\right) \tag{1}$$

where ρ and μ are the density and viscosity of the matrix at temperature T_m, x_m is the length of the channel filled by the matrix, and P_{co} and P_c are the pressures at the two ends

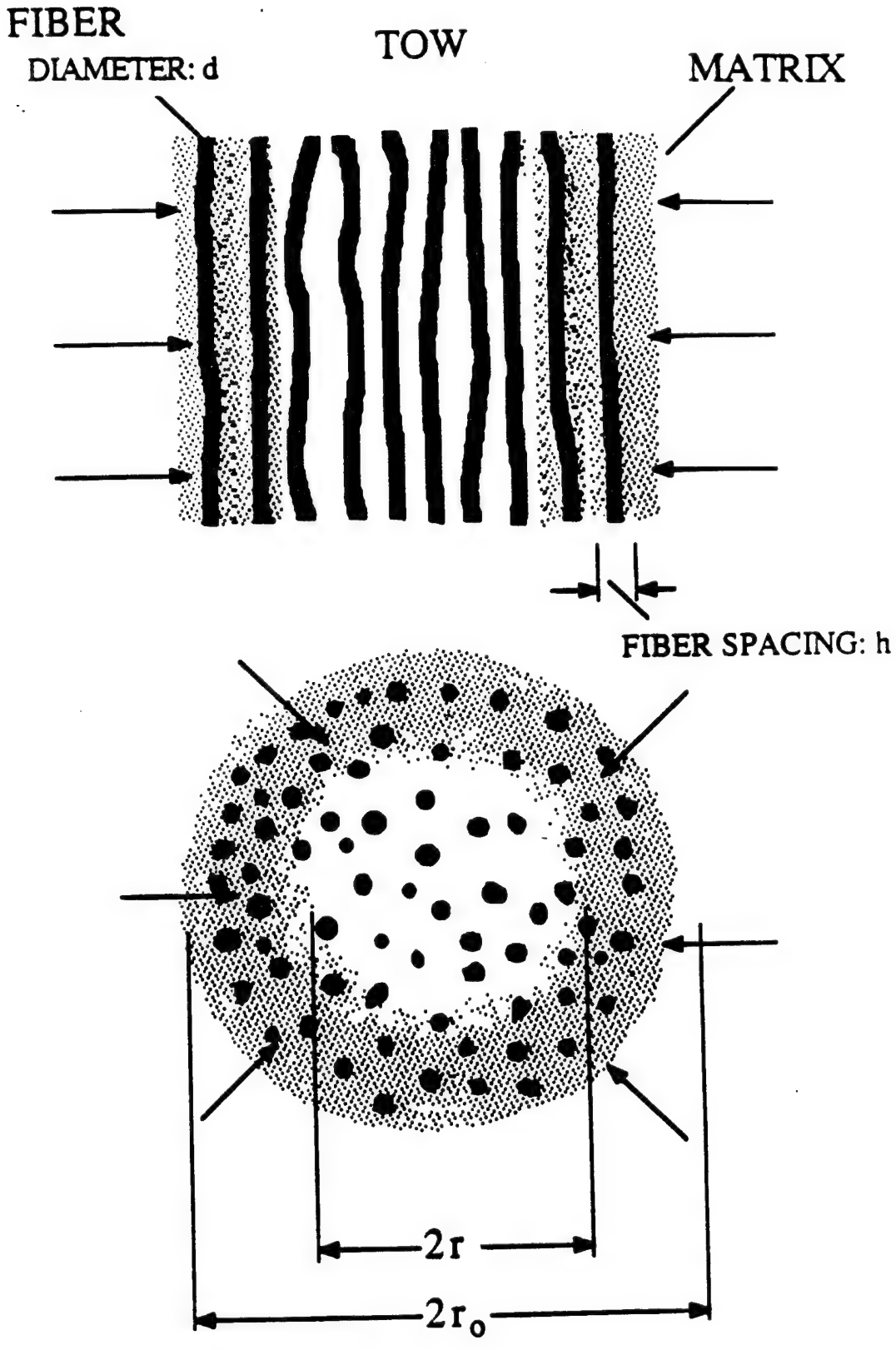

Figure 1. Illustration of the impregnation of a fiber tow.

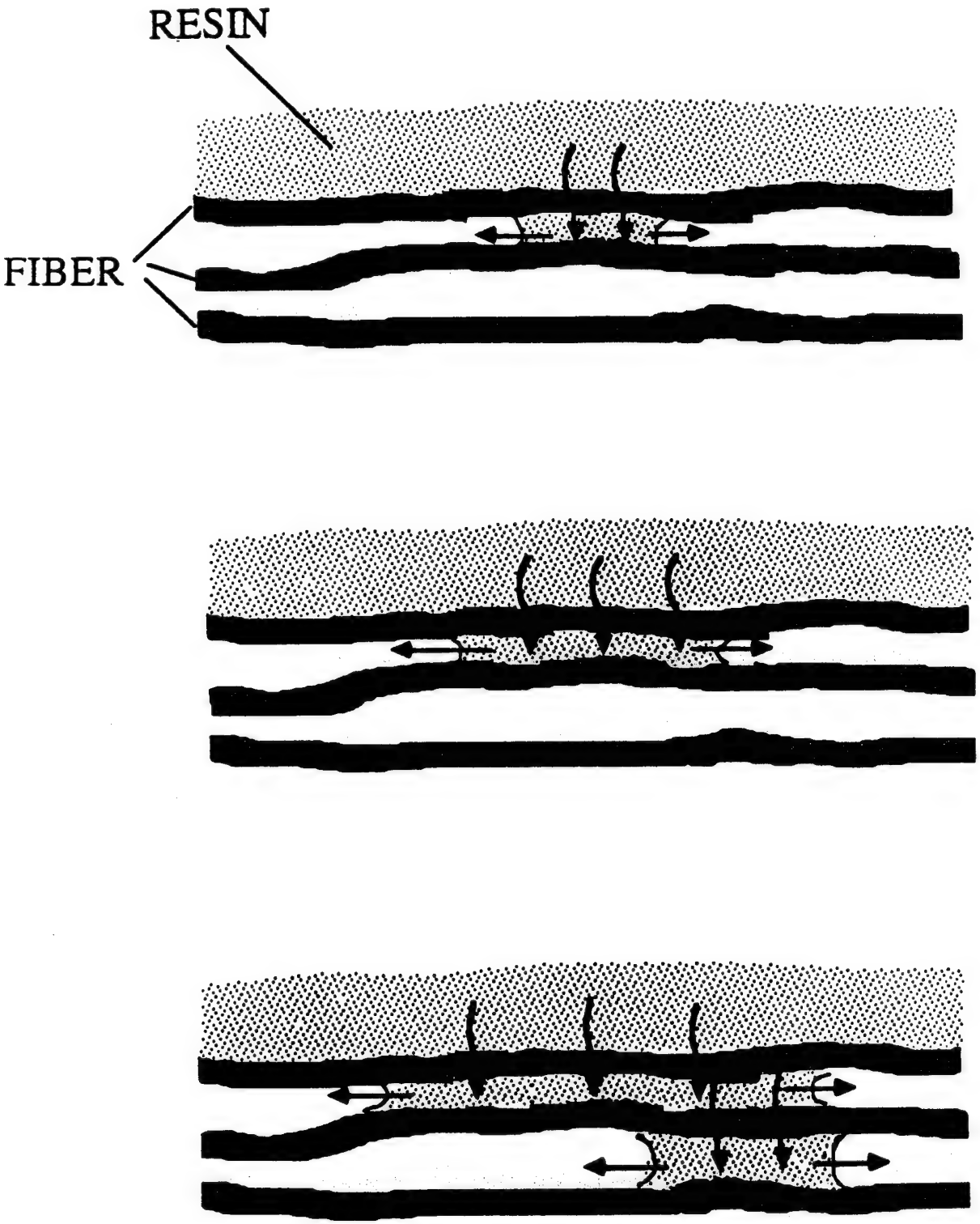

Figure 2. Illustration of the progressive motion of the matrix between fibers inside a tow.

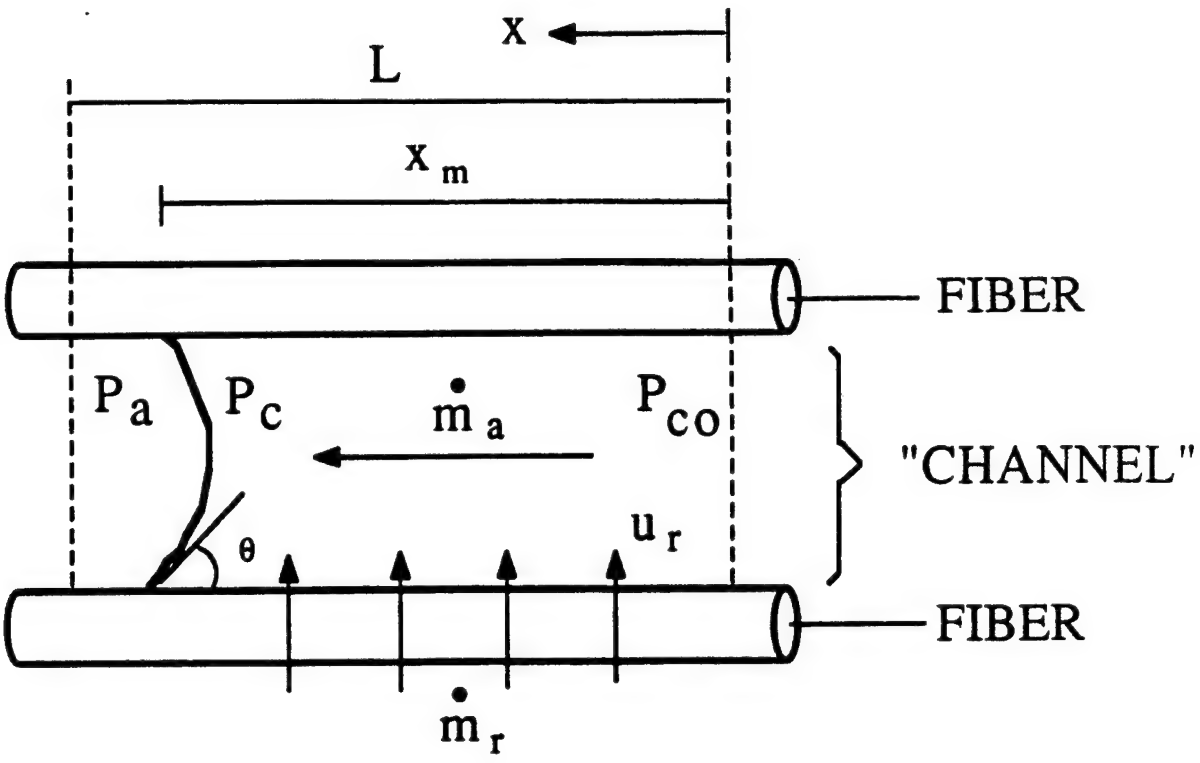

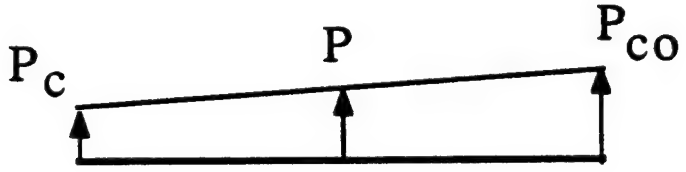

$$P = \frac{(P_c - P_{co})x}{x_m} + P_{co}$$

Figure 3. Annular channel used in modeling the matrix flow inside a tow.

of the channel (Figure 3). The pressure P_c is related to the pressure in the empty channel P_a through the surface tension σ. We assume that the channel is open to the ambient so that the pressure P_a is constant. The pressure difference across the meniscus can then be written as [5]

$$P_a - P_c = \frac{2}{h}\sigma\cos\theta \equiv \frac{2}{h}\sigma^* \tag{2}$$

where θ is the wetting angle and $\sigma^* = \sigma\cos\theta$.

The mass flow rate in the radial direction through an element of length dx is

$$d\dot{m}_r = \rho u_r (2\pi r)\, dx \tag{3}$$

u_r is the average radial velocity given by Darcy's law [5]

$$u_r = \frac{K_p}{\mu}\frac{dP}{dr} \tag{4}$$

K_p is the permeability perpendicular to the tow, and can be approximated by the expression given in Table 1. Equations (3) and (4) yield

$$\dot{m}_r = \frac{2\pi\rho K_p}{\mu \ln\frac{r}{r_o}} \int_o^{x_m} (P - P_a)\, dx \tag{5}$$

where P is the pressure at a distance x along the channel. P_a is the matrix pressure at the outside radius r_o of the tow, and is assumed to be the same as the pressure which exists inside the empty portion of the channel.

Conservation of mass requires that the lengthwise and axial mass flow rates be equal

$$\dot{m}_a = \dot{m}_r \tag{6}$$

By combining Equations (1) through (6), after lengthy but straightforward algebraic manipulations, we obtain

$$\frac{dx_m}{dt} = \frac{2\sigma^* K_p}{\mu h^2 r \ln r/r_o} \frac{x_m}{\left(\frac{6K_p}{h^3 r \ln r/r_0} x_m^2 - 1\right)} \tag{7}$$

Initially ($t = 0$) there is a small amount of matrix on the bottom of the channel. We take the length of this amount to be equal to the channel height h. The time required to fill the channel with matrix ($x_m = L$) is denoted by t_L. Thus we integrate Equation (7) from

Table 1

INPUT PARAMETERS REQUIRED FOR THE IMPREGNATION SUBMODEL

1) Initial tow radius, r_o
2) Fiber diameter, d
3) Average distance between two fibers (channel height), h
4) Channel length, L
5) Permeability of the tow,[a] K_p
6) Matrix viscosity, μ
7) Surface tension,[b] σ^*
8) Applied temperature, T_m

---

a) The permeability may be approximated by [6]

$$K_p = -\frac{d^2}{16}\epsilon^2 \left[\ln \epsilon + \frac{1}{2}\frac{\epsilon^4 - 1}{\epsilon^4 + 1}\right]$$

where

$$\epsilon = 1 - \frac{\pi}{4}\left(\frac{d}{h+d}\right)^2$$

b) In the temperature range of interest the surface may be expressed as

$$\sigma^* = \sigma_o^* e^{\alpha \frac{T - T_o}{T_o}}$$

where σ_o^* and α are constants which depend on the matrix, fiber, and interface, but are independent of temperature. T_o is an arbitrary reference temperature.

$x_m = h$ to $x_m = L$ and from $t = 0$ to $t = t_L$. This integration yields the following expression for the time required to fill a channel located at radius r

$$t_L = G\left[1 - Ir\ln\left(\frac{r}{r_o}\right)\right] \tag{8}$$

G and I are constants defined as

$$G \equiv \frac{3\mu h\left[(L/h)^2 - 1\right]}{2\sigma^*} \tag{9}$$

$$I \equiv \frac{h\ln(L/h)}{3K_p\left[(L/h)^2 - 1\right]} \tag{10}$$

It is interesting to note that Equation (8) is also obtained if the pressure along the fibers is taken to be constant instead of varying linearly with position, as is assumed in the above analysis. However, for constant pressure the value of G would be increased while the value of I would be decreased by a factor of two.

The time required to fill the tow to a depth of r (i.e., the time required to fill every channel between r_o and r (Figure 1)) is

$$t = \sum_{i=1}^{N_r}(t_L)_i \tag{11}$$

where N_r is the number of "layers" between $r = r_o$ and $r = r$. The thickness of each layer is

$$\Delta r = d + h \tag{12}$$

where d is the fiber diameter. Thus, the number of layers is $N_r = (r_o - r)/\Delta r$. We can replace the summation in Equation (11) by the integral

$$t = \int_{r_o}^{r} t_L\, dN_r = \int_{r_o}^{r} t_L\left(-\frac{dr}{\Delta r}\right) \tag{13}$$

Substitution of Equation (8) into Equation (13) and integration yields

$$t^* = (1 - r^*) + Jr^{*2}\ln r^* + \frac{J}{2}(1 - r^{*2}) \tag{14}$$

t^* and r^* are dimensionless time and position, respectively, and J is a dimensionless constant

$$t^* = \frac{\Delta r(t)}{Gr_o} = \frac{2\sigma^*(d/h + 1)}{3\mu\left[(L/h)^2 - 1\right]r_o}t \tag{15}$$

$$J = \frac{Ir_o}{2} = \frac{hr_o\ln(L/h)}{6K_p\left[(L/h)^2 - 1\right]} \tag{16}$$

$$r^* = r/r_o \tag{17}$$

Equation (14) provides the time required to impregnate the tow with matrix to a depth of $(r_0 - r)$. It is convenient to express the extent of impregnation by a parameter referred to as the degree of impregnation

$$D_{\text{imp}} = \frac{\text{area impregnated}}{\text{total tow area}} = \frac{\pi(r_o^2 - r^2)}{\pi r_o^2} = 1 - \left(\frac{r}{r_o}\right)^2 \tag{18}$$

In terms of the degree of impregnation Equation (14) is

$$t^* = (1 - \sqrt{1 - D_{\text{imp}}}) + J(1 - D_{\text{imp}}) \ln \sqrt{1 - D_{\text{imp}}} + \frac{J}{2} D_{\text{imp}} \tag{19}$$

The time required to fill the entire tow is ($r = 0$, and $D_{\text{imp}} = 1$)

$$t^*_{\text{imp}} = 1 + \frac{J}{2} \tag{20}$$

or, in terms of dimensional quantities, the time to complete the impregnation is

$$t_{\text{imp}} = \frac{3\mu r_o \left[(L/h)^2 - 1\right]}{2\sigma^*(d/h + 1)} \left\{1 + \frac{h r_o \ln(L/h)}{12 K_p [(L/h)^2 - 1]}\right\} \tag{21}$$

Impregnation—Method of Solution

The degree of impregnation as a function of time may be calculated by Equation (19). The time required to complete the impregnation may be calculated by Equation (20) or (21). The calculations can be facilitated by representing Equations (19) and (20) in graphical form. Graphical representation of these equations are given in Figures 4 and 5. Since these figures are in terms of dimensionless parameters they are not restricted to specific materials or specific tows but are applicable to different types of materials and different types of tows. The **actual** degree of impregnation and the **actual** impregnation time can be calculated from these figures once the parameters applicable to the given problem are known (see Table 1). Of the parameters required to calculate D_{imp} and t_{imp}, the tow radius r_o, the fiber diameter d, the distance between the fibers (channel height) h, and the channel length L can be determined from visual observation of the tow. The resin viscosity μ as a function of temperature can be measured by a viscometer. The permeability K_p can be estimated by the expression given in Table 1. The surface tension σ^* must be determined by matching the model to data obtained by impregnation tests. A procedure for these tests is described in the next subsection.

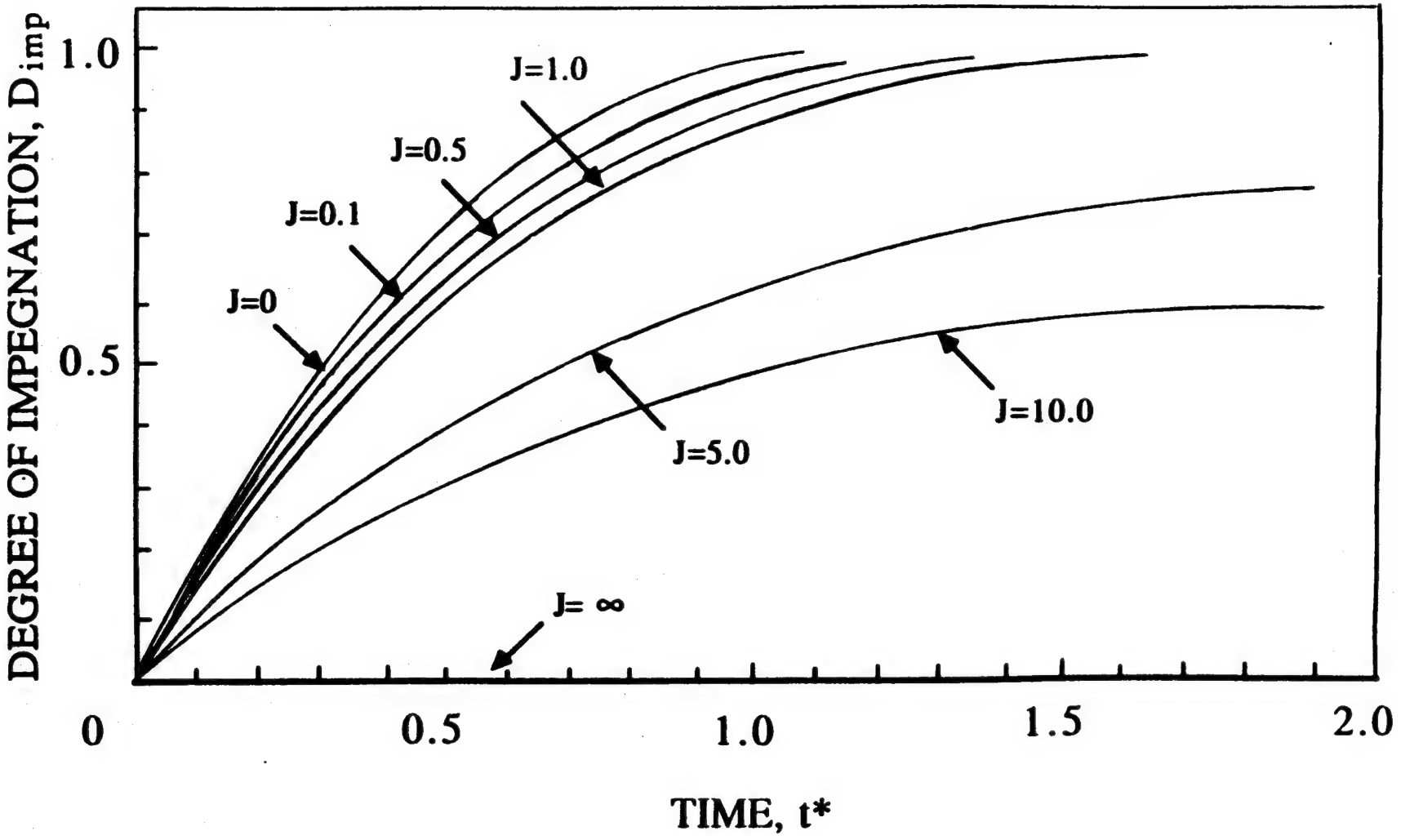

Figure 4. Degree of impregnation as a function of time (dimensionless, see Equation (19)).

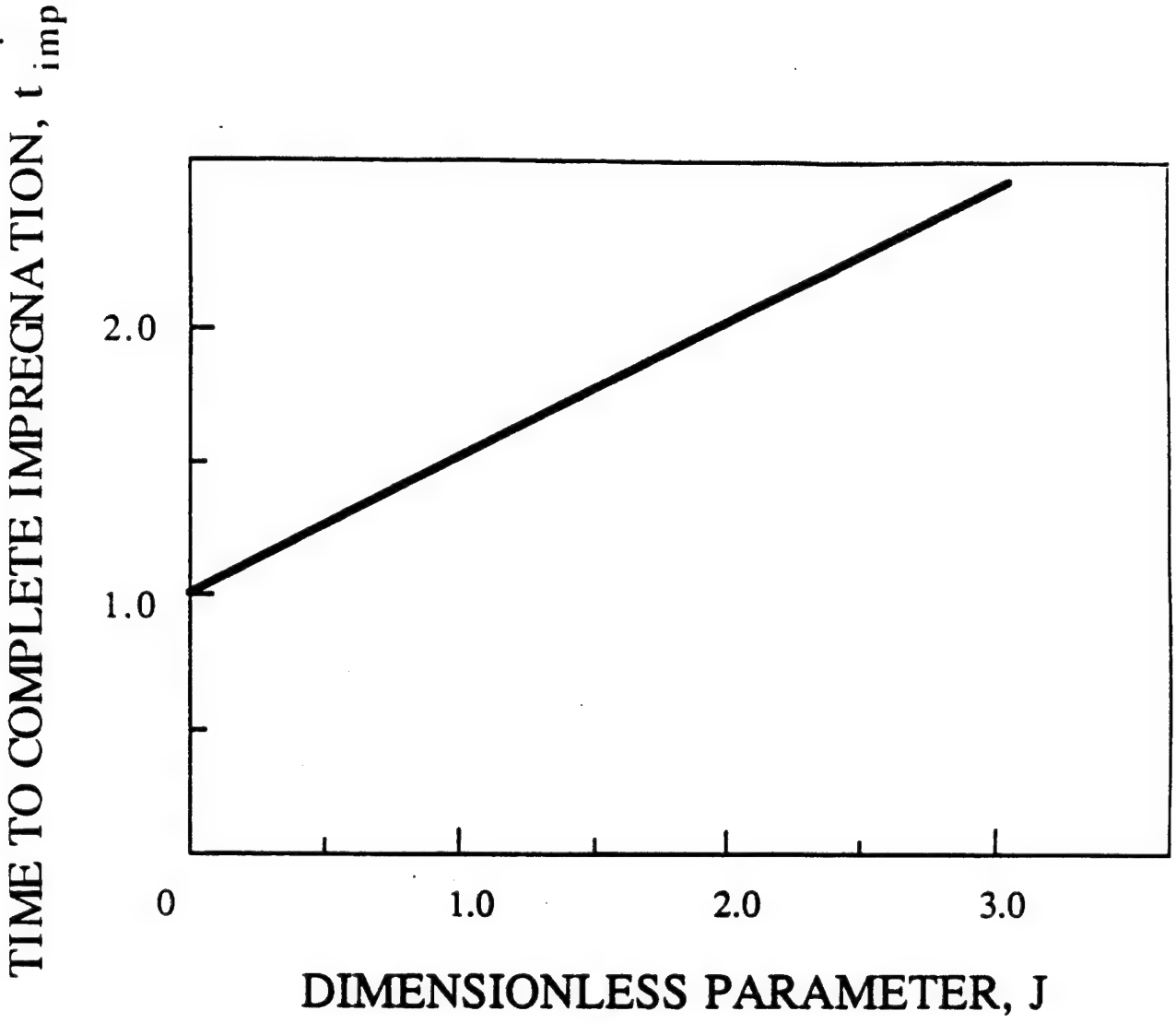

Figure 5. Time required to impregnate a tow characterized by the dimensionless parameter J (see Equation (20)).

The parameters required to calculate the degree of impregnation and the impregnation time were measured for T300/PEEK 150P (see next subsection). The measured values of the parameters are listed in Appendix A. With these parameters, the degree of impregnation as a function of time and the time of impregnation as function of tow size were calculated and plotted for impregnation occurring at 698°F (370°C) (Figures 6 and 7). The time required to complete the impregnation at different values of μ/σ^* were also plotted (Figure 8).

Finally, it is noted that Equations (19) through (21) were incorporated into a computer code which combines the calculations of all three submodels (impregnation, consolidation, crystallinity). This code is discussed in Section V.

Impregnation—Experimental Verification

Tests were performed to evaluate the validity of the impregnation submodel, to establish the procedure for determining some of the parameters required by this submodel, and to measure the parameters for one fiber-matrix system. In these tests Union Carbide T300 graphite fiber tows (6K) were impregnated with PEEK 150P polymer. Prior to the tests the sizing was removed from the fibers by the following procedure. The fibers were immersed in methylethylketone (MEK) for 24 hours, then were washed with fresh MEK in an ultrasonic cleaner for 30 minutes. This process was repeated. After the second treatment with fresh MEK the fibers were dried in a vacuum oven at 180°F (82.2°C) for two hours.

A fiber tow, treated in the above manner, was placed in an aluminum mold (Figure 9). The two ends of the tow were clamped so that the tow was suspended above the bottom of the mold. The mold was filled with PEEK 150P powder and placed in an oven kept at 698°F (370°C). The temperature of the matrix was monitored by a thermocouple. After a preset period of time the mold was removed from the oven and cooled to room temperature. The impregnated tow was removed from the mold, was cut perpendicular to the fibers, and the tow cross section was examined with an optical microscope. The number of impregnated fibers in the tow was counted, and the degree of impregnation was calculated by the expression

$$D_{\text{imp}} = \frac{\text{number of impregnated fibers}}{\text{total number of fibers}} \tag{22}$$

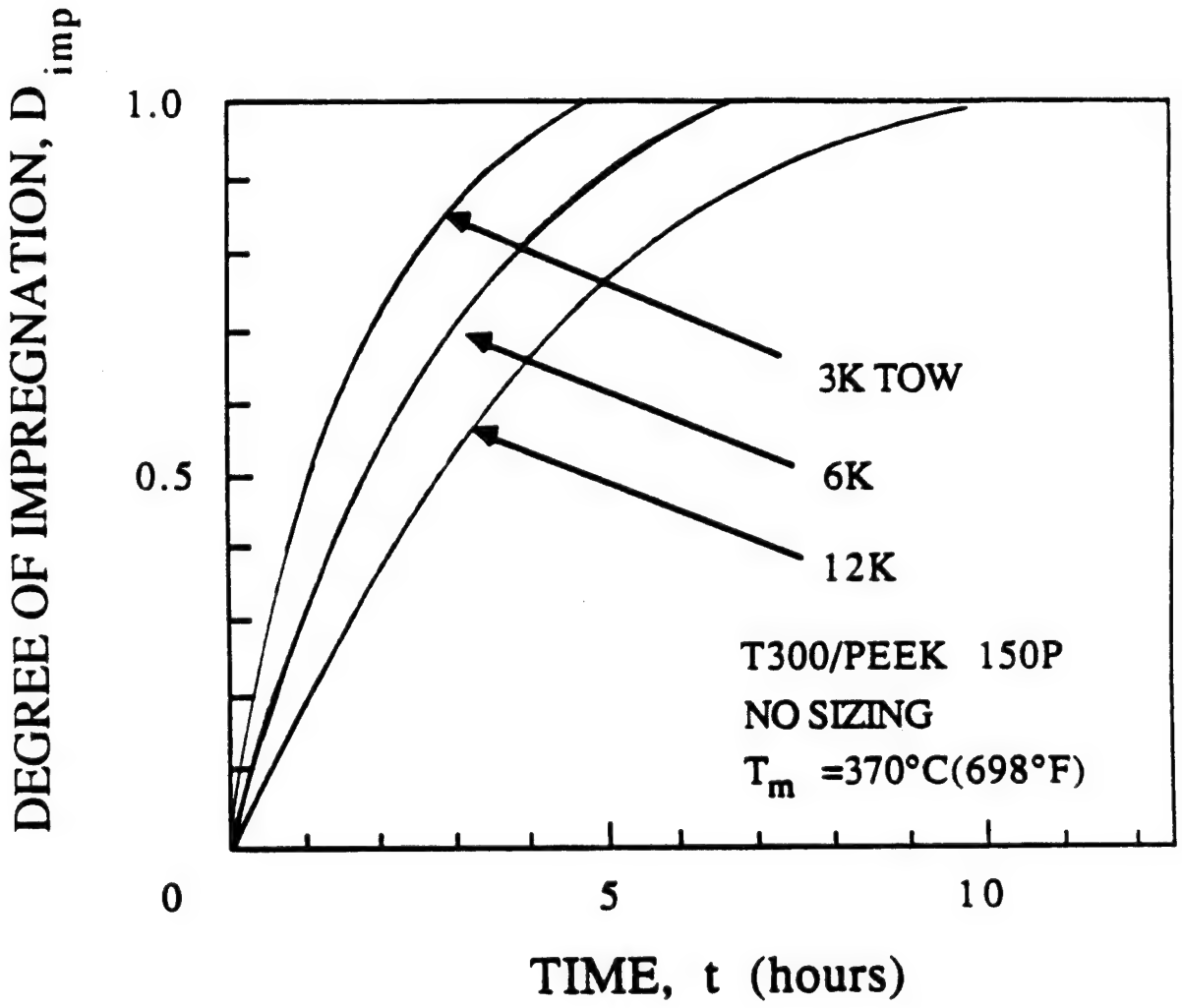

Figure 6. Degree of impregnation as a function of time as calculated by the model (see Equation (19)).

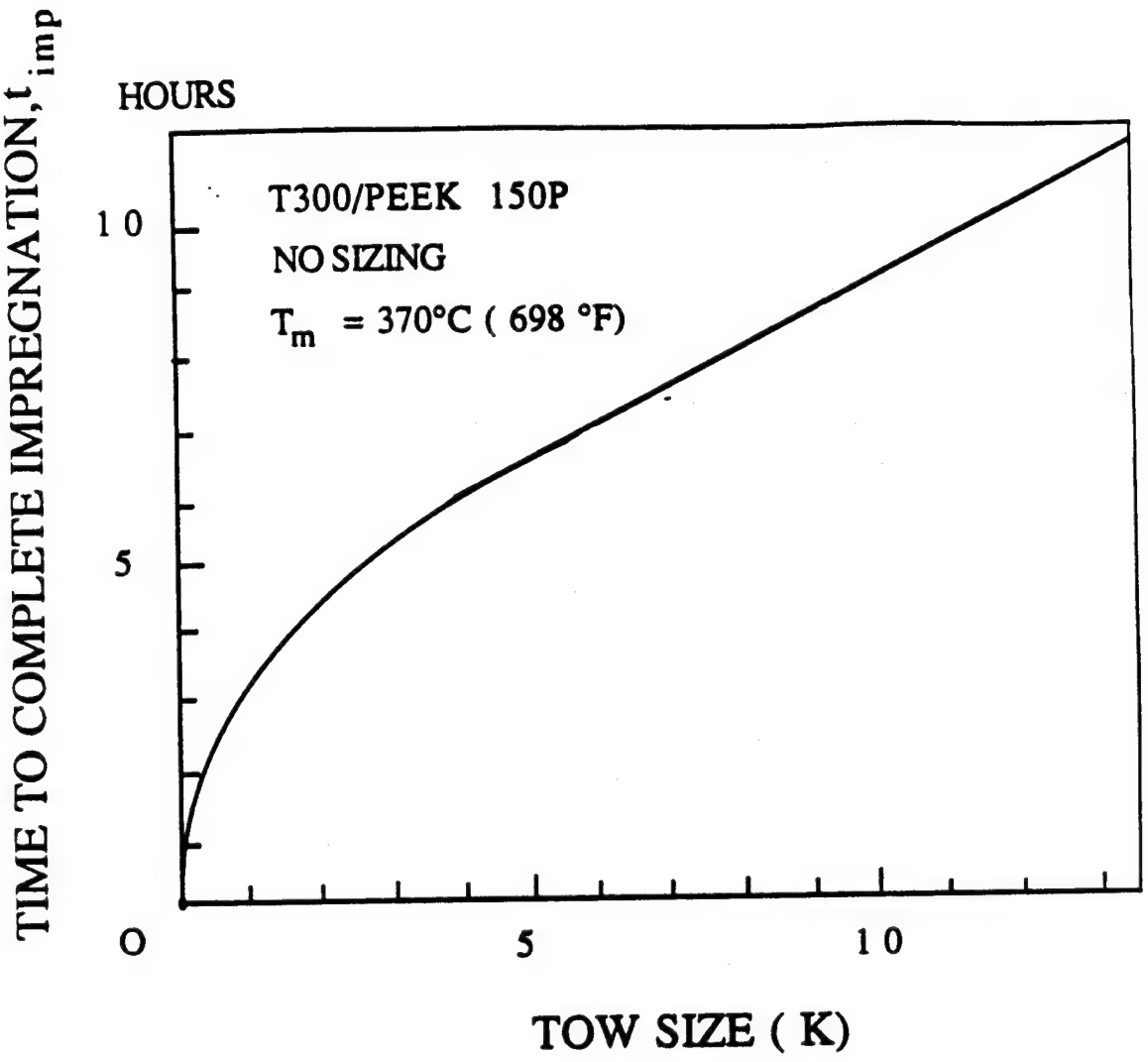

Figure 7. Time required to impregnate different size tows as calculated by the model (see Equation (21)).

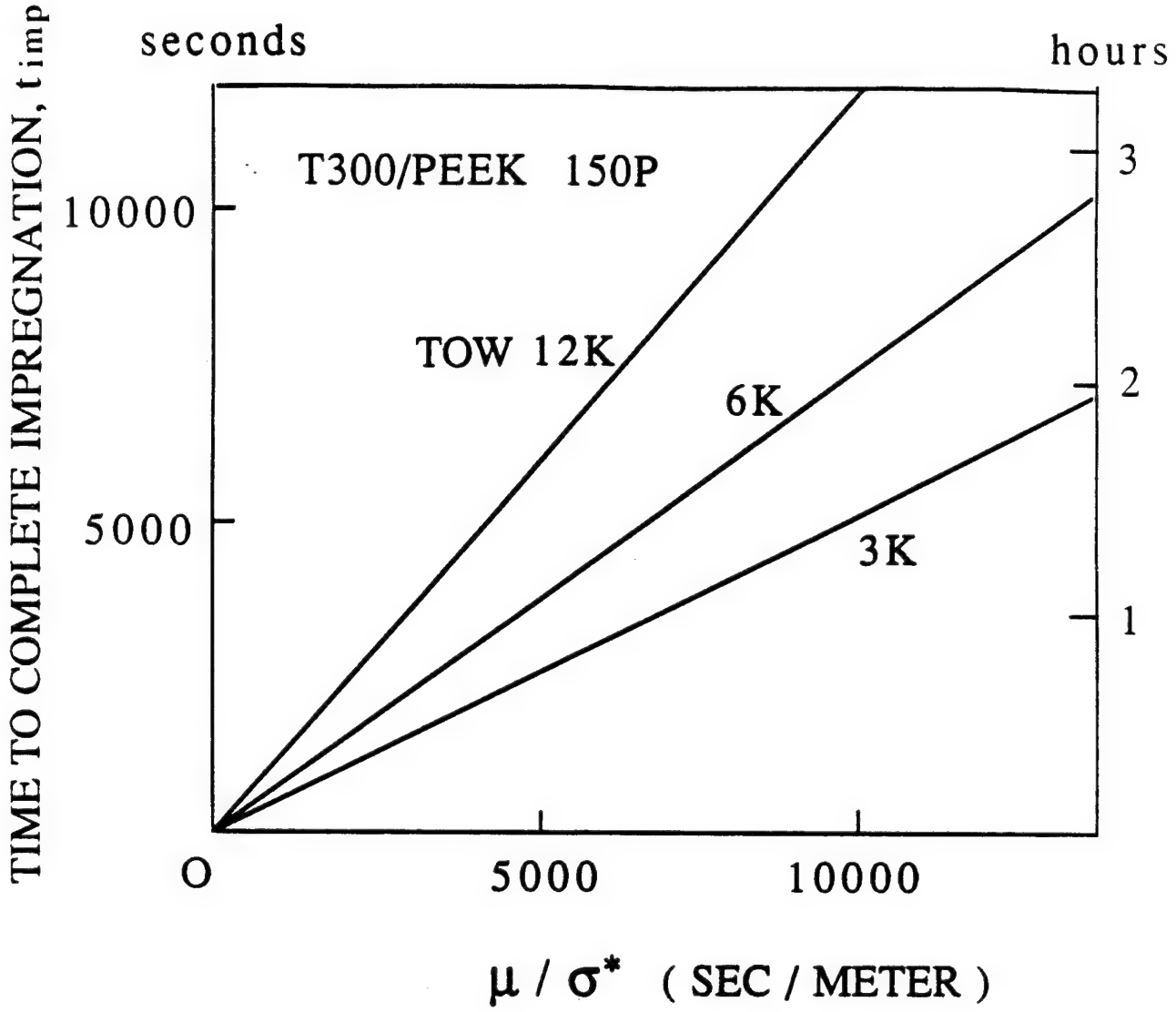

Figure 8. Time required to impregnate a tow as calculated by the model (see Equation (21)).

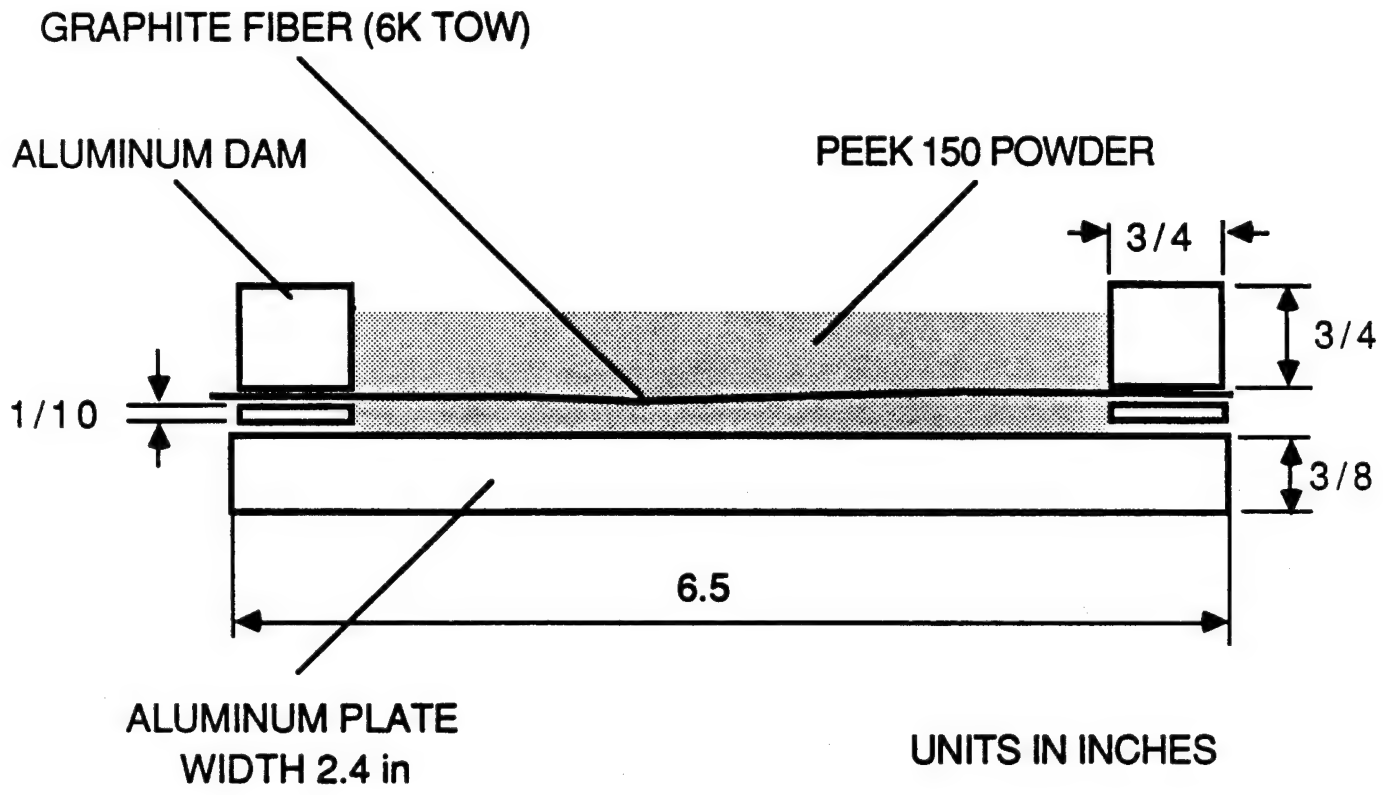

Figure 9. Schematic of the mold used in the impregnation tests.

This process was repeated with tows having been in the oven for different lengths of time. In this manner the degree of impregnation as a function of time was determined. The data are shown in Figure 10.

The degree of impregnation was also calculated by the impregnation submodel (Equation 19) for the conditions of the tests. The geometric parameters required in the calculations (channel height h, tow radius r_o, and fiber diameter d) were measured directly from photomicrographs of the tow cross section perpendicular to the fibers.

The average channel length L was determined from photomicrographs of tow sections parallel to the fibers. This was done in the following manner. First, the angles between different pairs of fibers were measured, and from these measurements an average angle Ω was computed. Second, the average channel length was calculated by

$$L = \frac{\text{channel height}}{\tan\Omega} = \frac{h}{\tan\Omega} \tag{23}$$

The viscosity of PEEK 150P was measured with a Rheometrics parallel plate type viscometer. The value of the surface tension σ^* was determined by fitting the model to data. The values of the material properties are given in Appendix A.

The degree of impregnation calculated by the model is included in Figure 10. There is reasonable agreement between the measured and calculated degree of impregnation, and this lends support to the validity of the model.

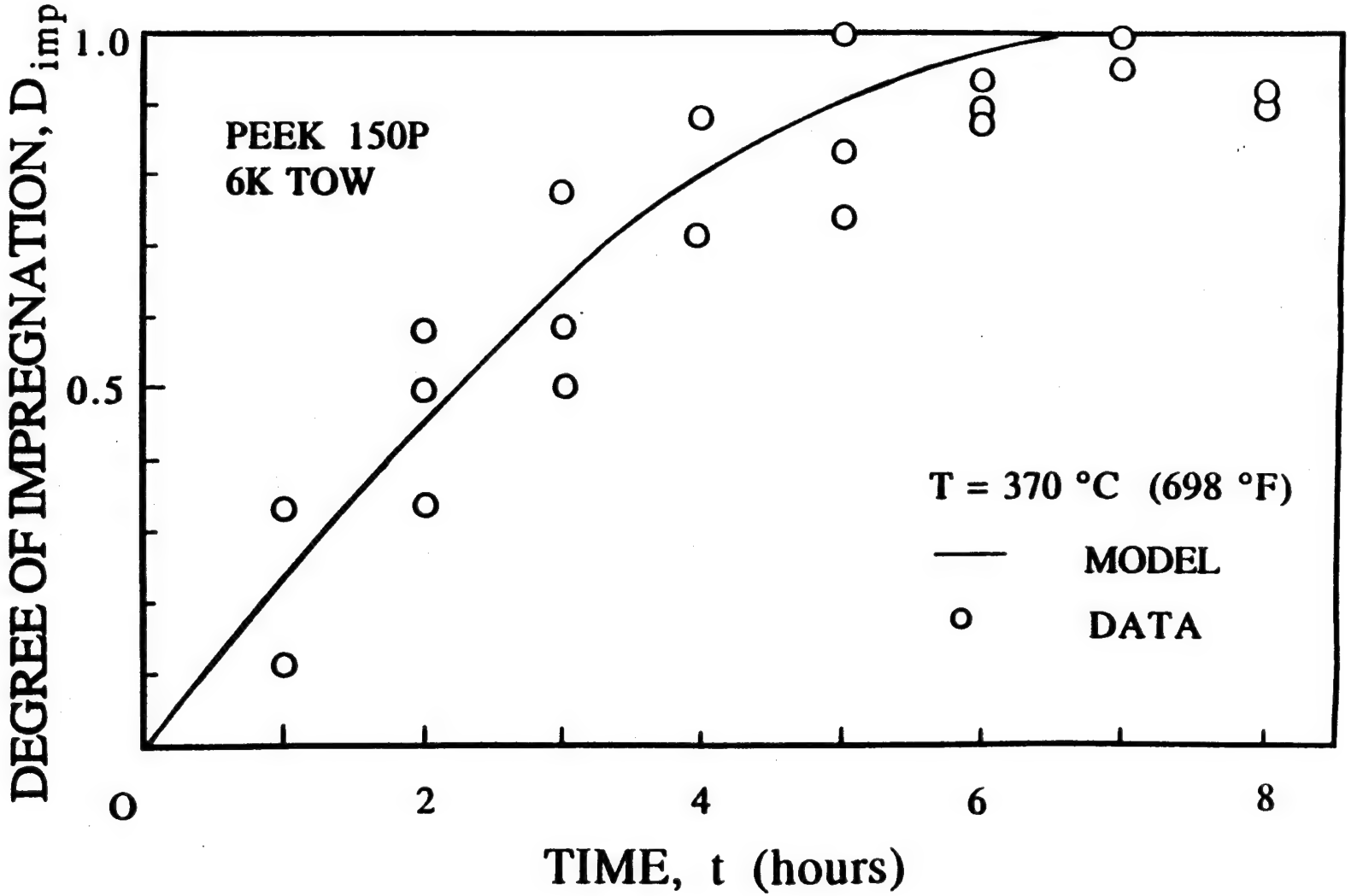

Figure 10. Degree of impregnation as a function of time. Comparisons of data and the results of the model.

Section III

CONSOLIDATION SUBMODEL

When thermoplastic composites are being processed individual plies consolidate into a laminate by bonding at the interfaces [7]. This bonding consists of two phenomena. First, two adjacent ply surfaces coalesce and come into "intimate contact". Second, bond forms at the ply interface by a process called autohesion. In the following, models are presented which describe the effects of the processing variables (temperature, pressure, time) on the intimate contact and autohesion processes. These processes occur simultaneously. However, for the sake of clarity, the models of these processes are developed separately.

Intimate Contact—Model

Laminates are formed by "laying up" plies. Since the ply surfaces are uneven, spatial gaps exist between the plies prior to the application of heat and pressure. When heated, most thermoset matrix composites, including epoxy, have sufficiently low viscosities and wetting abilities to coalesce the ply surfaces. For thermoplastics, even at elevated temperatures, the viscosity is too high to produce the desired degree of flow along the interface. Therefore, thermoplastic matrix composites must actually be deformed to produce intimate contact between adjacent surfaces.

Following Dara and Loos [7] we represent the irregular ply surface by a surface consisting of a series of rectangles (Figure 11). However, while in their model Dara and Loos utilized rectangles of different sizes, we take the rectangles to be identical. Due to the applied force (or pressure) the rectangular elements spread along the interface. We are interested in the extent of this spread (degree of intimate contact) as a function of applied temperature, force (pressure), and time. We also wish to calculate the time required to reach "complete" intimate contact.

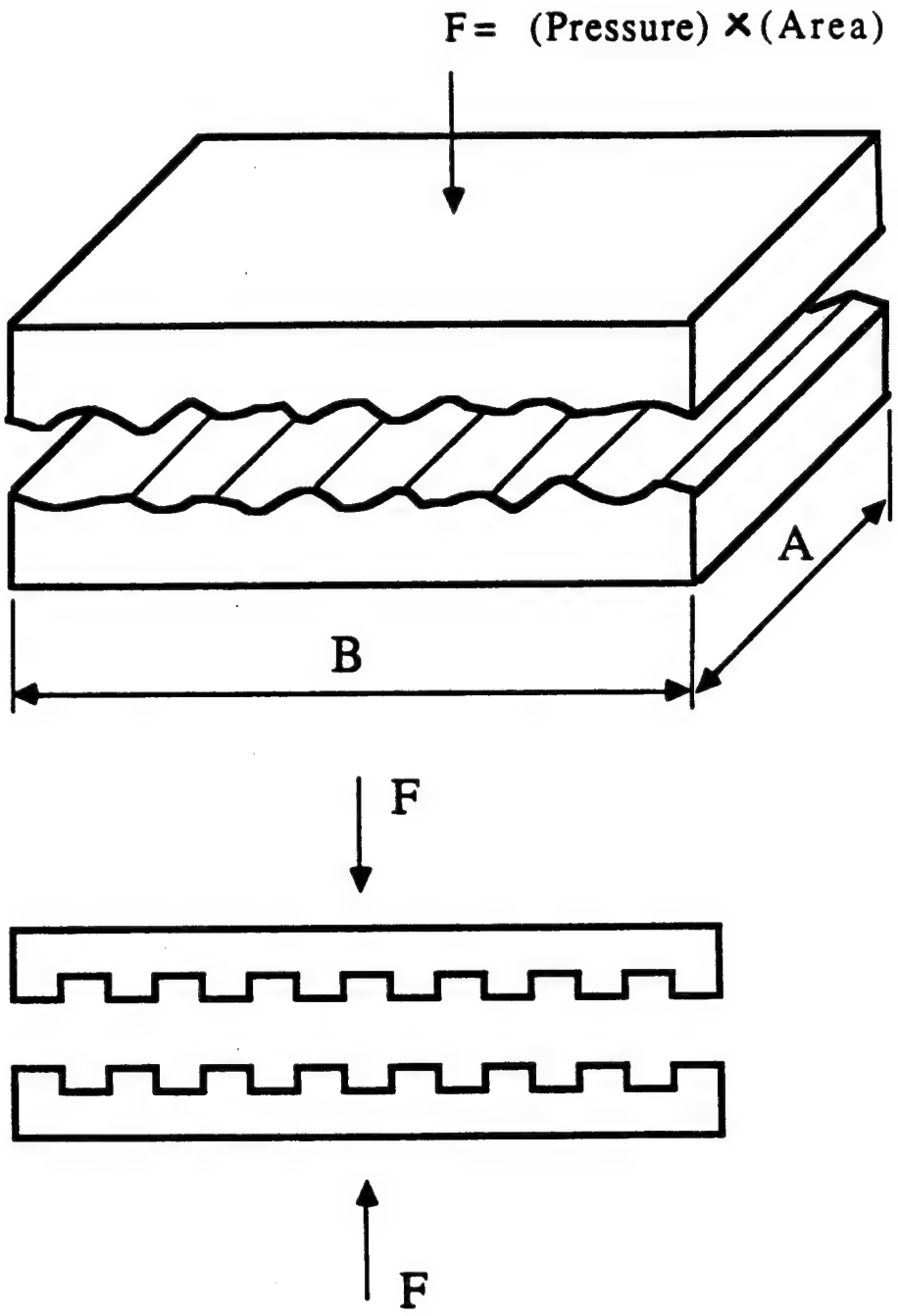

Figure 11. Illustration of the idealized interface used in the intimate contact model.

With reference to Figure 12, the degree of intimate contact is defined as

$$D_{\text{ic}} = \frac{b}{w_o + b_o} \tag{24}$$

where b_o and b are the initial ($t \leq 0$) and instantaneous (at time t) widths of each rectangular element, respectively, and w_o is the initial distance between two adjacent elements. During processing the volume of each element remains constant

$$V_o = a_o b_o = ab \tag{25}$$

where a_o and a are the initial and instantaneous heights of each rectangular element. Equations (24) and (25) yield the following expression for the degree of intimate contact

$$D_{\text{ic}} = \frac{a_o/a}{1 + w_o/b_o} \tag{26}$$

To proceed with the model we apply the law of conservation of mass to a control volume of width dy. Referring to Figure 12 we write

$$a\frac{du_y}{dy} + \frac{da}{dt} = 0 \tag{27}$$

y is the coordinate along the interface and t is time. By assuming that the flow is laminar, we write the average velocity u_y as [5]

$$u_y = -\frac{a^2}{12\mu_{mf}}\frac{dP}{dy} \tag{28}$$

Here μ_{mf} is the viscosity of the fiber-matrix mixture. In the space between two adjacent elements the pressure is P_e. The edge of the element ($y = b/2$), moves with a speed of db/dt. Thus, the boundary conditions corresponding to Equation (28) are

$$P = P_e \quad \text{and} \quad u_y = \frac{db}{dt} \quad \text{at} \quad y = b/2 \quad \text{for} \quad t > 0 \tag{29}$$

By combining Equations (27), (28), and (29), after algebraic manipulations, we obtain

$$P - P_e = \frac{6\mu_{mf}}{a^3}\frac{da}{dt}\left(y^2 - \left(\frac{b}{2}\right)^2\right) \tag{30}$$

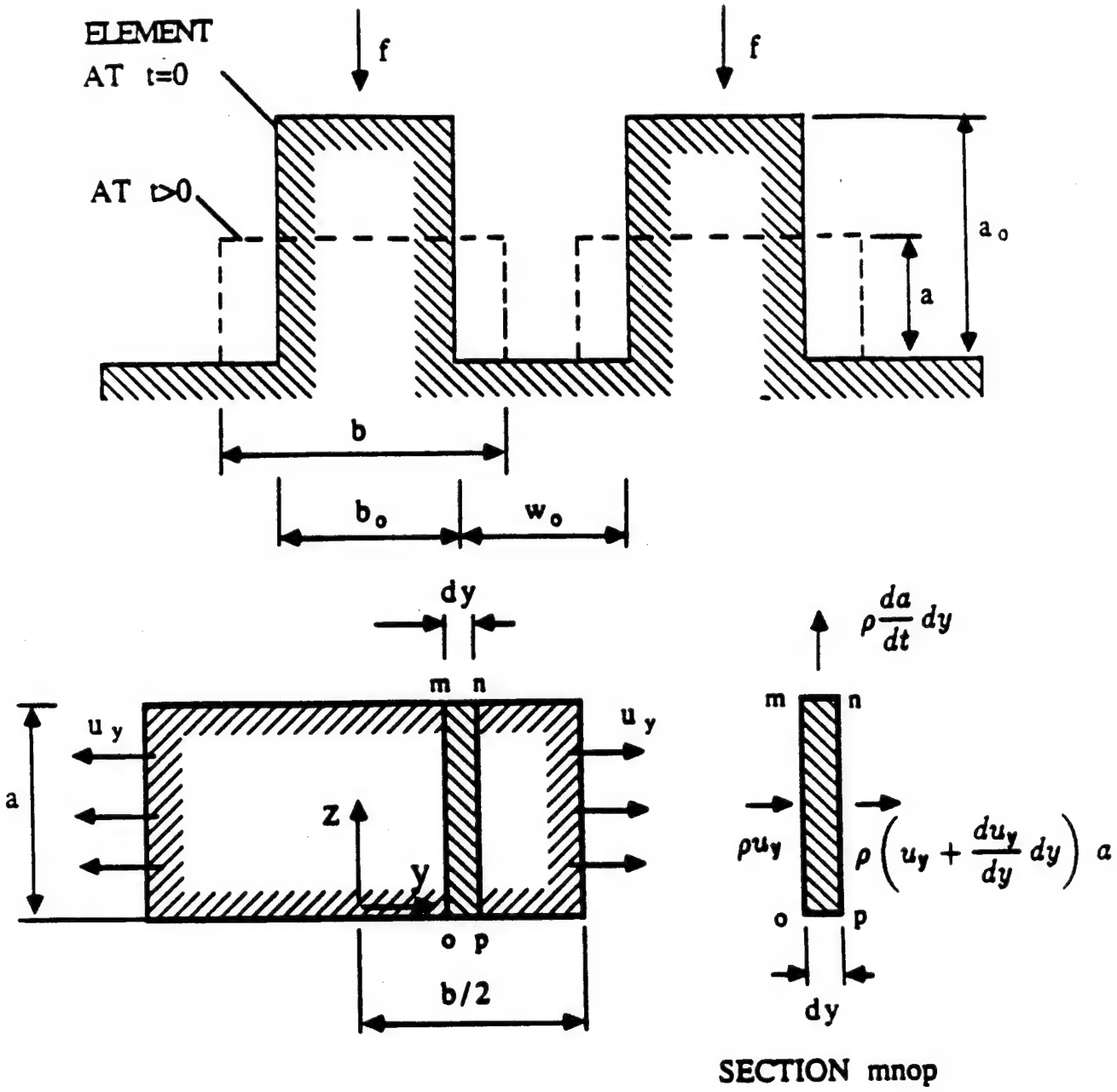

Figure 12. Top: Rectangular elements representing the uneven surface at time $t = 0$. Bottom: Illustration of one element at time t, and the control volume used in calculating mass flows.

The force applied to the entire ply of length A and width B is F (Figure 11). Correspondingly, the force applied per unit length to one element is

$$f = \frac{F}{A}\frac{1}{n} \tag{31}$$

where $n = B/(b_o + w_o)$ is the number of elements in a ply of width B. We write Equation (31) as

$$f = \frac{F}{A}\frac{(b_o + w_o)}{B} = P_{\text{app}}(b_o + w_o) \tag{32}$$

where P_{app} is the applied gauge pressure, and P_e is the ambient pressure which is taken to be the same as the pressure in the space between the rectangular elements. The force applied to an element must be balanced by the pressure inside the element

$$f = \int_{-b/2}^{b/2} (P - P_e)\, dy \tag{33}$$

Combination of Equations (25), (30), (32), and (33) and integration yields

$$\frac{a_o}{a} = \left[1 + \frac{5P_{\text{app}}}{\mu_{mf}}\left(1 + \frac{w_o}{b_o}\right)\left(\frac{a_o}{b_o}\right)^2 t\right]^{1/5} \tag{34}$$

Equations (34) and (26) provide the following expression for the degree of intimate contact

$$D_{\text{ic}} = \frac{1}{1 + \frac{w_o}{b_o}}\left[1 + \frac{5P_{\text{app}}}{\mu_{mf}}\left(1 + \frac{w_o}{b_o}\right)\left(\frac{a_o}{b_o}\right)^2 t\right]^{1/5} \tag{35}$$

Complete intimate contact is achieved when D_{ic} becomes unity. The height a corresponding to this condition is (see Equation 26)

$$a_{D_{\text{ic}}=1} = \frac{a_o}{1 + w_o/b_o} \tag{36}$$

Substitution of Equation (36) into Equation (35) results in the following expression for the time required to achieve complete intimate contact

$$t_{\text{ic}} = \frac{\mu_{mf}}{5P_{\text{app}}}\frac{1}{1 + w_o/b_o}\left(\frac{b_o}{a_o}\right)^2\left[\left(1 + \frac{w_o}{b_o}\right)^5 - 1\right] \tag{37}$$

Intimate Contact—Method of Solution

The degree of intimate contact and the time required to reach complete intimate contact can be calculated by Equations (35) and (37), respectively. The parameters required for the calculations are summarized in Table 2. The geometric parameters w_o/b_o and a_o/b_o can be measured from photomicrographs of the cross section of an uncompacted ply. The viscosity μ_{mf} can be obtained by matching the model to degree of intimate contact versus time data. A method for generating such data is given in the next subsection.

Values of w_o/b_o, a_o/b_o, and μ_{mf} for APC-2 are included in Appendix A. With these values the degree of intimate contact D_{ic} and the time to achieve complete intimate contact t_{ic} were calculated (solid lines in Figures 13 and 14). Similar plots can be generated for other types of materials once the values of the relevant parameters are known. Methods for determining these parameters are given in the next subsection.

Equations (35) and (37) were also incorporated into a computer code which simulates the entire manufacturing process (Section V).

Intimate Contact—Experimental Verification

The intimate contact model was evaluated by the following test procedure. The aluminum-steel mold shown in Figure 15 was placed into a hot press and was preheated to a given temperature. One ply of APC-2 was then placed between the top and bottom aluminum plates of the mold and a pressure was applied. After a certain amount of time the pressure was released and the mold was cooled to room temperature. The ply was then taken out of the mold and its surfaces were inspected. The areas of the uncompressed surfaces were measured, and from these measurements the degree of intimate contact was determined

$$D_{\text{ic}} = \frac{(\text{total surface area}) - (\text{uncompressed area})}{\text{total surface area}} \tag{38}$$

These tests were performed at 40 psig and 662, 680, and 698°F (350, 360, and 370°C), and at 40, 96, and 227 psig at 662°F (350°C). The results of these tests are included in Figure 13. There is good agreement between the results of the model and the data over the range of pressures and temperatures used in the tests.

Table 2

INPUT PARAMETERS REQUIRED FOR THE CONSOLIDATION SUBMODEL

Intimate Contact

1) Length of the plate, A
2) Width of the plate, B
3) Geometric ratios a_o/w_o and b_o/w_o (see Figure 12)
4) Matrix fiber viscosity, μ_{mf}
5) Force (or pressure) applied to the plate, F or P_{app}
6) Applied temperature, T_m

Autohesion

1) Proportionality constant, κ (see Equation 41)
2) Applied temperature, T_m

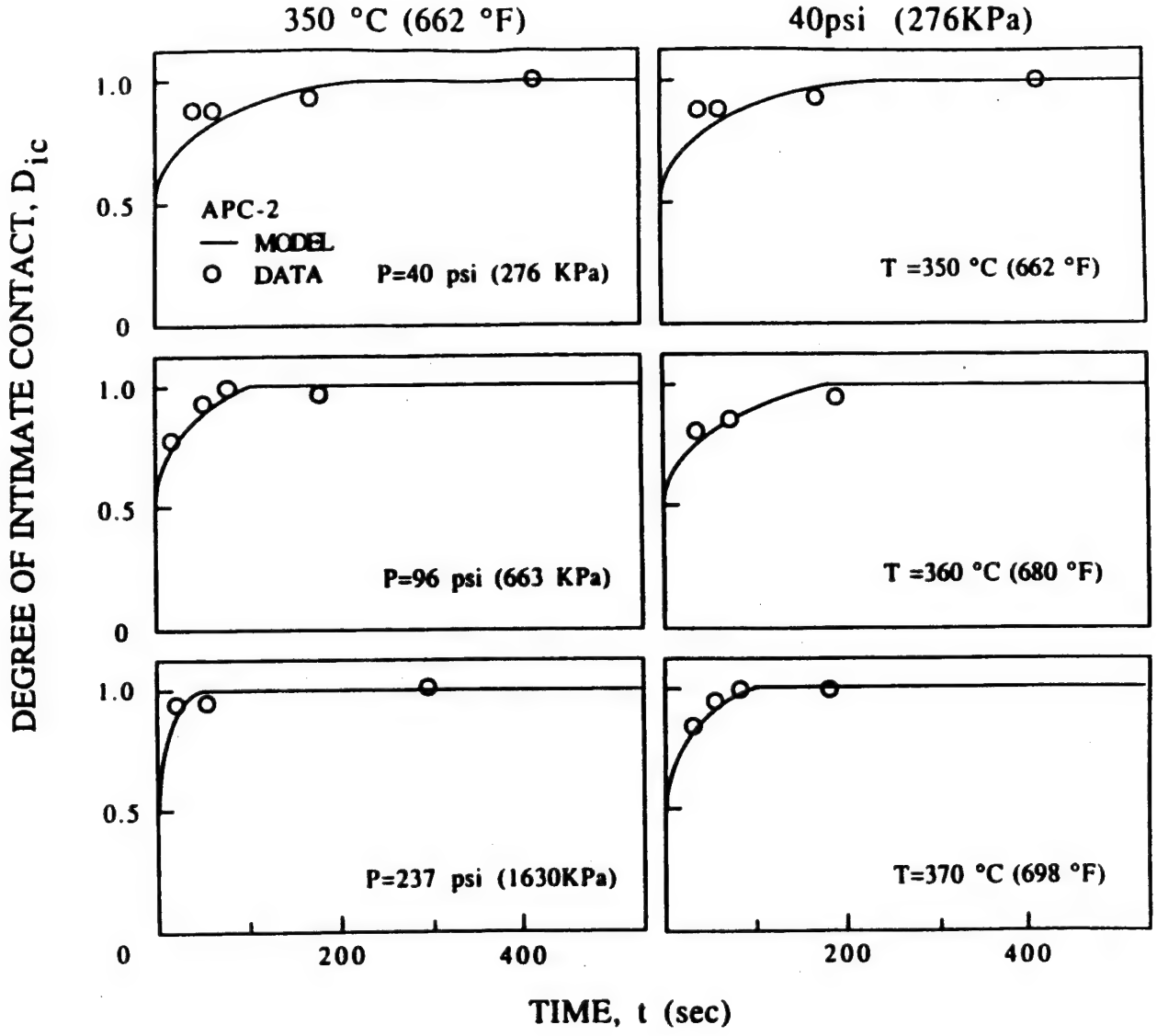

Figure 13. Degree of intimate contact versus contact time as a function of applied temperature and pressure. Comparison of the results of the model with data.

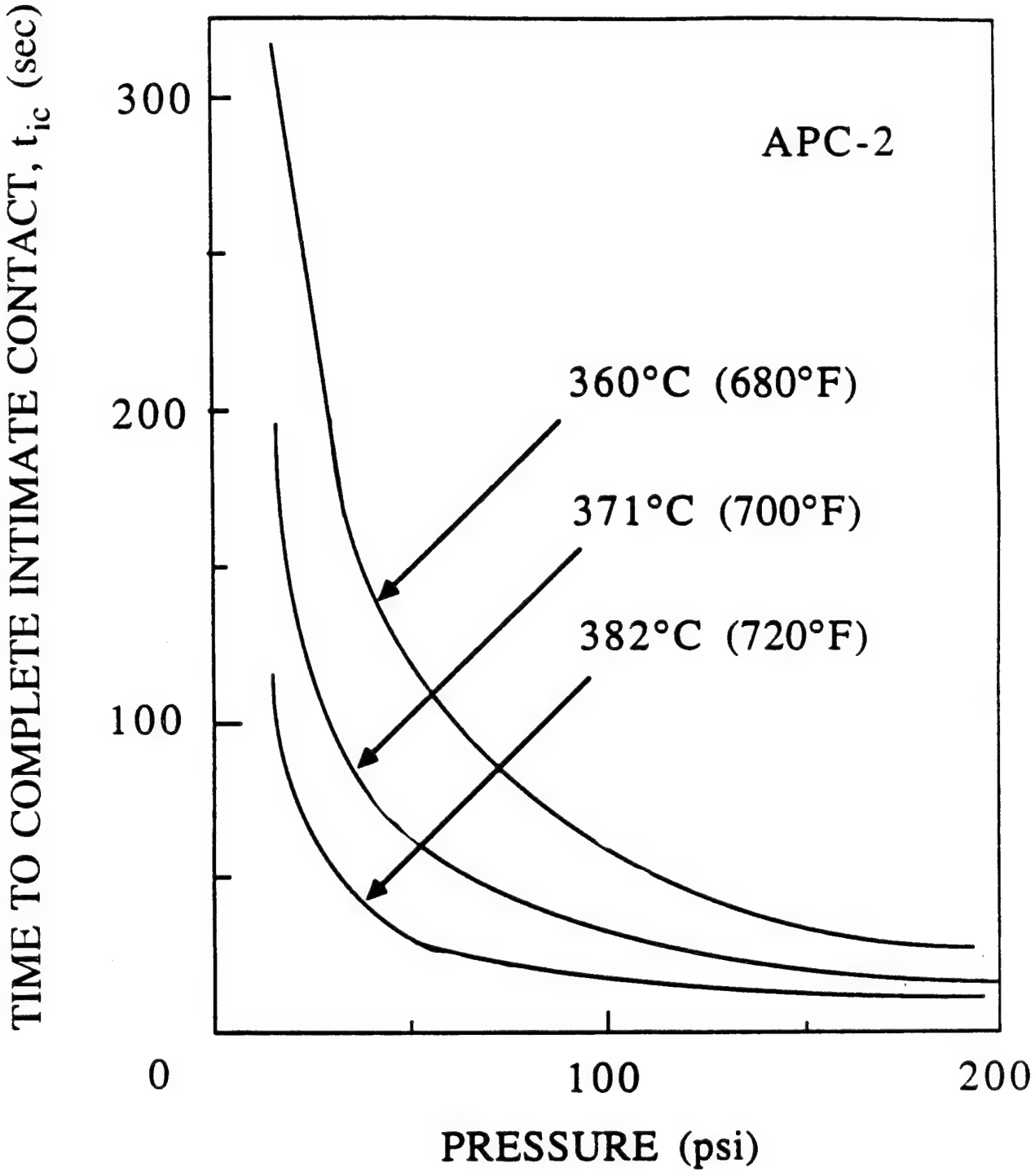

Figure 14. Time required for complete intimate contact ($D_{ic} = 1.0$) versus applied temperature and pressure.

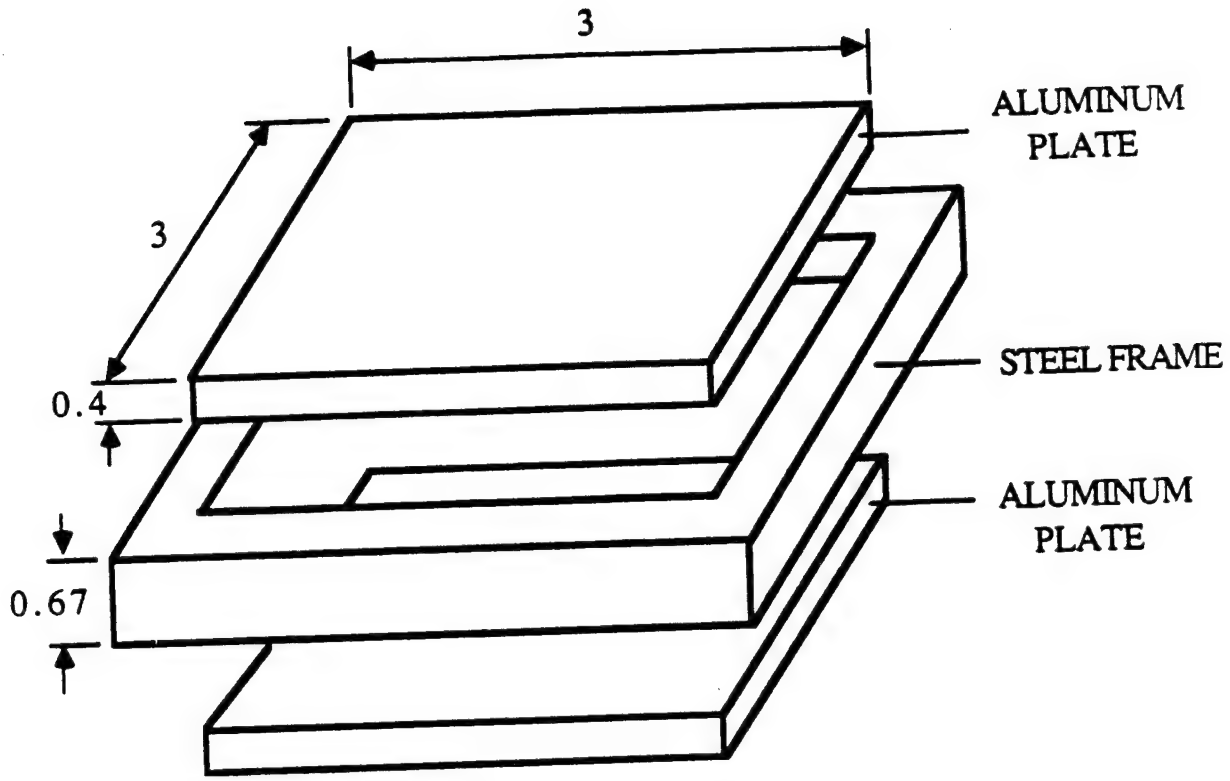

Figure 15. Mold used in the intimate contact tests.

Autohesion—Model

Once two adjacent interfaces come into intimate contact, a bonding process between the interfaces starts. In the case of two similar thermoplastic interfaces the bond is formed mostly by autohesion. During autohesion segments of the chain like molecules diffuse across the interface (Figure 16). The extent of the molecular diffusion and, hence, the bond strength increase with time.

A convenient way of characterizing the extent of autohesion is through the bond strength. Thus a degree of autohesion may be defined as [7]

$$D_{\mathrm{au}} = \frac{S}{S_\infty} \tag{39}$$

where S is the bond strength at time t and S_∞ is the ultimate bond strength, i.e., the strength of a completely bonded interface.

We approximate the autohesion by the following expression proposed by previous investigators (e.g., see References 7 through 10) for amorphous polymers

$$D_{\mathrm{au}} = \kappa t_a^{1/4} \tag{40}$$

where t_a is the time elapsed from the start of the autohesion process (i.e., the time when the interfaces come into intimate contact). κ is a constant which is related to the temperature through the Arrhenius relation

$$\kappa = \kappa_o \exp(-E/RT) \tag{41}$$

κ_o is a constant, E is the activation energy and R is the universal gas constant. It is noted that the crystallinity of the material resulting from cooling may affect the accuracy of Equation 40.

The time required to complete the autohesion process is discussed in the next section. First, experimental verification of the model is presented.

Autohesion—Experimental Verification

The autohesion model was verified by Dara and Loos [7] for UDEL P1700 polysulfone film. Dara and Loos measured the bond strength between two films brought into contact for

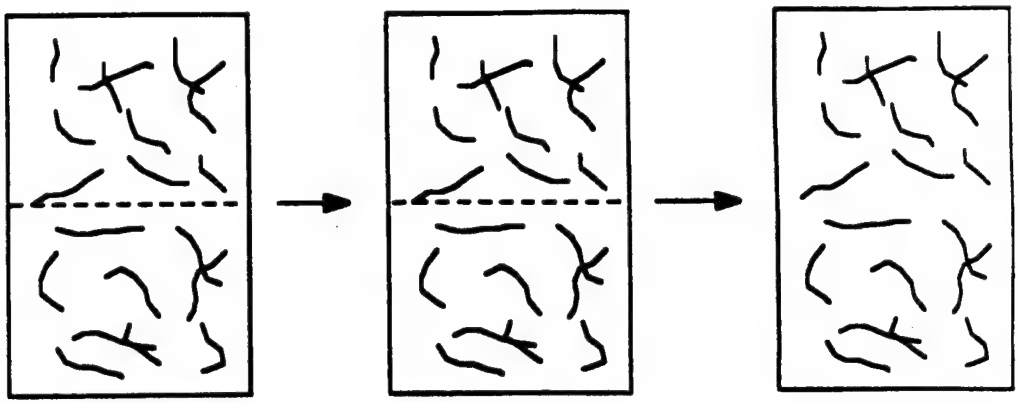

TIME	$t = 0$	$t > 0$	$t \infty$
STRENGTH	$S = 0$	S	S_∞
AUTOHESION	$D_{au} = 0$	$D_{au} = S/S_\infty$	$D_{au} = 1$

Figure 16. Illustration of the autohesion process.

a period of time at temperatures above the glass transition temperature. The semicrystalline PEEK 150 polymer must be processed above the melting temperature 644°F (340°C). At these temperatures the viscosity of PEEK 150P is very low and, hence, the method of Dara and Loos cannot be applied to PEEK 150P. The method could be applied to APC-2. The tests were performed as follows.

Two cross ply ($[0/90]_T$) APC-2 composite laminates were placed between two steel sample holders (Figure 17). A 0.001 inch thick aluminum foil, coated with Frekote 44 was placed between the two composite laminates. There was a 0.16 inch diameter hole in the center of the aluminum foil.

The assembly described above was placed in a hot press maintained at either 698, 716, or 734°F (370°C, 380°C, or 390°C). A light load (18 lbf) was applied to assure contact between the laminates. After a certain amount of time the assembly was removed from the press and was quenched in cold water. The tensile strength of the bond was then measured by placing the assembly into a mechanical tester and by applying a tensile load to the steel sample holders. (The APC-2 bonded to the steel without glue.) The degree of autohesion was calculated by

$$\text{Degree of autohesion} = \frac{\text{bond strength at time } t}{\text{max bond strength (at } t \to \infty)} \tag{42}$$

The data thus obtained are given in Figure 18. The model ($D_{au} \sim t^{1/4}$) is represented by the solid lines in this figure. There is reasonable agreement between the data and the model.

The tests were repeated at different pressures. As seen from the data in Figure 19, within the pressure range tested, the applied pressure does not have a marked effect on the degree of autohesion.

Finally it is noted that the constant κ can be obtained by fitting Equation 40 to the data. An expression of κ obtained in this manner is given in Appendix A.

Degree of Bond

Once intimate contact is established at a point along the interface autohesion, and thus the bonding process, starts. The degree of bonding D_b at time t can be calculated by the

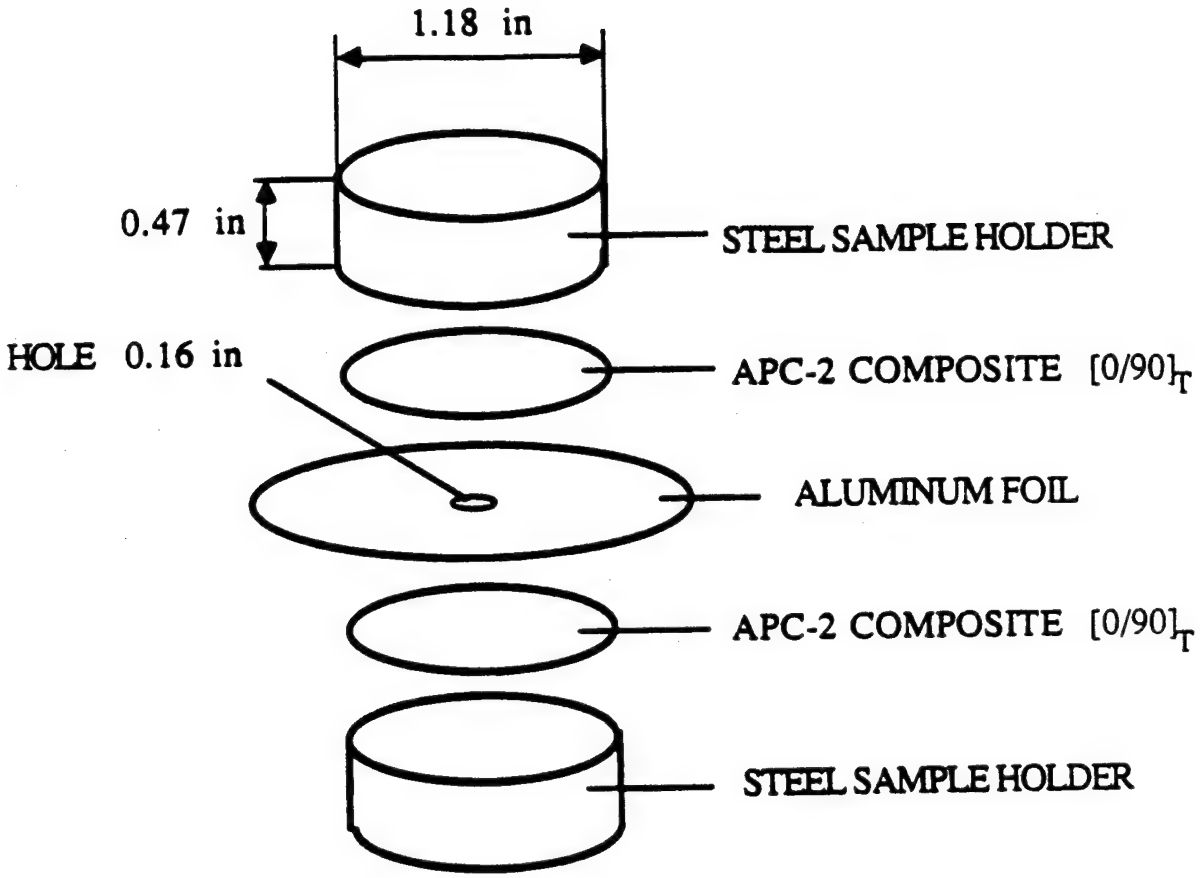

Figure 17. Illustration of the test used to measure autohesion.

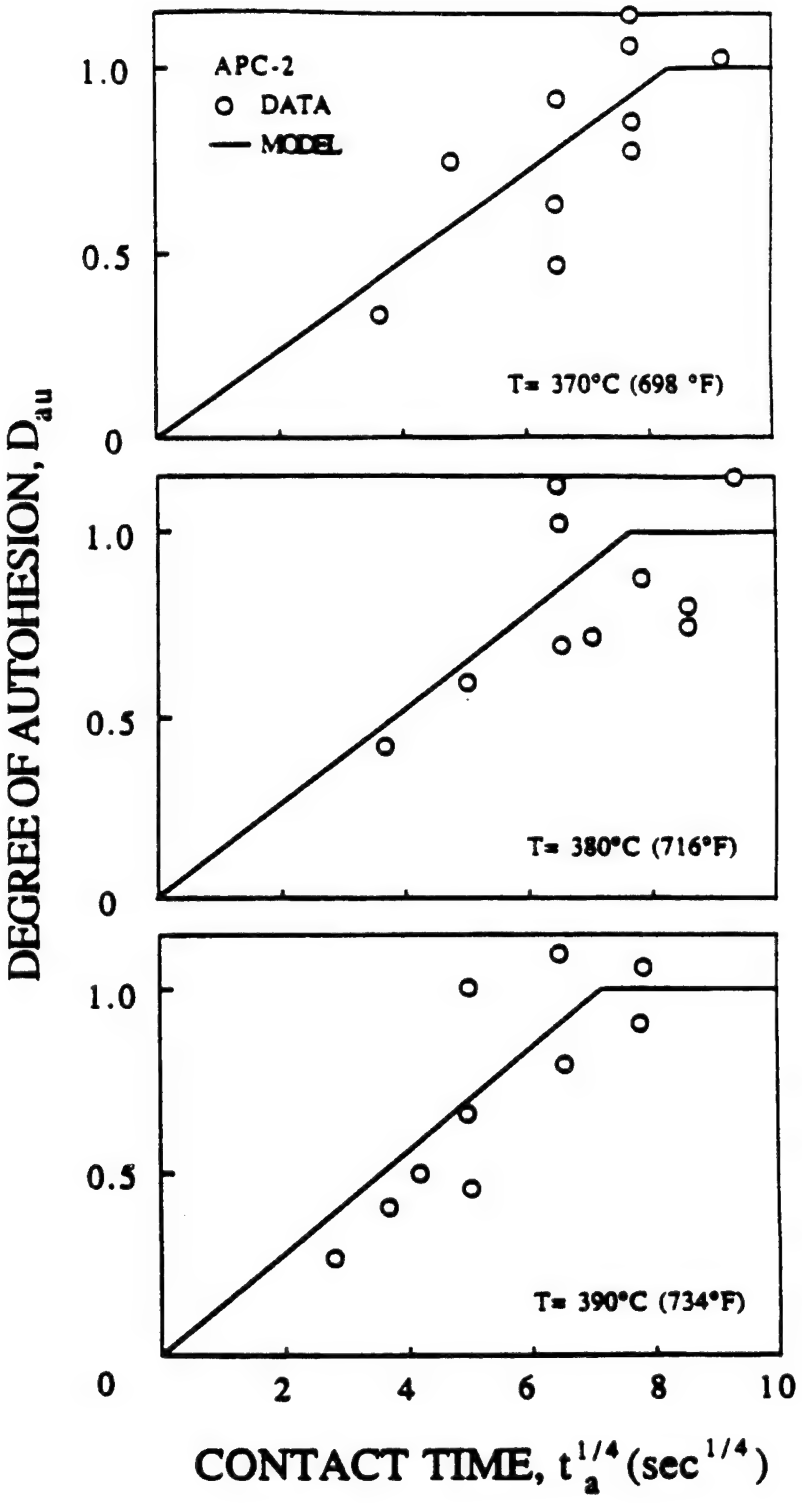

Figure 18. Degree of autohesion as a function of time for different temperatures.

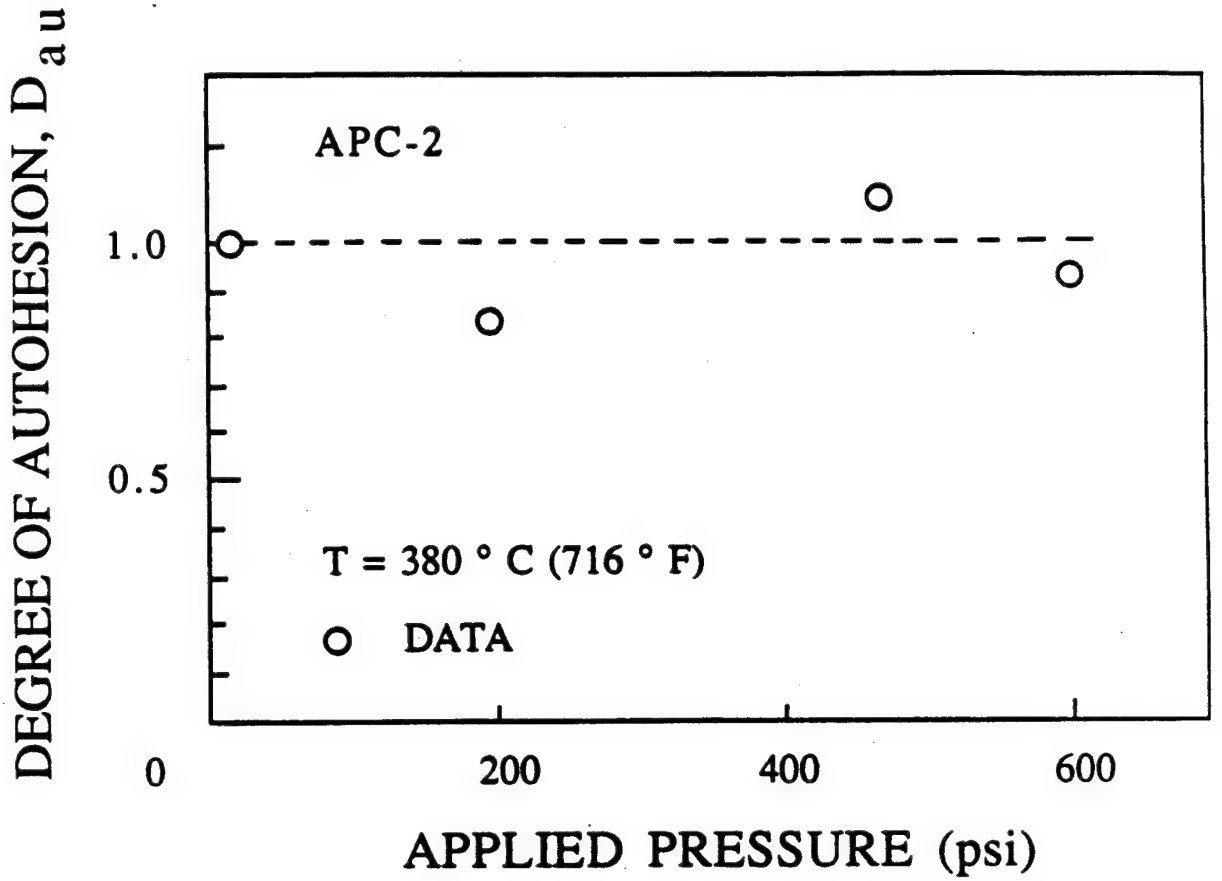

Figure 19. Autohesion as a function of pressure.

expression

$$(D_b)_{\text{at } t} = [(D_{\text{ic}})_{\text{at } \Delta t} - (D_{\text{ic}})_{\text{at } 0}] \left[\kappa\,(t-\Delta t)^{1/4}\right] + [(D_{\text{ic}})_{\text{at } 2\Delta t} - (D_{\text{ic}})_{\text{at } \Delta t}] \left[\kappa\,(t-2\Delta t)^{1/4}\right] + \cdots \tag{43}$$

or

$$(D_b) = \sum_{i=1}^{t/\Delta t} \left[(D_{\text{ic}})_{i\Delta t} - (D_{\text{ic}})_{(i-1)\Delta t}\right] \left[\kappa(t-i\Delta t)^{1/4}\right] \tag{44}$$

where Δt is an arbitrary time step. D_{ic} is the degree of intimate contact given by Equation (35).

Bonding is complete when D_b becomes unity. Thus the time required to complete the bonding t_b is to be calculated by

$$1 = \sum_{i=1}^{t_b/\Delta t} \left[(D_{\text{ic}})_{i\Delta t} - (D_{\text{ic}})_{(i-1)\Delta t}\right] \left[\kappa(t_b-i\Delta t)^{1/4}\right] \tag{45}$$

The degree of bonding D_b as function of time, temperature, and pressure, and the bonding time t_b as function of temperature and pressure were calculated for APC-2. The results are given in Figures 20 and 21. From these figures the degree of bonding and the time required to achieve full bonding can readily be estimated. To facilitate the calculations for conditions and materials not included in these figures, Equations (44) and (45) were also incorporated into the computer code developed for simulating the entire manufacturing process (Section V).

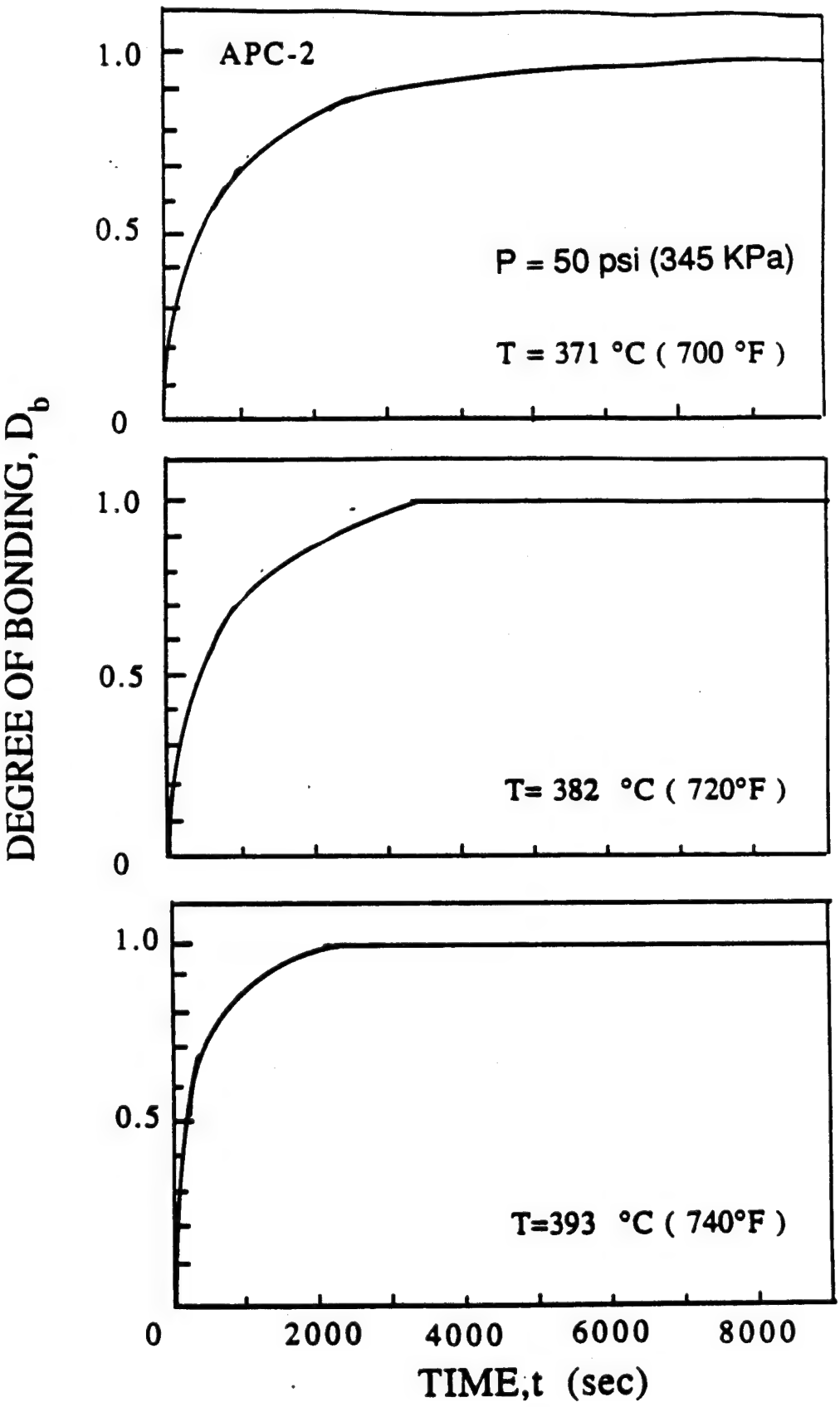

Figure 20. Degree of bonding as a function of time for different temperatures.

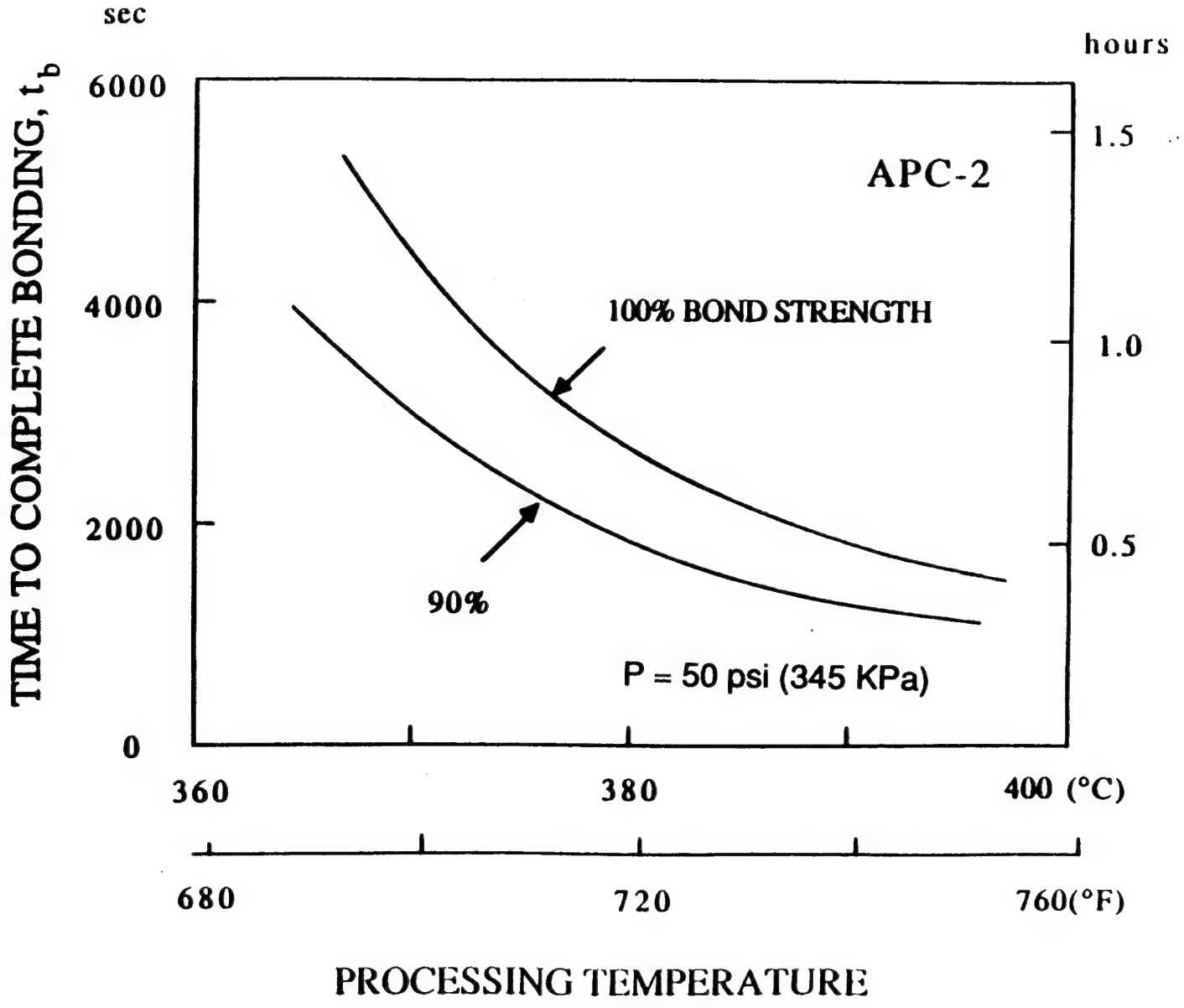

Figure 21. The time required to complete the bond as a function of applied temperature.

Section IV

CRYSTALLINITY SUBMODEL

For semicrystalline thermoplastic matrix composites the degree of crystallinity affects significantly the mechanical properties of the composite. The desired crystallinity is achieved during the processing by cooling the composite from the melt temperature T_m at an appropriate cooling rate. The objective here is to establish a model which relates the cooling rate applied during processing to the crystallinity of the material. For clarity, the model is developed for a flat plate in which the temperature varies only across the plate but not along the plate (one dimensional problem, Figure 22). The model could readily be extended to more complex geometries. In applying the model it must be borne in mind that the model was developed to aid in the selection of the processing variables. No attempt was made to study the detailed molecular processes and the morphologies involved in processing thermoplastics.

During cooling the crystallinity of the polymer changes. The instantaneous degree of crystallinity depends on the temperature and on the rate of change of the temperature. Therefore, to determine the degree of crystallinity as a function of position and time, the temperature distribution inside the laminate must be known at all times. For a flat plate the temperature distribution can be calculated by the following form of the conservation of energy [11]

$$\rho C \frac{\partial T}{\partial t} = \frac{\partial}{\partial z}\left(k \frac{\partial T}{\partial z}\right) + m_m \frac{dc}{dt} H_u \tag{46}$$

where t is time, z is the coordinate normal to the plate, T is the temperature, ρ is the density, C is the specific heat, and k is the thermal conductivity of the composite. Expressions for estimating the latter three parameters are given in Table 3.

The second term on the right-hand side of Equation (46) represents the heat generated due to crystallization. In this term c is the crystallinity of the matrix, m_m is the matrix mass fraction, and H_u is the theoretical ultimate heat of crystallization of the polymer at 100 percent crystallinity.

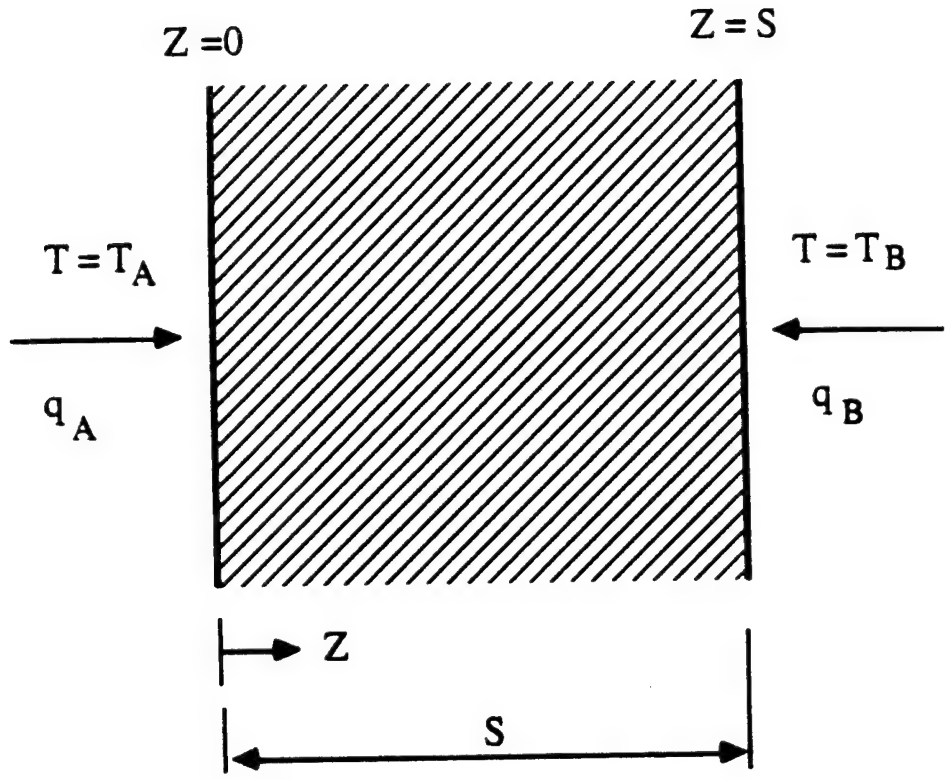

Figure 22. Geometry used in the crystallinity submodel.

Table 3

INPUT PARAMETERS REQUIRED FOR THE CRYSTALLINITY SUBMODEL

Geometry

1) Number of plies in the plate, N
2) Thickness of one ply, s_o

Polymer[a]

3) Mass fraction, m_m
4) Density, ρ_m
5) Specific heat, C_m
6) Thermal conductivity, k_m
7) Theoretical ultimate heat of crystallization, H_u
8) Relationship between crystallinity, cooling rate, and temperature

Fiber[a]

9) Density, ρ_f
10) Specific heat, C_f
11) Thermal conductivity, k_f

Mechanical Properties

12) Mechanical properties as function of crystallinity (optional)

Processing Variables

13) Applied temperature or heat flux (T_A and T_B or q_A and q_B)

---

a) The density, specific heat, and thermal conductivity of the composite may be approximated by the expressions [12, 13]

$$\rho = v_m \rho_m + (1 - v_m)\, \rho_f$$

$$C = m_m C_m + (1 - m_m)\, C_f$$

$$k = \left[(1 - \sqrt{1 - v_m}) + \frac{1}{\sqrt{1/(1 - v_m)} + (k_m/k_f - 1)} \right] k_m$$

where the subscripts m and f refer to the matrix and fiber respectively. v_m is the matrix volume fraction

$$v_m = \left[1 + (\rho_m/\rho_f) \left(\frac{1}{m_m} - 1 \right) \right]^{-1}$$

Equation (46) contains two dependent variables, the temperature T and the crystallinity c. Therefore, to proceed with the solution an additional expression is needed relating the crystallinity to the temperature. This expression is established by utilizing the fact that for a given material, the rate of degree of crystallinity depends on the cooling rate and on the instantaneous temperature. This dependence can be expressed symbolically as

$$\frac{dc}{dt} = g\left(\frac{dT}{dt}, T\right) \tag{47}$$

The function g is a material property which must be obtained experimentally. A procedure for determining this function is described in Appendix B.

Solutions to Equations (46) and (47) require that the initial and boundary conditions be specified. Initially, (prior to the start of cooling) the composite is at the uniform temperature T_i having zero crystallinity. Thus, the initial conditions corresponding to Equation (46) are

$$\left.\begin{aligned} T &= T_i \\ c &= 0 \end{aligned}\right\} \qquad \begin{aligned} t &< 0 \\ 0 \leq z &\leq s \end{aligned} \tag{48}$$

where s is the thickness of the plate. During processing either the surface temperatures (T_A and T_B) or the heat fluxes (q_A and q_B) on the two surfaces of the plate must be specified (Figure 22). In terms of the surface temperatures the boundary conditions are

$$\begin{aligned} T &= T_A \quad z = 0 \quad t \geq 0 \\ T &= T_B \quad z = s \quad t \geq 0 \end{aligned} \tag{49}$$

In terms of the heat fluxes the boundary conditions are

$$\begin{aligned} q &= q_A \quad z = 0 \quad t \geq 0 \\ q &= q_B \quad z = s \quad t \geq 0 \end{aligned} \tag{50}$$

Equations (46) through (50) define the problem under consideration.

Crystallinity—Method of Solution

The temperature and the crystallinity as functions of position and time can be calculated by Equations (46) through (50). The solutions to these equations require numerical procedures. Therefore, a finite element algorithm was developed for performing the calculations. This algorithm was incorporated into a computer code which simulates the entire

manufacturing process (Section V). The input parameters required for the calculations are summarized in Table 3.

To illustrate the type of information which can be generated by the crystallinity submodel, temperature and crystallinity distributions as functions of time, as well as the average crystallinity as a function of cooling rate were calculated for APC-2 composites. The material properties used in the calculations are listed in the Appendices. The results are presented in Figures 23 through 25. In these figures the cooling rates indicated are the cooling rates on the plates' surfaces. It is interesting that, according to the calculations, even for the comparatively thick ($s = 0.2$ inch) plates, the crystallinity is quite uniform across the plate for cooling rates up to 1000°F/min. Only at the extremely high cooling rate of 10,000°F/min is there a small variation in crystallinity inside the plate. This is reassuring because uniform crystallinity implies uniform material properties.

Finally, it is observed that, as expected, the average crystallinity of the plate changes with cooling rate (Figure 25). At cooling rates below 100°F/min (i.e., at the cooling rates often used in practice) the average crystallinity is nearly independent of the plate thickness.

By generating results such as shown here, the cooling rates (and the corresponding surface temperatures or surface heat fluxes) can be selected which result in a composite of the desired crystallinity.

Crystallinity—Experimental Verification

The validity of the crystallinity submodel described above was assessed by two types of tests. First, the crystallinities of PEEK 150P polymer specimens cooled at different rates were measured. Second, during cooling the temperatures inside APC-2 composites were recorded. The data thus obtained were compared to the results of the model.

The apparatus and procedures used in the tests were described in References 14–16. Hence, details of the experiments are not given here. Essentially, in the tests, the specimens were heated to 720°F (382°C) and then cooled to room temperature. The surface temperatures of the specimens T_s were measured. An average cooling rate was computed by

$$\dot{Q} = \frac{(T_S)_{\text{at } 720°F} - (T_S)_{80°F}}{(\Delta t)} \tag{51}$$

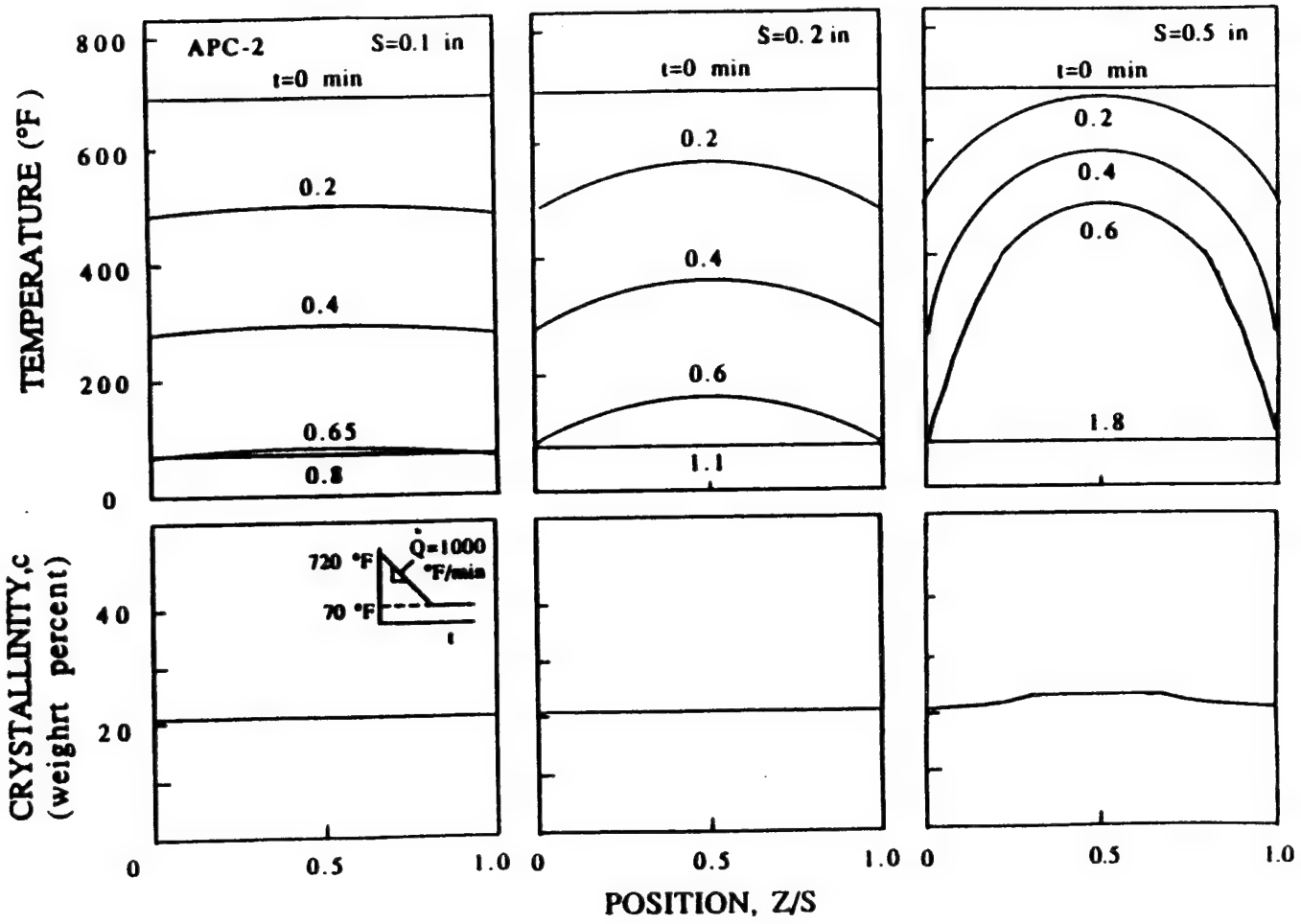

Figure 23. Top: The temperature distribution as a function of time in APC-2 plates. Bottom: Crystallinity distribution after cooling to 70°F. Results of the model computed for a surface cooling rate of 1000°F/min.

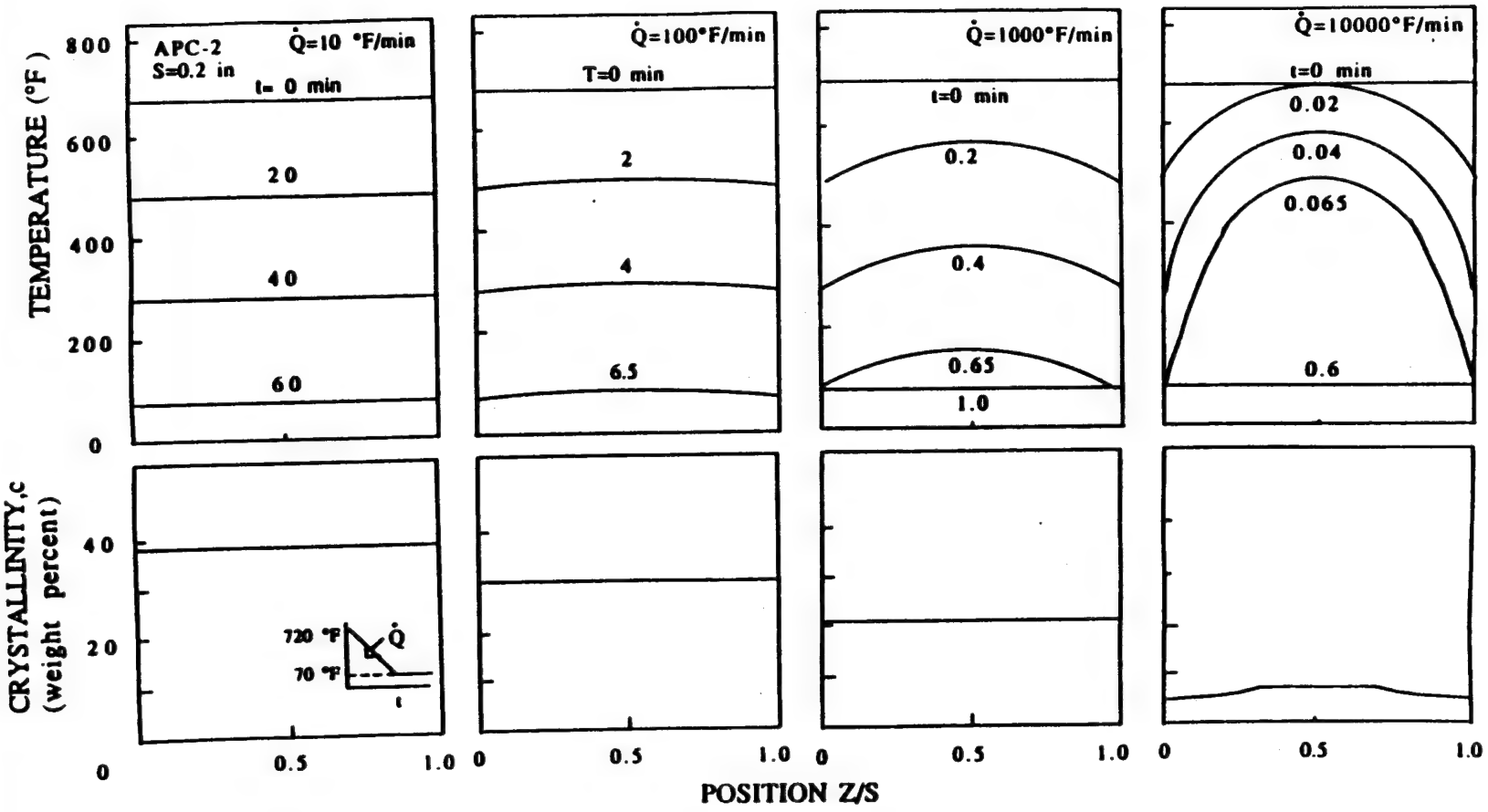

Figure 24. Top: The temperature distribution as a function of time. Bottom: Crystallinity distribution after cooling to 70°F. Results of the model computed for a 0.2 in thick APC-2 plate. Cooling rates indicated are the surface cooling rates.

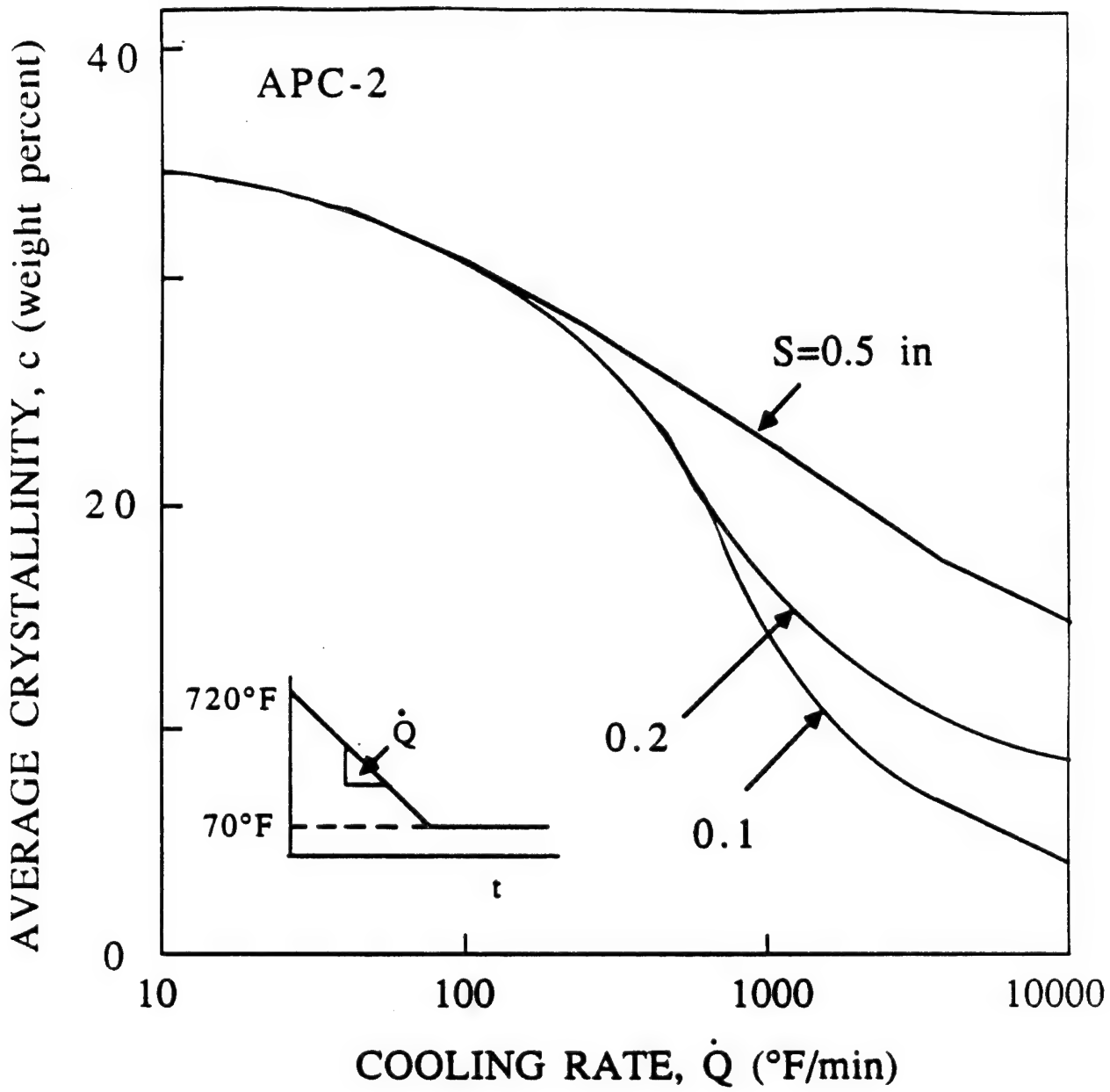

Figure 25. Average crystallinity as a function of surface cooling rate for an APC-2 composite. Results of the model.

where Δt is the time required to decrease the surface temperature from 720°F to 80°F. For APC-2 the temperatures were also recorded at the midpoint inside the composite.

After having been cooled to room temperature the crystallinities of the specimens were determined by differential scanning calorimetry (DSC). A small sample taken from the specimen (~40 mg) was enclosed in an aluminum sample pan and placed into the DSC cell. The heat flow in the cell as a function of temperature was measured at a constant heating rate of 36°F/min. The crystallinity was determined from the expression (Figure 26)

$$c_{\text{measured}} = \frac{H_F}{H_u} \tag{52}$$

where H_F is the net amount of heat absorbed on heating from the glass transition temperature (293°F) to 720°F as measured by the DSC. H_u is the ultimate heat of fusion and is 130 J/gram [17]. The crystallinities of some of the PEEK 150P specimens were also determined by wide angle X-ray diffraction [15]. The crystallinities measured by DSC and X-ray agreed closely. In evaluating the crystallinities of the APC-2 composites adjustments were made for the fiber content using the expression

$$c = [(c)_{\text{measured}}]/(WP) \tag{53}$$

where WP is the weight percent of the polymer in the composite. Since the polymer density depends on the crystallinity, an iterative procedure was used to calculate WP [15]. This procedure was based on a nominal fiber volume fraction of 0.59.

The crystallinities of 1/8 inch thick PEEK 150P plates specimens manufactured at three different cooling rates are presented in Figure 27. The temperatures recorded at the middle of 3/16 inch thick APC-2 composites are shown in Figure 28.

The crystallinities and the center temperatures were also computed by the crystallinity submodel. The material properties used in the calculations are listed in the Appendices. The calculated values of the temperatures and crystallinities and temperatures are included in Figures 27 and 28. There are good agreements between the data and the results of the model.

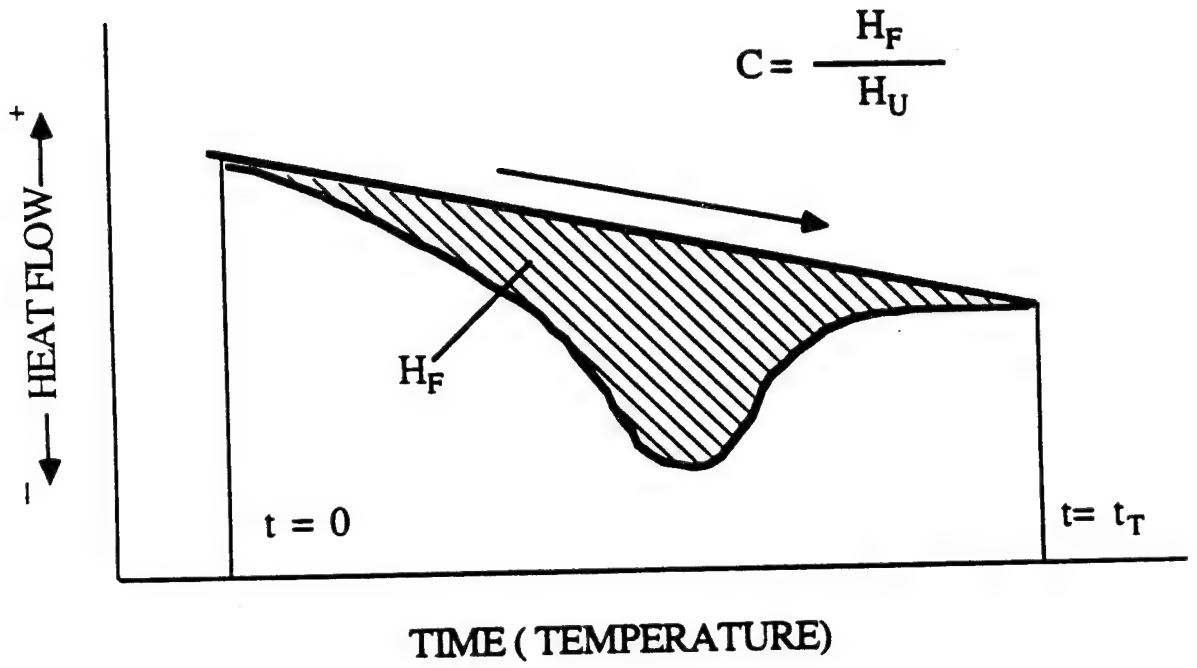

Figure 26. Illustration of the results obtained on heating a PEEK 150P polymer or APC-2 composite sample in the DSC.

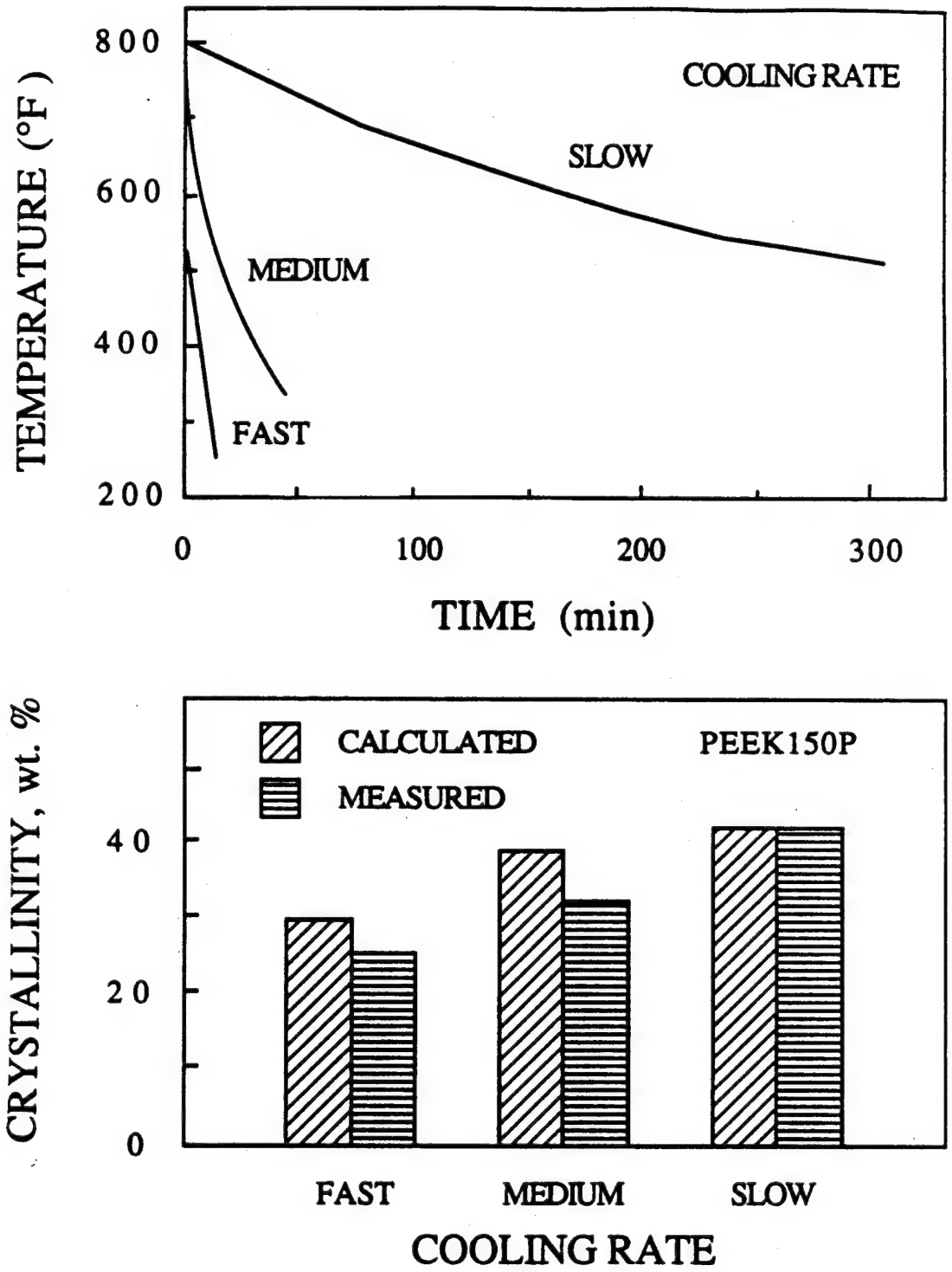

Figure 27. Average crystallinities of PEEK 150P plates cooled at different rates. Comparisons between the measured and calculated crystallinities. Top: Cooling cycle used in the manufacture of the plates.

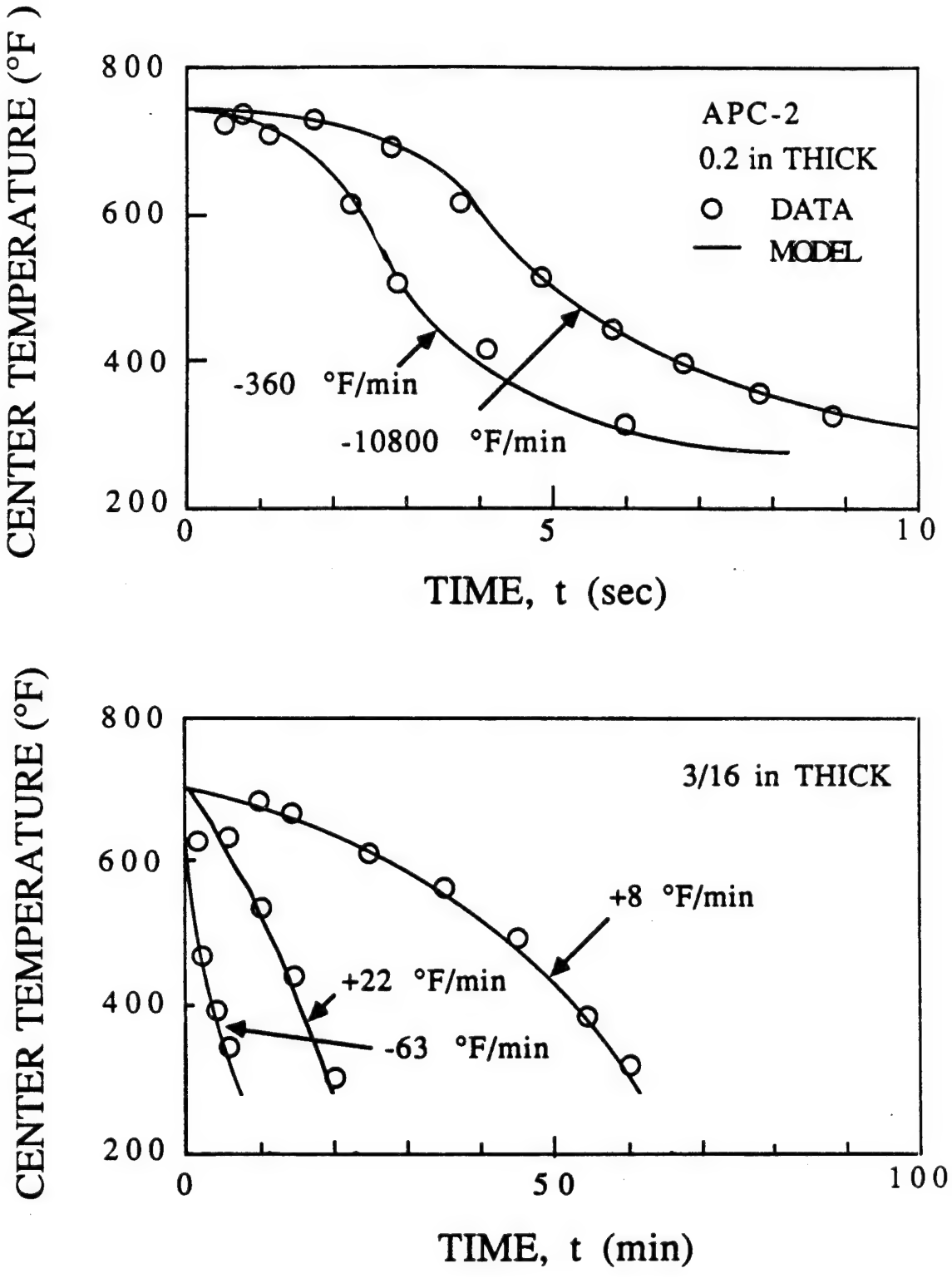

Figure 28. Temperature in the middle of APC-2 plates cooled (heated) at different rates. Comparison between the data and the results of the model.

Section V

NUMERICAL PROCEDURE

Solution to the impregnation, intimate contact, autohesion, and crystallinity submodels may be obtained individually by the methods described in conjunction with each submodel. Some of the solutions are simple, while other require extensive numerical computations. For convenience, all of the four submodels were incorporated in a user friendly computer code designated as PLASTIC. The input parameters required by this code are summarized in Tables 1 through 3. The output provided by the code is given in Table 4 and in Figure 29. With this code each processing step can be studied individually. The code can also be used to analyze processes where two or more phenomena occur simultaneously. The model, and the corresponding code, should thus be useful in the study of the processing of thermoplastic matrix composites, and in establishing the processing parameters (temperature, pressure, time) most suitable in a given application.

Table 4

OUTPUT PROVIDED BY THE THERMOPLASTIC PROCESSING MODEL AND THE PLASTIC CODE

Impregnation Submodel

1) Degree of impregnation as a function of time.
2) Time required to complete the impregnation.

Consolidation Submodel

3) Degree of intimate contact as a function of time.
4) Time required for complete intimate contact.
5) Degree of autohesion as a function of time.
6) Time required for complete autohesion.
7) Degree of bonding as a function of time.
8) Time required for complete bonding.

Crystallinity Submodel

9) Temperature inside the material as a function of position and time during cooling.
10) Crystallinity inside the material as a function of position and time during cooling.
11) Crystallinity as a function of position inside the material after completion of the processing.
12) Average crystallinity of the material after processing.
13) Mechanical properties as a function of position inside the material.

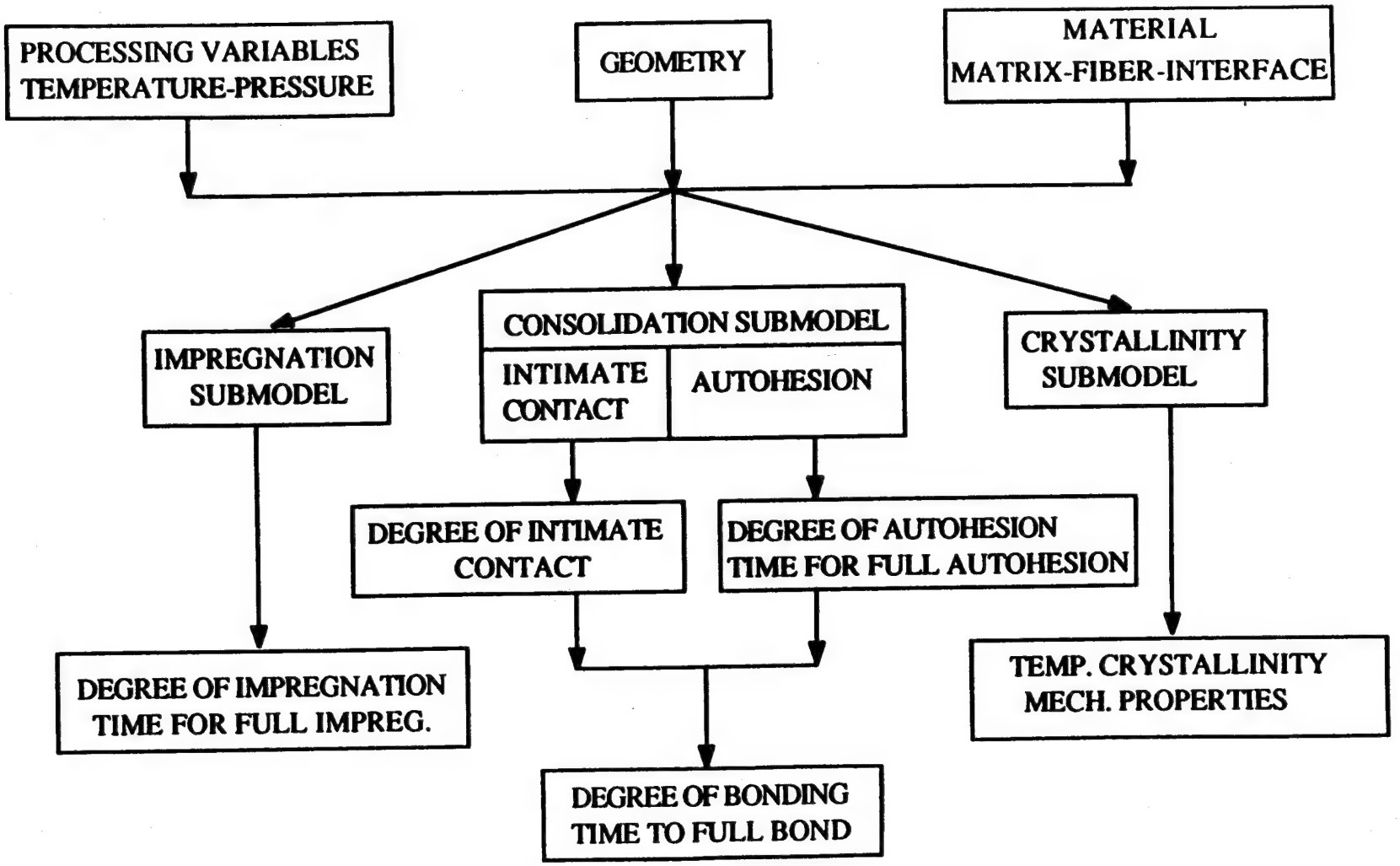

Figure 29. Illustration of the output of the thermoplastic processing model.

Section VI

MECHANICAL PROPERTIES

The mechanical properties of thermoplastic matrix composites can be related directly to the crystallinity of the polymer. Thus, once the variations of the mechanical properties with the crystallinity are established by tests, the mechanical properties resulting from a given cooling rate can simply be determined from the model, as follows. First the crystallinity is calculated by the model. Second, the mechanical property is calculated from the known crystallinity—property relationship. Mechanical properties of PEEK 150P polymer and APC-2 composite as functions of crystallinity were measured during this investigations. These tests and the results are described in the following sections (Sections VII and VIII).

Section VII

MECHANICAL PROPERTIES—TEST METHODS

The test specimens were cut out of plates manufactured by the procedures described below.

Manufacturing PEEK 150P

The PEEK 150P plates were made by placing the polymer, in powder form, in an aluminum mold. Two molds were used; one was $10 \times 7 \times 1/2$ inch, and the other was $6 \times 1\frac{3}{4} \times 0.2$ inch (Figures 30 and 31). The first mold was used to achieve crystallinities above 25 percent. The second mold was used to make plates with lower crystallinity.

The 10-inch mold consisted of a base and a cover, as shown in Figure 30. The PEEK 150P powder was poured into the mold. Then, with the cover removed, the mold was placed into an oven and heated to 750°F. This temperature was chosen because local order has been reported to remain in the PEEK melt unless the polymer is heated above its equilibrium melting temperature [17]. Blundell and Osborn estimated this temperature to be 743°F [18]. It is very difficult to achieve low crystallinity if the polymer is melted at too low a temperature.

The mold was kept at this temperature for two hours to allow air and vapor bubbles to escape from the polymer. The cover was placed on top of the polymer melt and the mold was kept at 750°F for an additional 15 minutes. The polymer was then cooled to room temperature by blowing air past the mold. The cooling rate was controlled by regulating the air flow rate. During cooling, the temperature was monitored by a Type J thermocouple located in the center of the polymer plate. Because of the long time at high temperature, the top surface of the PEEK plate was covered with a black film, presumably degraded PEEK. This film was removed by sanding before further processing. The bottom surface was also

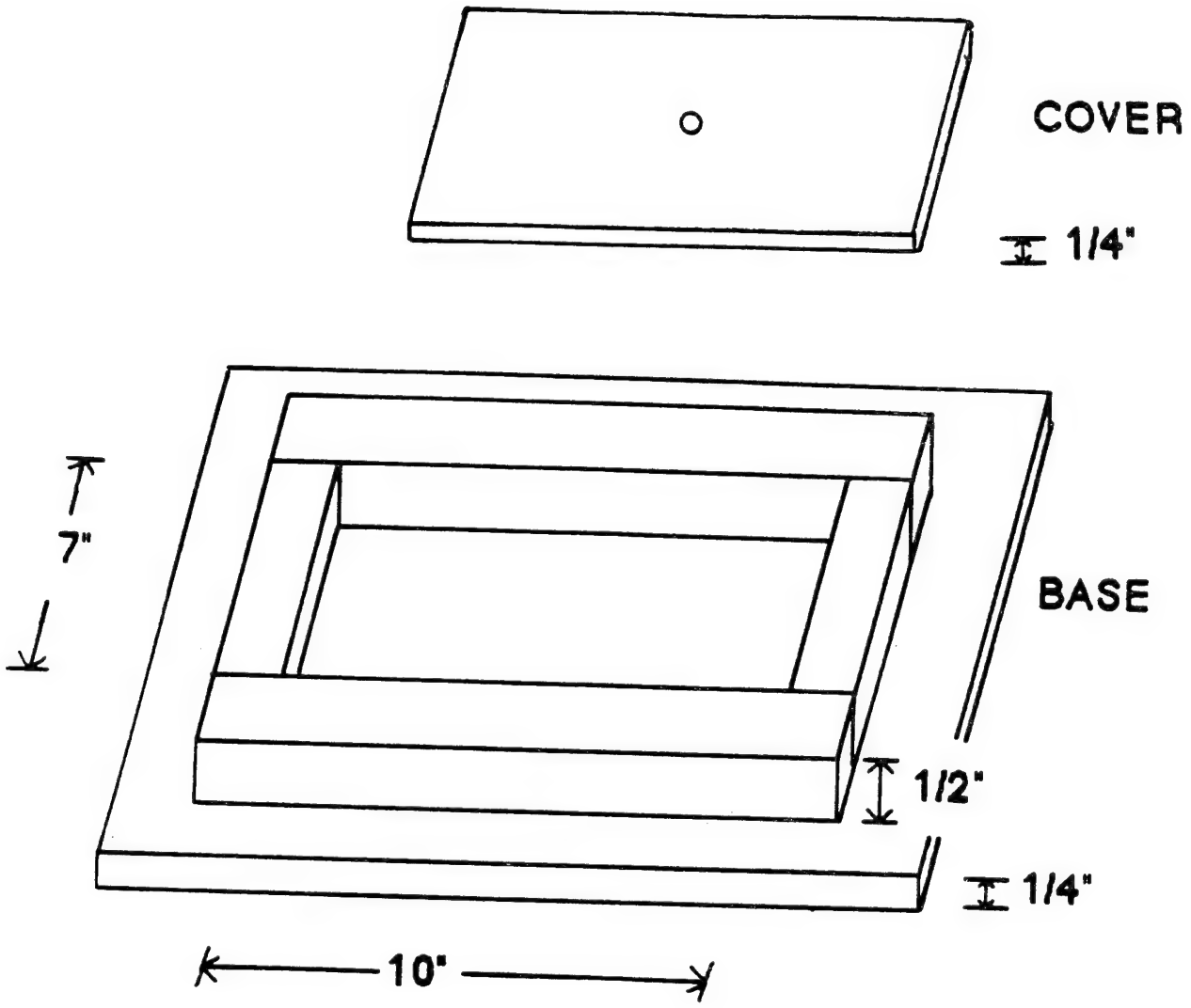

Figure 30. Mold used for preparing PEEK 150P specimens having crystallinities above 25 percent.

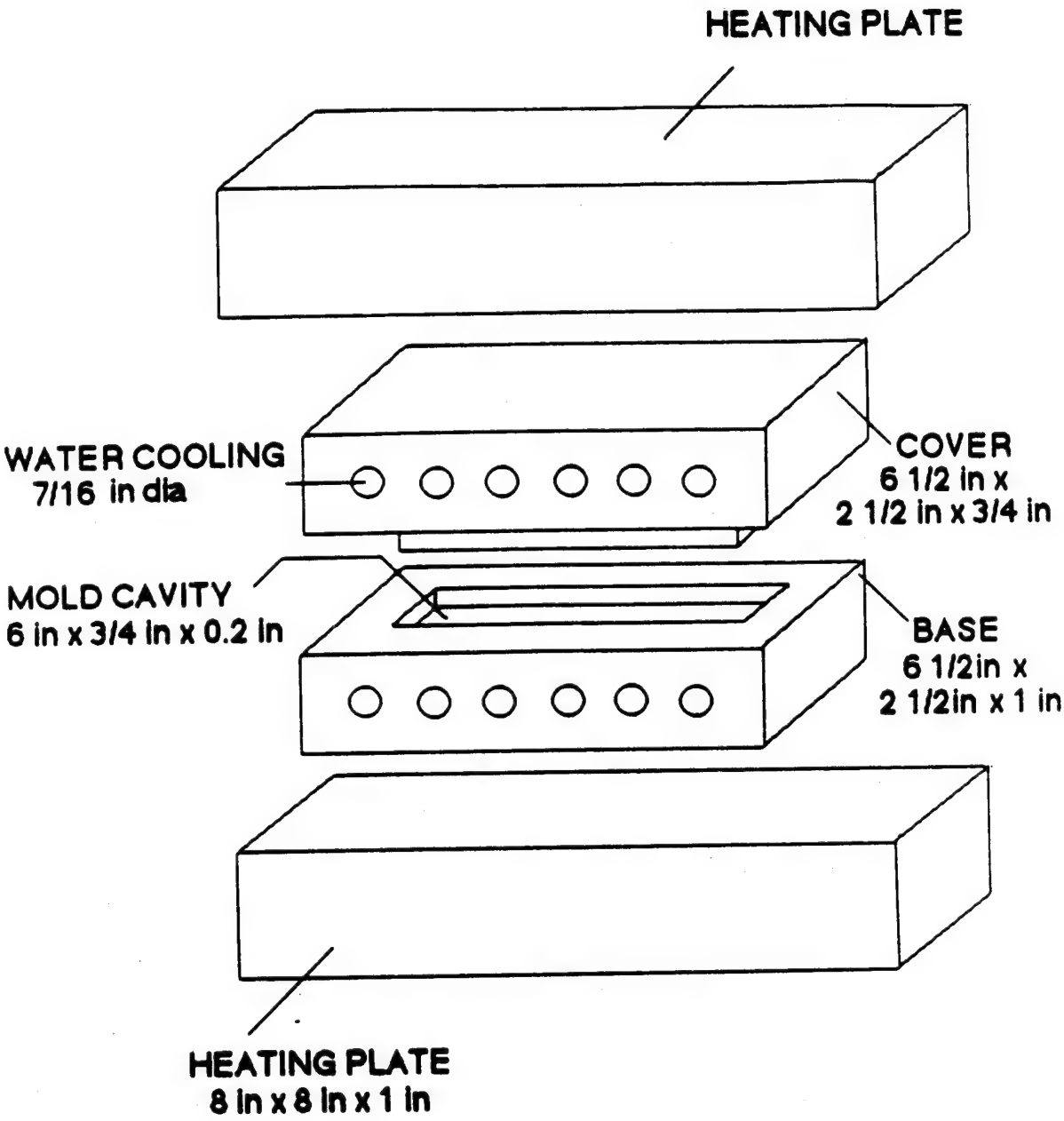

Figure 31. Mold used for preparing specimens of less than 20 percent crystallinity.

sanded away because it contained many voids. The interiors of the plates were virtually free of voids.

The 6-inch mold was provided with heaters as well as with built-in cooling channels (Figure 31). Details of this apparatus were described elsewhere [19] and are not repeated here. Only the essential features of the mold are given below. Six 7/16 inch diameter holes were provided in the top and the base of the mold. Cold water could be passed through these holes to provide rapid cooling. The cooling rates were adjusted by regulating the water flow up to 30 gallons per minute. Heating plates, containing 1500-watt cartridge heaters, were placed above and below the mold. The heating plate-mold assembly could be placed into a press which could exert a pressure on the material inside the mold—polymer or composite—during the entire manufacturing process, i.e., during heating and cooling.

Prior to processing in the 6-inch mold, the PEEK 150P powder was dried in an oven at 300°F for three hours. The mold was then filled with the powder to a depth of about 0.15 inch. The cover was placed on the mold and the mold was inserted into the press. The temperature of the mold was raised to 390°F under a pressure of 1500 psig. After 5 minutes, PEEK 150P powder was added to increase the thickness of the plate. With the cover in place the mold was remounted in the press. A pressure of 1500 psig at 390°F was again applied for 5 minutes. Then the pressure was removed and the mold temperature was raised to 750°F and held for 20 minutes without pressure being applied. The data of Lee and Porter [20] and Ma et al. [21] suggest that the time at high temperature was not long enough for significant degradation to occur in the polymer. At the end of 20 minutes the heaters were turned off, and insulating plates were inserted between the heating plates and the mold. The pressure was raised to 300 psig and the cooling water flow was started. The mold temperature dropped to room temperature in 5 to 10 seconds.

During the entire manufacturing process the temperature was monitored by an Omega Type *J* subminiature thermocouple mounted on the inside center of the base of the mold.

Manufacturing APC-2

The APC-2 composite plates used in this study were provided by ICI and the Swedish

National Defense Institute. These plates were 0.05 and 0.2 inch thick (8 and 34 plies) and contained unidirectional AS4 graphite fibers. Some of the test specimens were cut directly from these plates. In addition, sections of the plates were reprocessed in the 6 inch mold described above to obtain test specimens with lower levels of crystallinity. The procedure was essentailly the same as that used for the PEEK 150P polymer. The mold was placed into the press, a pressure of 200 psig was applied, and the temperature was raised to 750°F in 20 to 25 minutes. The temperature was kept at 750°F and the pressure at 200 psig for 10 minutes. Again, this short time at high temperature is not expected to allow the matrix to degrade significantly. The heaters and the pressure were then turned off and insulating plates were inserted between the heating plates and the mold; the pressure (200 psig) was reapplied, the water was turned on, and the plates were cooled to room temperature within 3 to 10 seconds.

Annealing PEEK 150P and APC-2

Some of the PEEK 150P polymer and APC-2 composite plates were annealed as follows. Plates were processed in the 6-inch mold using a high cooling rate, resulting in plates with low (below 20 percent) crystallinities. After the plate was cooled to room temperature the mold was reheated in 20 to 25 minutes to 480°F [18]. During this reheat no pressure was applied for the PEEK 150P polymer and 200 psig was applied for the composite. Once 480°F was reached, the temperature was kept at this level for 60 minutes. The mold was then cooled to room temperature.

Differential Scanning Calorimetry and X-ray Inspection

The crystallinities of polymer and composite samples were determined using differential scanning calorimetry (DSC) and the peak area calculation method [22]. Although for PEEK of low crystallinity the density gradient technique is more accurate than DSC [23], the presence of voids in composites makes density measurements impractical for APC-2. Therefore, DSC was used in this study.

A small sample taken from the plate (~10 mg) was enclosed in an aluminum sample pan and placed into the DSC cell. The heat flow in the cell as a function of temperature

was measured at a constant heating rate of 36°F/minute. The crystallinity was determined from the expression

$$c = \frac{H_T}{H_{\text{ULT}}} \tag{54}$$

where H_T is the net amount of heat absorbed on heating from the glass transition temperature (293°F) to 720°F as measured by the DSC. H_{ULT}, the ultimate heat of crystallization of 100 percent crystalline polymer, was taken to be 130 J/g [18].

In evaluating the crystallinities of the APC-2 composite, adjustments were made for the fiber content using the expression

$$c = \left[(c)_{\text{measured}}\right] / (WP) \tag{55}$$

where WP is the weight percent of the polymer in the composite. Since the density of the polymer depends on the crystallinity, an iterative procedure was used to calculate the weight percent polymer in the composite. This procedure was based on a nominal fiber volume fraction of 0.59.

The measured crystallinities versus cooling rates are given in the next section (Results). It is noted here that the crystallinities as a function of cooling rate of PEEK 150P measured in this study by DSC agree reasonably well with those obtained by Velisaris and Seferies [24] for PEEK 450P using the density gradient technique (Figure 32). The differences in crystallinities at high cooling rates may be due to differences in the material tested or differences in the measuring techniques.

In addition to differential scanning calorimetry, the crystallinities of some PEEK 150P plates were determined by wide-angle X-ray diffraction using a Picker diffractometer with copper K_α radiation. The scans were analyzed using a method discussed by Young [25] and applied to PEEK by Blundell and Osborn [18]. A straight line was drawn on the diffraction scan between 2θ values of 10° and 36° to subtract background radiation. (θ is the angle of incidence of the incoming X-ray beam.) The area under the diffraction curve and above this line was then divided into the crystalline and amorphous peaks, as illustrated in Figure 35. The ratio of the area of the crystalline peak to the area of the amorphous peak equals the weight ratio of crystalline to amorphous material. The crystallinities measured by X-ray

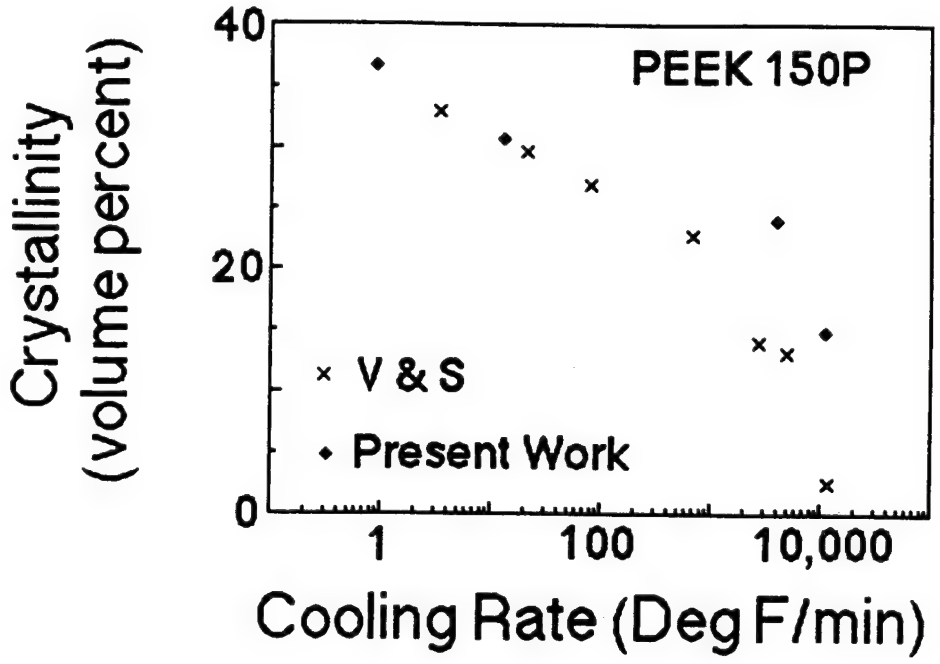

Figure 32. Crystallinity of PEEK as a function of cooling rate. Data of Velisaris and Seferis [24] for PEEK 450P and data from the present work for PEEK 150P.

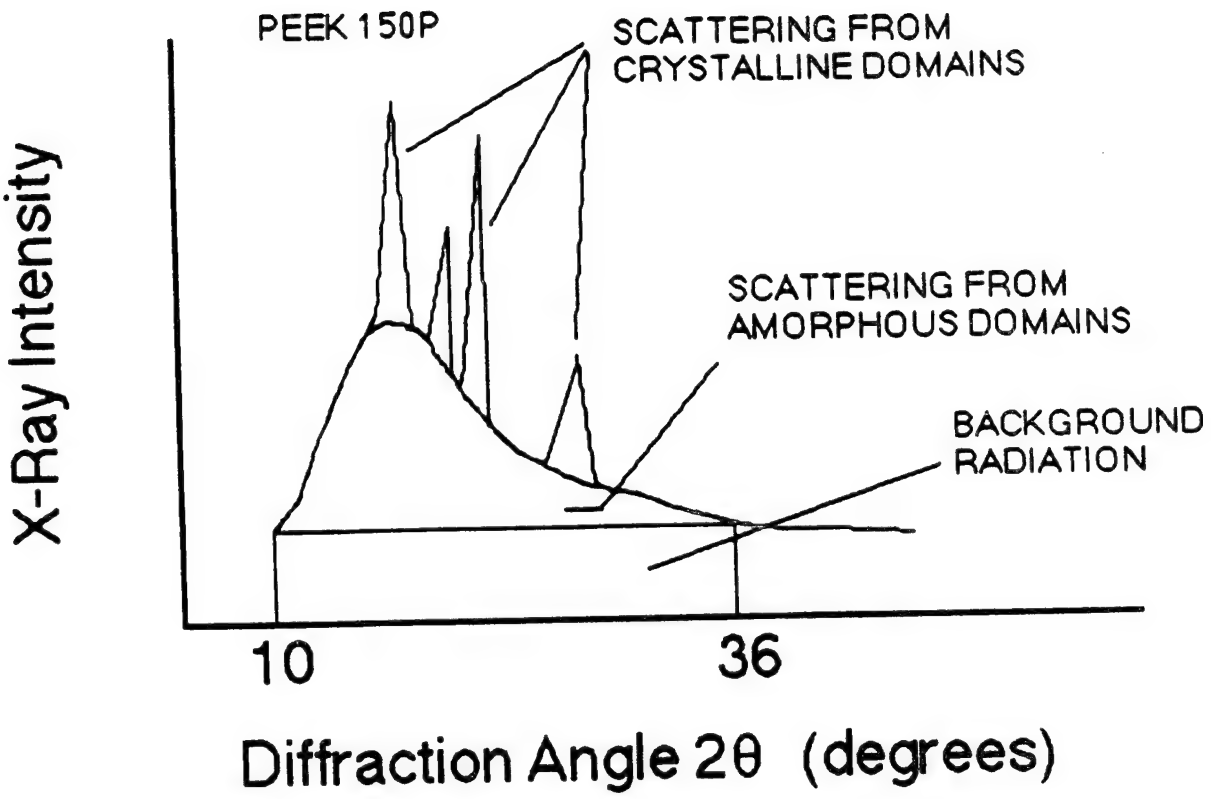

Figure 33. A typical X-ray scan of semicrystalline PEEK 150P, showing the background radiation and the scattering from crystalline and from amorphous domains in the sample.

diffraction and by DSC agree closely, both for specimens processed by cooling only and for annealed specimens (Figure 34).

It is recognized that the crystallinity may vary across the plate. In order to estimate the nonuniformities in crystallinities, the crystallinities across a 0.2 inch thick APC-2 plate were calculated for "low" cooling rates, using the method described in Reference 26. The results, given in Figure 35, show that the crystallinities are very uniform across the plates. Hence, for low cooling rates nonuniformities in crystallinity are not expected to affect significantly the properties measured in this investigation. At "fast" cooling rates there might be a crystallinity gradient across the plate. For example, DSC measurements on 0.06 inch thick PEEK 150P plates, cooled at 11,000°F/min, showed that the crystallinity varied from 16 percent at the surface to 23 percent in the center. Similar variations were observed by Velisaris and Seferis [24] in 0.15 inch thick PEEK 450P plates cooled at 50°F/min.

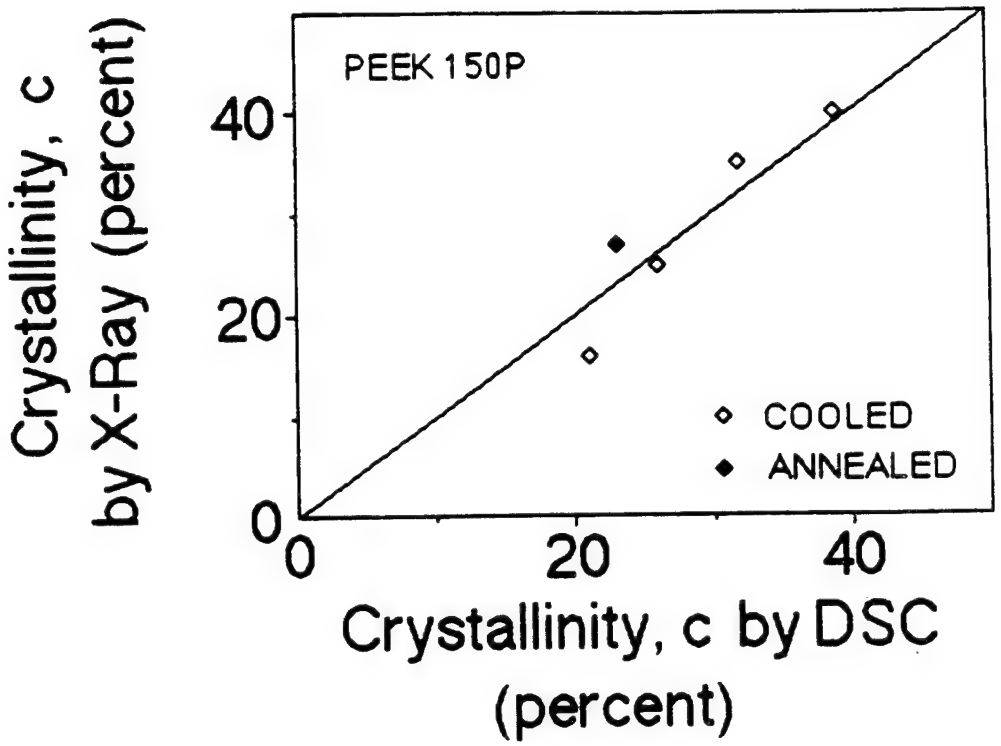

Figure 34. A comparison of the crystallinities of PEEK 150P as measured by DSC and by X ray.

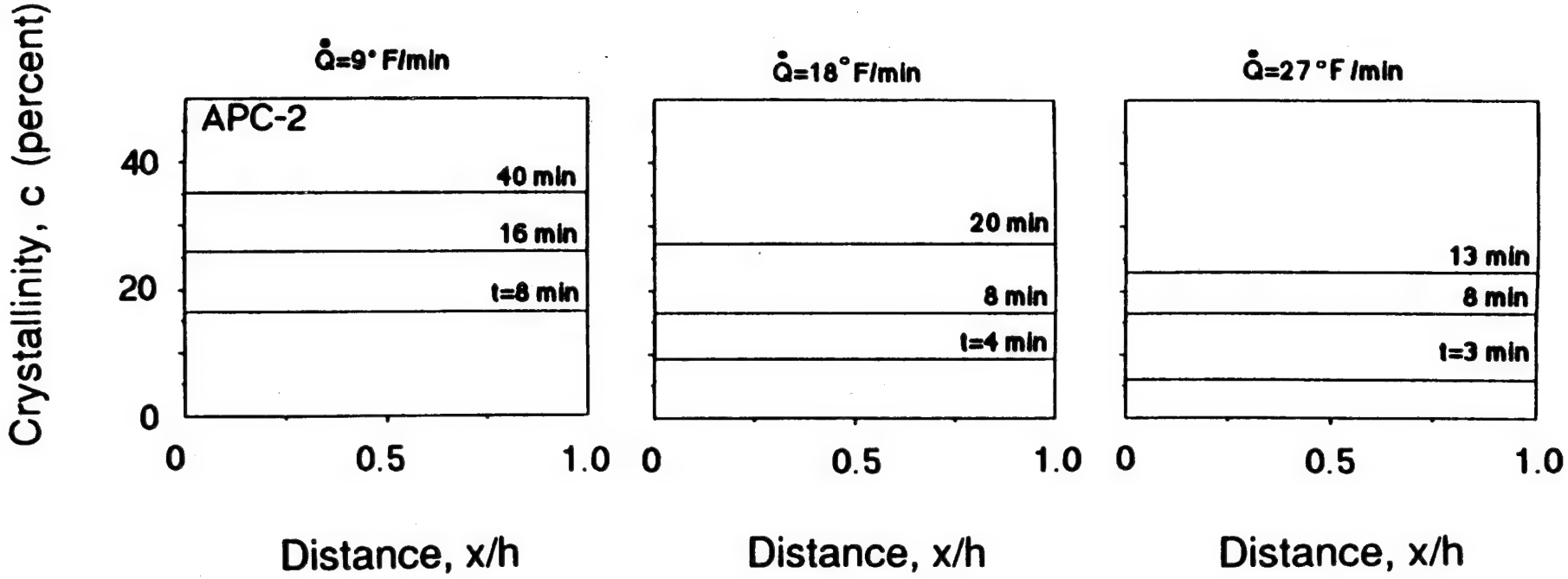

Figure 35. Calculated distributions of crystallinity in thick APC-2 plates at different cooling rates $\dot{Q}$.

Section VIII

MECHANICAL PROPERTIES—RESULTS

Tests were performed to relate the mechanical properties of PEEK 150P polymer and APC-2 composite to the crystallinity of the polymer. The results of the tests are summarized below. It is emphasized that these results are meant primarily to aid in engineering analyses. No attempt has yet been made to generate data of sufficient accuracy for a study of the detailed molecular processes and morphologies involved.

PEEK 150P Polymer

The PEEK 150P polymer test specimens were cut with a band saw from plates made by the procedures described in the previous section. Six types of mechanical properties were measured at different crystallinities: tensile, compressive, and shear strengths, tensile and shear moduli, and mode I fracture toughness.

The tensile properties were measured with 6-in long (1/4 inch by 1/10 inch) dog-bone specimens (Figure 36). Data were taken at a crosshead speed of 0.2 inch/minute. The moduli were determined from strains measured with a 1 inch gauge length extensometer. The results are presented in Table 6 and Figure 37, where each point is the average of at least four tests. The tensile strengths S_t and tensile moduli E_t of specimens prepared by cooling only can be fitted by the expressions

$$S_t = 8.2 + 0.17\ c \tag{56}$$

$$E_t = 404 + 4.0\ c + 0.075\ c^2 \tag{57}$$

where c is the crystallinity in percent. Jones et al. [27] reported a yield strength of 15.1 ksi for PEEK of unspecified grade and crystallinity. This value is within the range of the tensile strengths found in the current work (Table 6).

The shear properties of PEEK 150P were determined by the Iosipescu method [35]. The geometry of the test specimens is shown in Figure 38. The tests were performed at a

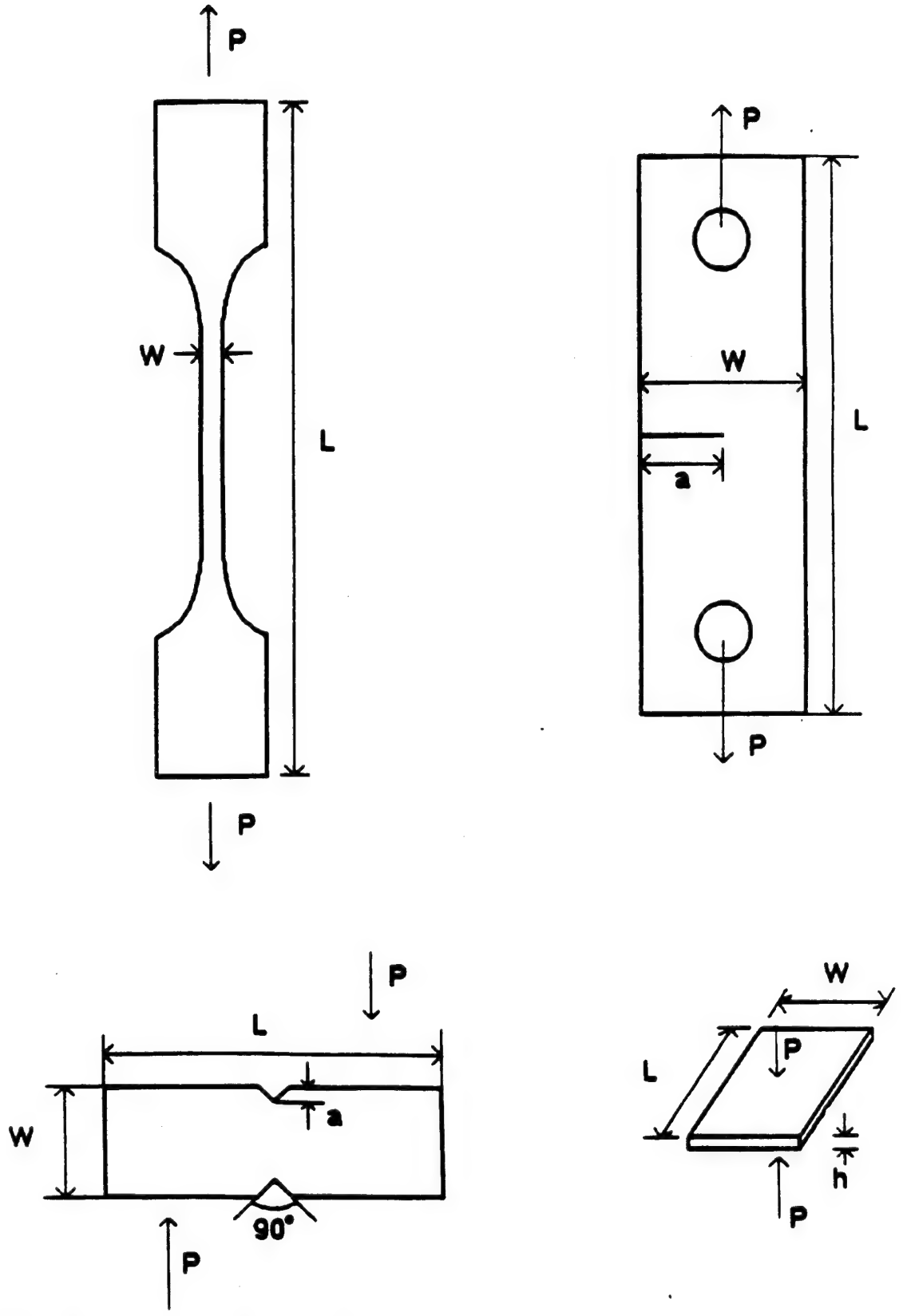

Figure 36. Geometries of PEEK 150P test specimens. The specimen dimensions are specified in Table 5.

Table 5

GEOMETRIES OF THE TEST SPECIMENS

Specimen	Length L (in)	Width w (in)	Thickness h (in)	Notch Length (in)	Remarks
Tensile	6	1/4	1/10	–	PEEK150P
Shear	3	3/4	1/10	0.15	PEEK150P
Compressive	3/8	3/8	$\approx$1/10	–	PEEK150P
Single edge notched fracture	5	$1\frac{1}{2}$	0.06–0.15	3/4	PEEK150P
Edge notched flexure	4	3/4	0.2	1	APC-2
Center notched	6	$1\frac{1}{8}$	0.05	$\approx$1/8	APC-2
Center notched (off axis)	6	$1\frac{1}{8}$	0.05	$a \sin\theta = \frac{1}{8}$ –	APC-2
Rail shear	6	6	0.05	1/2	APC-2

Table 6

MEASURED PROPERTIES OF PEEK 150P

Average Cooling Rate °F/min.	Crystallinity c percent	Tensile Strength (ksi)	Tensile Modulus (ksi)	Compressive Strength (ksi)	Shear Strength (ksi)	Shear Modulus (ksi)	Apparent Fracture Toughness (ksi $\sqrt{in}$)
11,000	16	10.5	510	22	6.2	175	10.5
4,000	26	13.4	520	24	9.4	165	5.4
13	33	14.1	640	25	10.4	195	3.3
0.9	39	14.5	670	27.5	10.3	205	2.6
11,000 + annealed for 1 hr. at 480°F	27	16.5	630	33	9.2	200	5.6

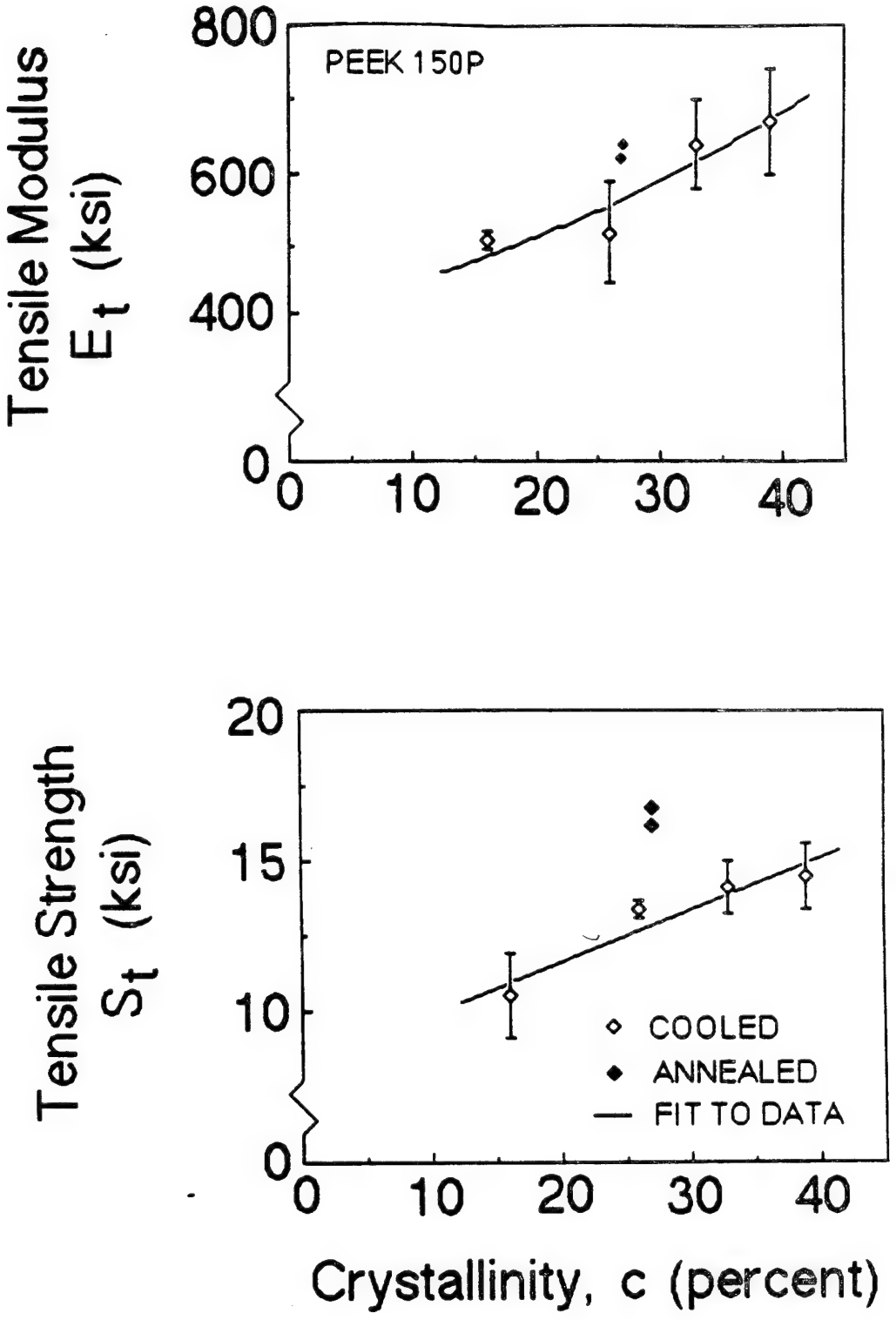

Figure 37. Tensile properties of PEEK 150P as functions of crystallinity. The error bars represent the standard deviation of the data.

loading rate of 0.24 inch/minute. The moduli were evaluated using strain gauges attached to the specimens. The results are given in Table 6 and Figure 38, where each point is the average of four measurements. The shear strength S_s and modulus E_s data of specimens prepared by cooling only were fitted by the expressions

$$S_s = 4.9 + 0.10\ c + 0.0015\ c^2 \tag{58}$$

$$E_s = 140 + 1.59\ c \tag{59}$$

where again, c is in percent. The foregoing data show that the strength and stiffness in both tension and shear increase with crystallinity. The likeliest reason for the rise in modulus is the high stiffness of the crystal lattice [29].

The strength of PEEK 150P in compression was measured using 3/8 inch square by approximately 1/10 inch thick specimens (Figure 36). The specimens were compressed between two plates at a rate of 0.2 inch/minute. The general form of the load versus deflection curves is shown in Figure 39. As this figure illustrates, it is difficult to define a unique compression strength. Therefore, the compression strength was defined as the point where the slopes of the first two adjacent segments intersect. The compression strengths thus obtained are presented in Table 6 and Figure 40. In this figure and table each point is the average of at least five data. The compression strength S_c data in Figure 39 for specimens prepared by cooling only can be represented by the expression

$$S_c = 18 + 0.22\ c \tag{60}$$

where c is in percent.

It is seen that the strength in compression changes very little with crystallinity for specimens prepared by cooling only. However, due to the highly nonlinear behavior of the material during compression (Figure 39), these data must be interpreted with caution. In fact, the shape of the load-deflection curves suggests that some change in crystal structure occurs at the point where the curve bends over sharply. X-ray scans of compressed specimens did indeed reveal a considerable reduction in crystallinity after the specimen was loaded significantly past the deflection point. Specimens of 16 percent crystallinity before compression

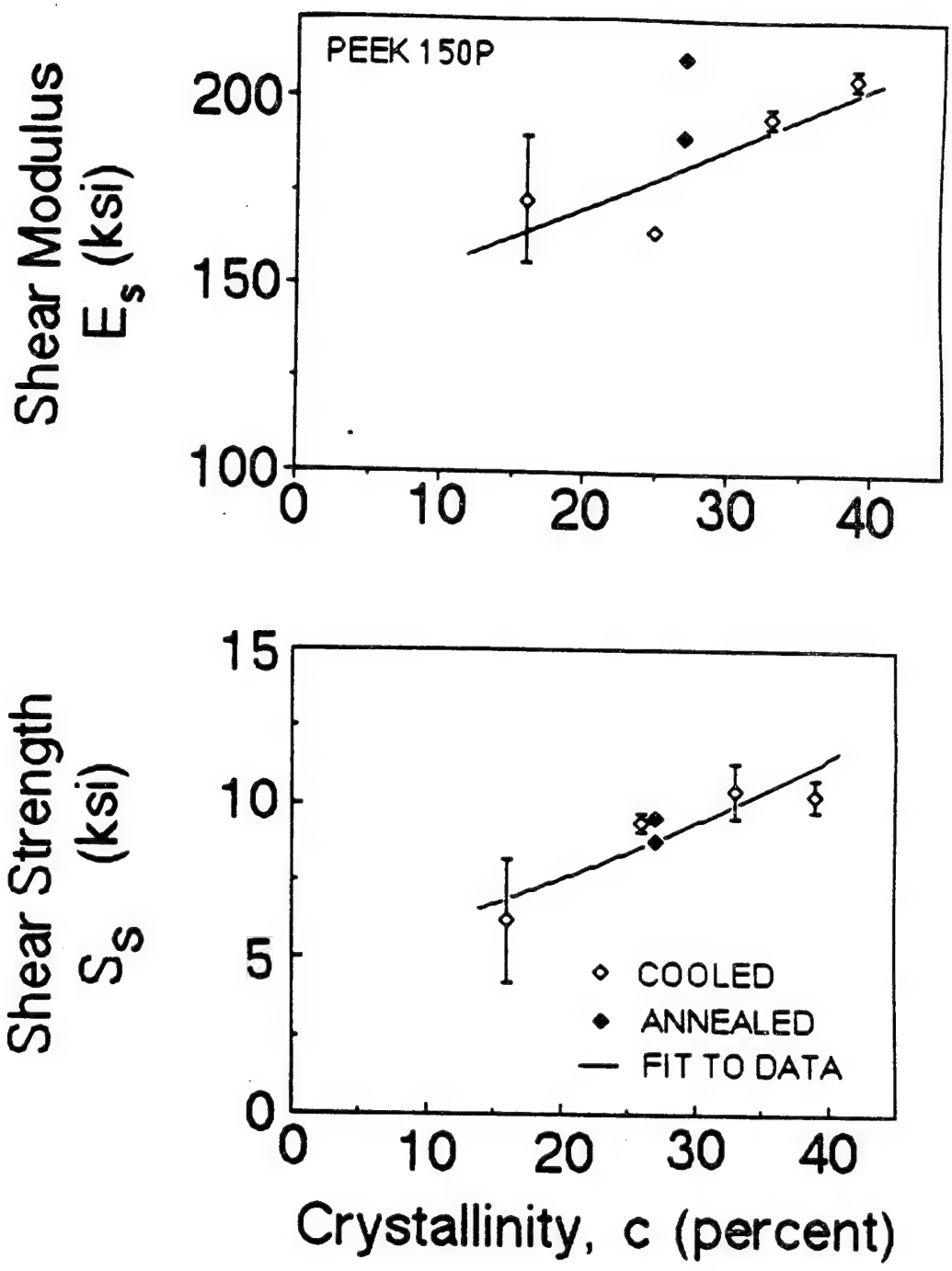

Figure 38. Shear properties of PEEK 150P as functions of crystallinity. The error bars represent the standard deviation of the data.

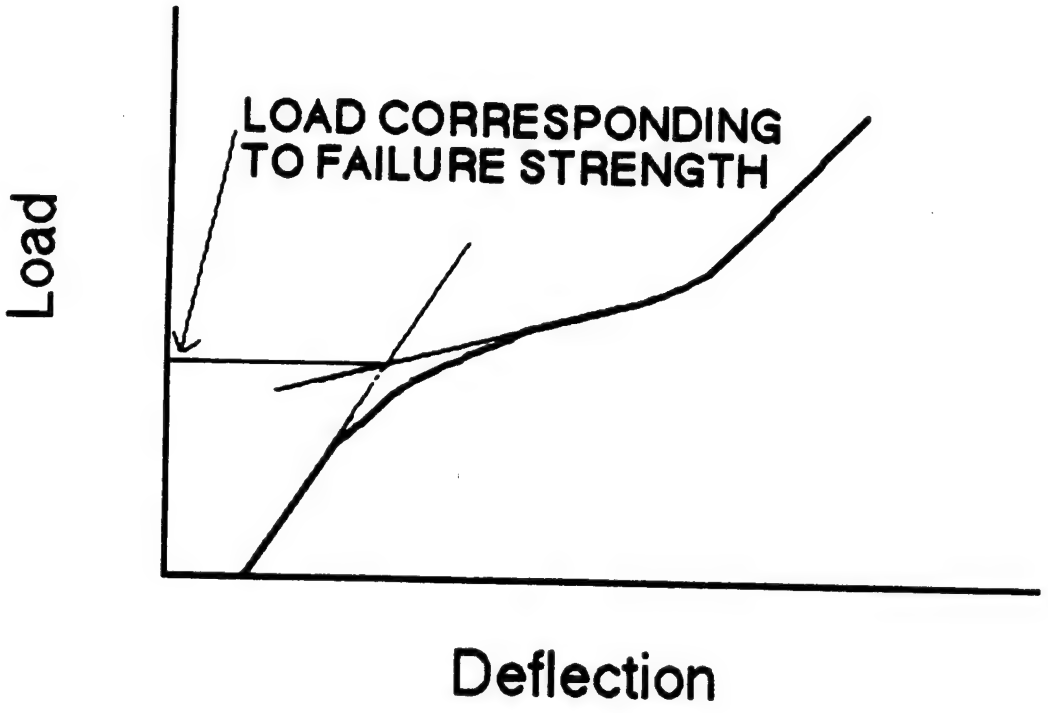

Figure 39. A typical load-deflection curve during compression tests of PEEK 150P.

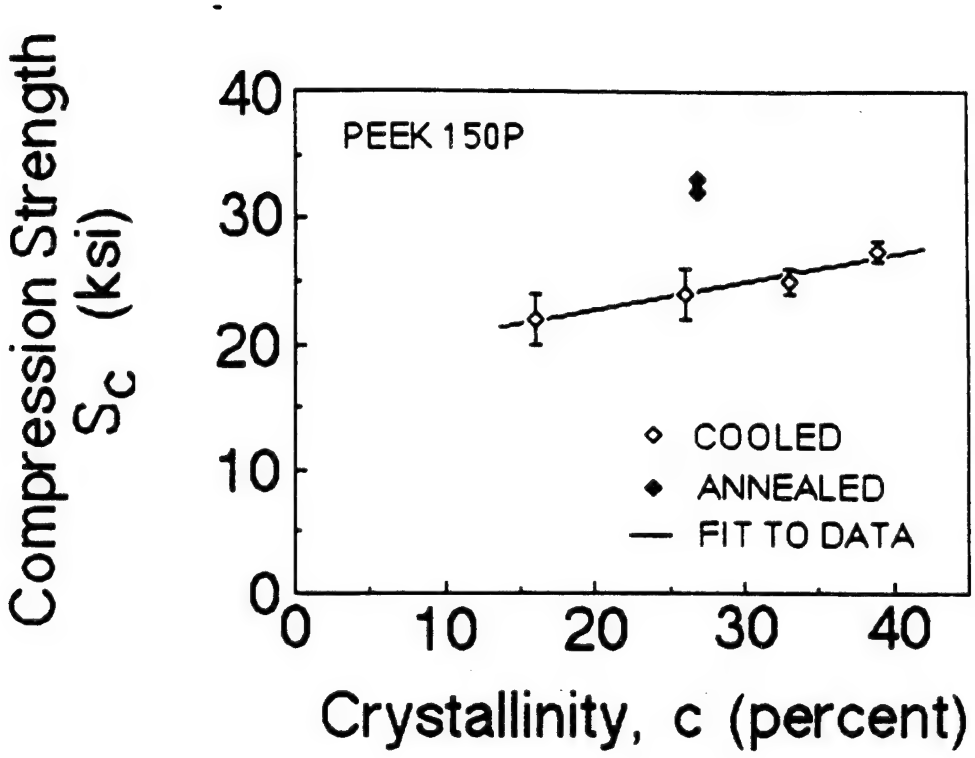

Figure 40. Strength in compression of PEEK 150P as a function of crystallinity. The error bars represent the standard deviation of the data.

were less than 5 percent crystalline thereafter, while specimens at 27 percent crystallinity before compression were afterwards only 16 percent crystalline.

Finally, the mode I fracture toughness of PEEK 150P at various degrees of crystallinity was measured using single edge notched specimens (Figure 36) pulled to failure at 0.2 inch per minute. A fracture toughness K is calculated by [30]

$$K = \frac{PY\sqrt{a}}{hw} \tag{61}$$

where P is the failure load in lbf, a is the initial crack length in inches, h is the specimen thickness in inches, and w is the specimen width in inches. Y is the dimensionless finite width correction factor computed by

$$Y = 1.99 - 0.41\left(\frac{a}{w}\right) + 18.7\left(\frac{a}{w}\right)^2 - 38.48\left(\frac{a}{w}\right)^3 + 53.85\left(\frac{a}{w}\right)^4 \tag{62}$$

If the test specimen is in plane strain, the measured fracture toughness K is the actual fracture toughness K_{IC}; if plane strain conditions are not met during the test then K is an apparent fracture toughness symbolized by K_Q.

The plane strain condition is met if the ratio R is less than unity [30]

$$R \equiv \frac{K}{S_t\sqrt{\frac{h}{2.5}}} \tag{63}$$

As can be seen from Table 7, only specimens of 33 and 39 percent crystallinity were in plane strain; therefore, only at these crystallinities are the measured toughnesses for PEEK 150P equal to K_{IC}. At lower crystallinities the measured fracture toughness is an apparent fracture toughness K_Q. A sufficient increase in specimen thickness would produce plane strain in these specimens. Unfortunately, it is extremely difficult, if not impossible, to make thick specimens of low and uniform crystallinity. The measured values of the fracture toughnesses are given in Table 6 and Figure 41, where each point is the average of at least five data. The decrease in toughness with increasing crystallinity is quite pronounced. A similar trend has been observed for isotactic polystyrene [31].

The fracture toughness data obtained in this study may be compared with the data of Karger-Kocsis and Friedrich [32], Klei [33], and Jones et al. [27]. Karger-Kocsis and Friedrich

Table 7

THE PLANE STRAIN CRITERION
FOR FRACTURE TOUGHNESS TESTING OF PEEK 150P

Crystallinity c (percent)	Measured Fracture Toughness K $(ksi\sqrt{in})$	Tensile Strength $S_t(ksi)$	Thickness h (inches)	R	Remarks
16	10.4	10.5	0.06	6.4	$K = K_Q$
26	5.4	13.4	0.13	1.8	$K = K_Q$
27[a]	5.6	16.5	0.06	2.2	$K = K_Q$
33	3.3	14.1	0.15	0.96	$K = K_{IC}$
39	2.6	14.7	0.15	0.72	$K = K_{IC}$

[a]Annealed.

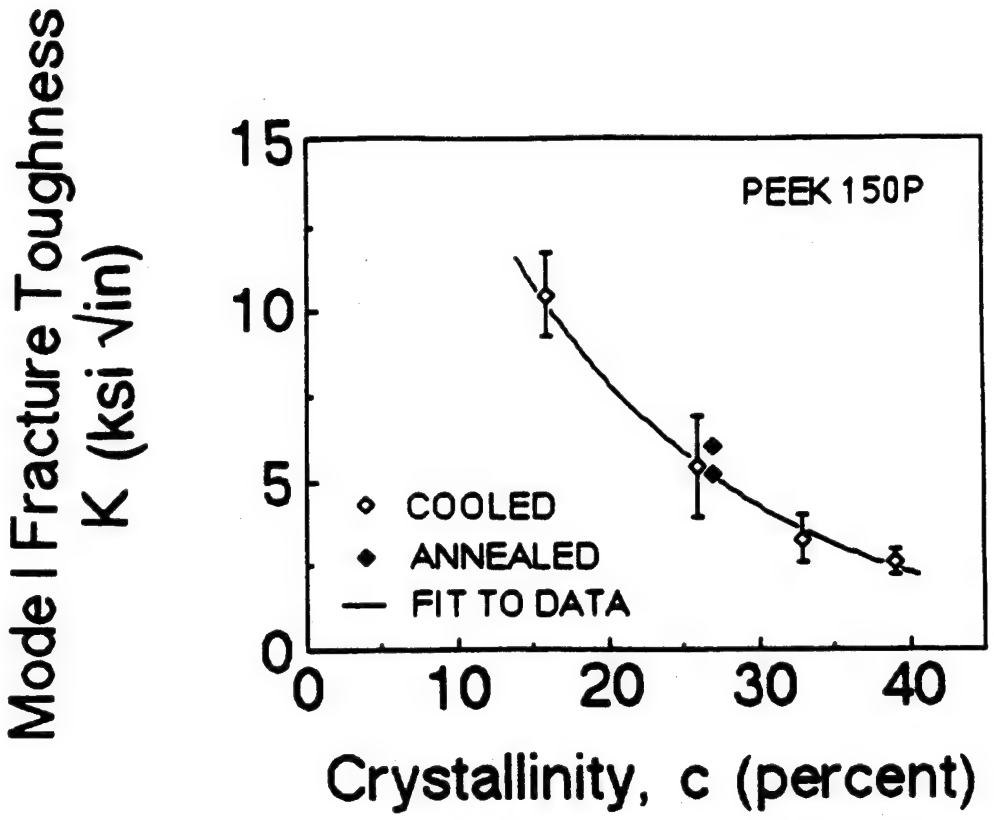

Figure 41. Measured Mode I fracture toughness of PEEK 150P as a function of crystallinity. The error bars represent the standard deviation of the data.

measured the fracture toughness of PEEK 450P of 24 and 30 percent crystallinities. At the lower crystallinity the fracture toughnesses were 6 to 6.3 ksi$\sqrt{\text{in}}$ (at 0.04 inch/min strain rate) and 0.9 to 2.1 ksi$\sqrt{\text{in}}$ (at 0.4 inch/min). At the higher crystallinity the fracture toughnesses were 5.2 and 0.8 ksi$\sqrt{\text{in}}$ at 0.04 and 0.4 inch/min strain rates, respectively. These fracture toughness values are similar to those obtained in the present investigation (see Table 6 and Figure 41).

Klei [33] reported the fracture toughnesses of PEEK at 21 to 25 percent crystallinity. The grade of PEEK used in the tests was unspecified. The toughnesses measured by Klei (11 to 15 ksi$\sqrt{\text{in}}$) are somewhat higher than those presented here (2.5 to 11 ksi$\sqrt{\text{in}}$). The differences in toughness obtained by Klei and by us may be due to differences in material, in testing speeds (0.02 inch/min versus 0.2 inch/min), or sample thickness (0.1 inch versus 0.15 inch).

Jones et al. [27] did not specify either the grade of PEEK or the crystallinity used in their tests. They measured the toughness of PEEK as 4.1 ksi$\sqrt{\text{in}}$ (at a testing speed of 3.9 inch/min), a value comparable to those presented here.

We measured the tensile, compressive, and shear properties and the fracture toughness for annealed as well as for cooled-only specimens. The results are included in Table 6 and in Figures 37, 38, 40, and 41. From these data, it appears that annealed specimens are stronger in both tension and compression than cooled-only specimens of comparable crystallinity. However, the shear strengths, the tensile and shear moduli, and the fracture toughnesses of annealed specimens are similar to those of cooled-only specimens of the same crystallinity.

APC-2

For APC-2 composite, the Mode I and Mode II fracture toughnesses (K_{IC} and K_{IIC}) and fracture energies (G_{IC} and G_{IIC}) as well as the mixed mode stress intensity factors (K_I and K_{II}) were determined for crystallinities ranging from 0 to 33 percent.

The Mode I fracture toughnesses were measured using center notched specimens, with the notch being parallel to the fibers and normal to the load (Figure 42). The notching procedure is given in [34]. Tensile load was applied at a crosshead speed of 0.07 inch/minute.

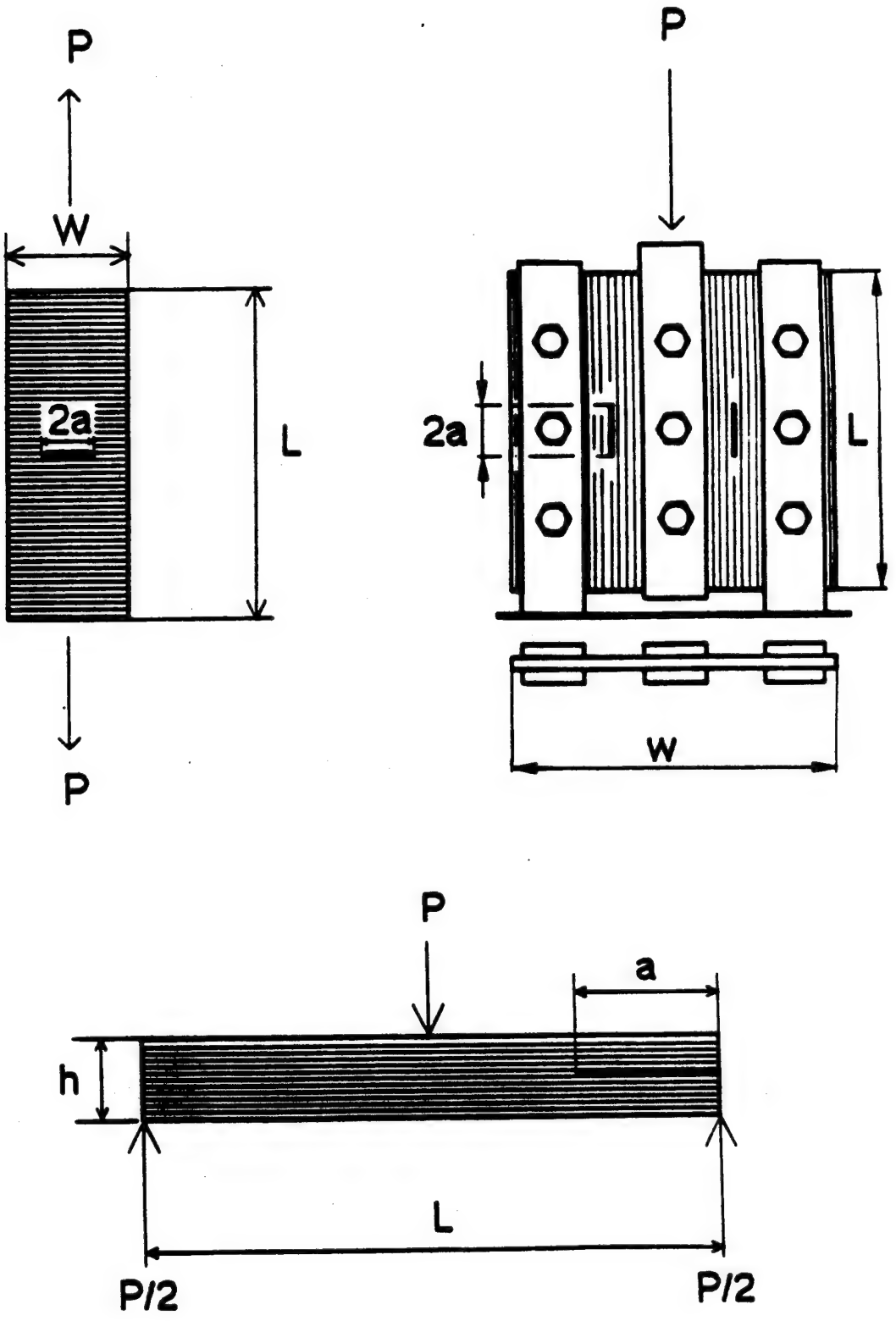

Figure 42. Geometries of APC-2 test specimens. The specimen dimensions are specified in Table 5. Top left: center notched (CN), top right: rail shear (RS), bottom: edge notched fracture.

The fracture toughness was calculated by the expression [35]

$$K_{IC} = \frac{PY\sqrt{a}}{hw} \tag{64}$$

where P is the load at which failure occurs and, as before, h and w are the thickness and the width of the specimen. $2a$ is the initial notch length. Y is the finite width correction factor defined as

$$Y = 1.77 + 0.227\left(\frac{2a}{w}\right) - 0.510\left(\frac{2a}{w}\right)^2 + 2.7\left(\frac{2a}{w}\right)^3 \tag{65}$$

From the known values of K_{IC}, the Mode I critical strain energy release rates G_{IC} (referred to here in short as the Mode I "fracture energies") were calculated by the formula [36]

$$G_{IC} = K_{IC}^2 \frac{1}{(2E_L E_T)^{1/2}} \left[\left(\frac{E_L}{E_T}\right)^{1/2} - \nu_{LT} + \frac{E_L}{2G_{LT}}\right]^{1/2} \tag{66}$$

where E_L and E_T are the longitudinal and transverse elastic ply moduli, G_{LT} is the shear ply modulus and ν_{LT} is the ply Poisson ratio. In the calculations E_L and ν_{LT} were taken to be constant [37] and having the values given in Table 8. The transverse and shear moduli and the Poisson ratio were estimated from the measured polymer properties given in Table 8 and the micromechanics formulae given in Table 9. The properties thus estimated are given in Table 10.

The Mode II fracture toughnesses were measured using either rail shear (RS) or edge notched fracture (ENF) specimens (Figure 42). The rail shear test was performed on specimens of high crystallinity. Edge notched fracture tests were used with specimens at low crystallinities because these specimens (processed in the 6-inch mold) were too small for the rail shear test.

For the rail shear specimens, load was applied at a rate of 0.03 inch/minute. The fracture toughness was calculated from the measured failure load P by [39]

$$K_{IIC} = \frac{P}{2hL}\sqrt{\pi(a)} \tag{67}$$

where h and L are the specimen thickness and length, and $2a$ is the initial notch length. Correction for finite width was not applied because such a correction was shown to be unnecessary for the type of specimens used in this study [39].

Table 8

PROPERTIES USED IN CALCULATING
THE ELASTIC PROPERTIES OF APC-2 GIVEN IN TABLE 10

Fiber	
Volume fraction, $v_f = 0.58$	measured
Poisson's ratio, $\nu_f = 0.27$	from [37]
Transverse modulus, $E_{Tf} = 2.32$ Msi	from [37]
Longitudinal shear modulus, $G_f = 1.2$ Msi	from [37]
Matrix	
Volume fraction, $v_m = 0.42$	measured
Matrix modulus, E_m	from Table 6
Stress Partitioning Parameters: $\eta_{LT} = 0.2$, $\eta_T = 0.5$.	from procedure in [37]
Composite	
Poisson's ratio, $\nu_{LT} = 0.28$	from [37]
Longitudinal modulus, $E_L = 19.4$ Msi	from [37]

Table 9

MICROMECHANIC EQUATIONS USED
IN CALCULATING ELASTIC PROPERTIES OF APC-2
(Tsai-Hahn [38])

Longitudinal Shear Modulus, G_{LT}	$\frac{1}{G_{LT}} = \frac{1}{v_f + \eta_{LT} v_m} \left(\frac{v_f}{G_f} + \frac{\eta_{LT} v_m}{G_m} \right)$
Transverse Tensile Modulus, E_T	$\frac{1}{E_T} = \frac{1}{v_f + \eta_T v_m} \left(\frac{v_f}{E_{Tf}} + \frac{\eta_T v_m}{E_m} \right)$
Poisson's Ratio of the Matrix, ν_m	$\nu_m = \frac{\nu_c - v_f \nu_f}{v_m}$
Shear Modulus of the Matrix, G_m	$G_m = \frac{E_m}{2(1+\nu_m)}$

E Tensile modulus

G Shear modulus

V Volume fraction

η Stress partitioning parameter in the Tsai-Hahn equations

ν Poisson's ratio

Subscripts

f Fiber

m Matrix

L Longitudinal direction

T Transverse direction

Table 10

ELASTIC PROPERTIES USED IN CALCULATING
THE FRACTURE ENERGY G_{IC}
AND FRACTURE TOUGHNESS K_{IIC} OF APC-2

Crystallinity c (percent)	Transverse modulus $E_T(Msi)$	Shear modulus $G_{LT}(Msi)$
0–20	1.19	0.71
25	1.21	0.72
28	1.29	0.74
33	1.37	0.78

E_T and G_{LT} were calculated using the equations in Table 9 and the data in Table 8.

Load was applied to the ENF specimens at the rate of 0.1 inch/minute. The fracture energy G_{IIC} was computed from the measured failure load P by the expression [40]

$$G_{IIC} = \frac{9a^2P^2C}{2w(2L^3 + 3a^3)} \tag{68}$$

Again, L, w, and a represent the length and width of the specimen and the initial notch length. C is the compliance due to bending and is the ratio of the measured deflection at the loading position divided by the load. The mode II fracture toughness K_{IIC} is related to the Mode II fracture energy G_{IIC} by [36]

$$K_{IIC} = \left(G_{IIC}\sqrt{2}E_L\right)^{1/2} \left\{ \left(\frac{E_L}{E_T}\right)^{1/2} - \nu_{LT} + \frac{E_L}{2G_{LT}} \right\}^{-1/4} \tag{69}$$

The meanings of the symbols are the same as for Equation 66. K_{IIC} values were calculated from this equation, with the moduli E_L, E_T, G_{LT} and the Poisson ratio ν_{LT} determined in the same manner as discussed above (see Equation 66).

The Mode I and Mode II fracture toughnesses and fracture energies as functions of crystallinity are presented in Table 11 and Figures 43 through 44. Each data in this table and figures is the average of at least three tests.

The following observations can be made from the data in Figures 43 and 44. First, the mode II fracture toughnesses obtained by rail shear and edge notched fracture specimen tests agree very closely. Second, at corresponding crystallinities, the fracture toughnesses obtained from specimens which were cooled only were nearly the same as the fracture toughnesses of specimens which were first cooled rapidly then heated ("annealed"). This observation suggests that neither the fracture toughness nor the fracture energy is sensitive to processing history, but depends mainly on the value of the crystallinity. Third, the fracture toughnesses and fracture energies decrease with increasing crystallinity.

The data in Figures 43 and 44 were fitted with curves, which can be described by the equations

$$K_{IC} = 4.3 - 0.007\,c - 0.001\,c^2 \quad \text{ksi}\sqrt{\text{in}} \tag{70}$$

$$K_{IIC} = 9.2 - 0.005\,c - 0.002\,c^2 \quad \text{ksi}\sqrt{\text{in}} \tag{71}$$

Table 11

FRACTURE PROPERTIES OF APC-2 AS A FUNCTION OF CRYSTALLINITY

Cooling rate (°F/min)	Crystallinity c (percent)	Fracture Toughness Mode I $K_{IC}(ksi\sqrt{in})$	Fracture Toughness Mode II $K_{IIC}(ksi\sqrt{in})$	Fracture Energy Mode I G_{IC} (lbf/in)	Fracture Energy Mode II G_{IIC} (lbf/in)
18000	0	4.3	9.2	11.5	12.1
6500	0	4.4	8.9	11.8	12.7
4300	14	4.3	9.0	11.3	12.3
1700 to 430°F 90 from 430°F	20	4.1	8.4	10.2	10.7
18000+ annealing for 60 min. at 480°F	25	3.3	8.3	6.7	10.3
72	28	3.4	8.1	6.8	9.7
27	33	3.2	6.8	5.6	6.7

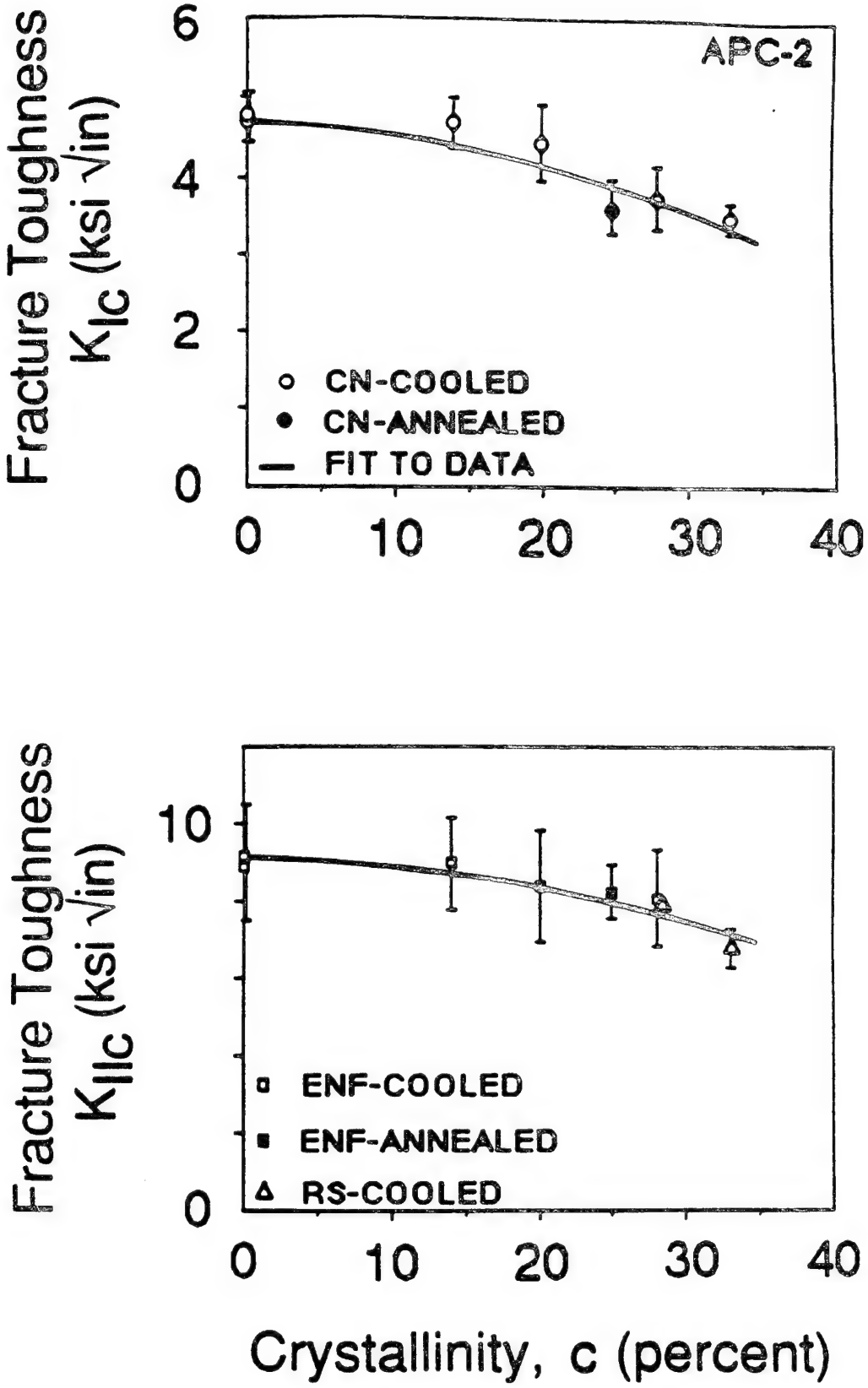

Figure 43. Mode I and Mode II fracture toughness of APC-2 as a function of crystallinity. The error bars represent the standard deviation of the data. CN = center notched, ENF = edge notched fracture, RS = rail shear specimen (see Figure 42).

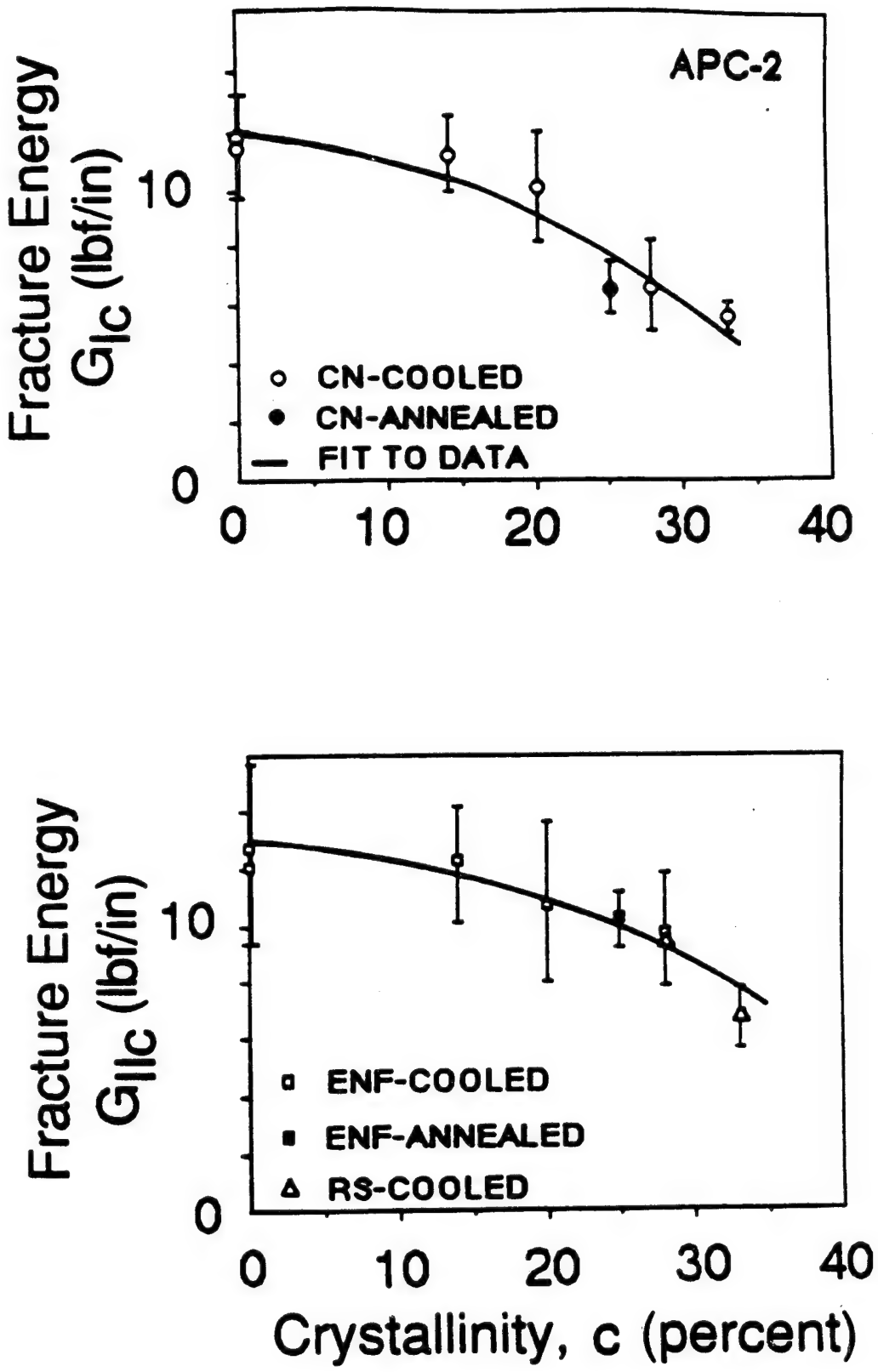

Figure 44. Mode I and Mode II fracture energy of APC-2 as a function of crystallinity. The error bars represent the standard deviation of the data. CN = center notched, ENF = edge notched fracture, RS = rail shear specimen (see Figure 42).

$$G_{IC} = 12.01 - 0.022\,c - 0.006\,c^2 \quad \text{lbf/in} \tag{72}$$

$$G_{IIC} = 12.78 - 0.024\,c - 0.004\,c^2 \quad \text{lbf/in} \tag{73}$$

where c is the degree of crystallinity in percent.

The Mode I fracture toughness obtained in this investigation can be compared to the value given by Donaldson [41], who measured the fracture toughness of APC-1. Donaldson's result of 3.4 ksi$\sqrt{\text{in}}$ is the same as our valve obtained at 28 percent crystallinity (see Table 11).

Mode I and Mode II fracture energies of APC-2 have previously been reported in References 42 through 45. Russel and Street [42], Smiley and Pipes [43] and Leach et al. [44] obtained G_{IC} values of 8.8, 9.1, and 13.8 to 16.5 lbf/in, respectively. These values are similar to those obtained during the course of this study (5.6 to 11.8 lbf/in, Table 11). Russell and Street [42] and Carlsson et al. [45] reported G_{IIC} values of 10.1 and 10.6 lbf/in, respectively. These values are also in the range of those values measured here (6.7 to 12.7 lbf/in, Table 11).

Finally, the stress intensity factors K_I and K_{II} were measured under mixed mode loading conditions, using specimens with crystallinities ranging from 0 to 33 percent. The test specimen is shown in Figure 45. Notches of length $2a$ were inserted parallel to the fibers. Specimens with fiber and notch angles of $\theta = 45$, 30, and 20 degrees were tested at a crosshead speed of 0.07 inch/minute. The stress intensity factors at the point of failure were calculated from the measured failure loads using the expressions [36]

$$K_I = \frac{P}{(w)(h)}\sqrt{\pi a}\sin^2\theta \tag{74}$$

$$K_{II} = \frac{P}{(w)(h)}\sqrt{\pi a}\sin\theta\cos\theta \tag{75}$$

No finite width correction factors were used, since none are known to us for off-axis center-notched specimens. The data are presented in Figure 46. Each point in this figure is the average of at least three measurements.

It has been suggested in the past that the mixed mode stress intensity factors for composites can be related by the equation [46]

$$\left(\frac{K_I}{K_{IC}}\right)^2 + \left(\frac{K_{II}}{K_{IIC}}\right)^2 = 1 \tag{76}$$

In Figure 46 the above equation was also included. As can be seen, the quadratic failure criterion represented by Equation 76 describes the data well over the entire range of crystallinities tested. This supports the observations made by previous investigators [34, 47] that the mixed mode fracture of thermoplastic composites is controlled by the total fracture energy.

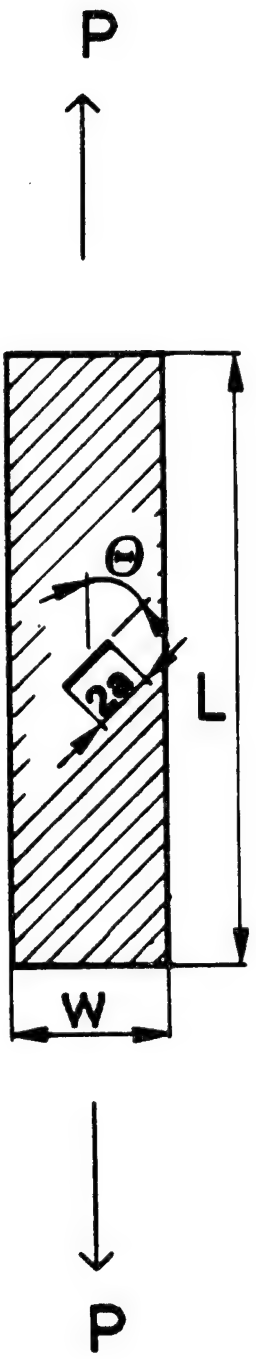

Figure 45. Geometry of mixed-mode fracture specimens of APC-2. The specimen dimensions are specified in Table 5.

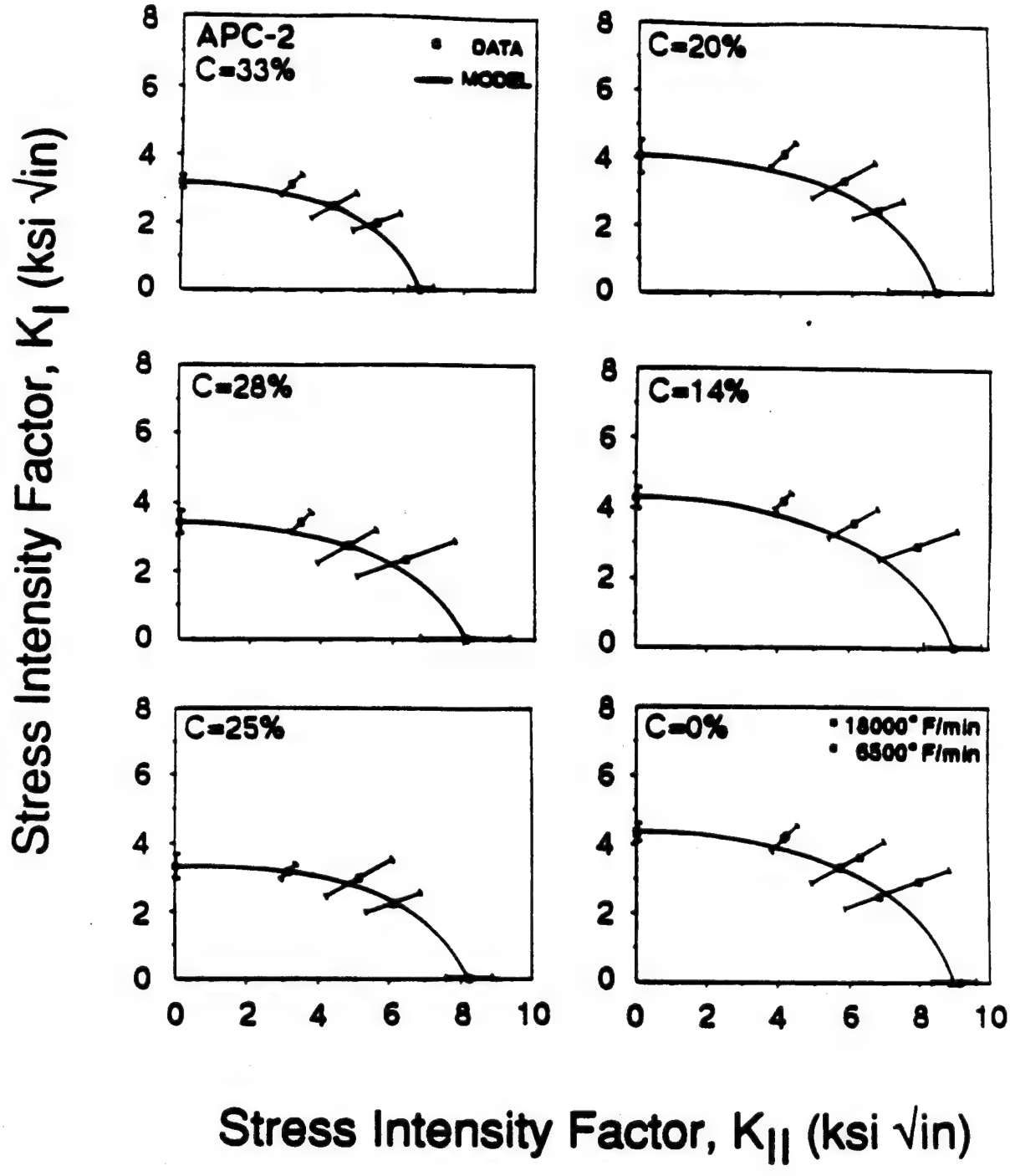

Figure 46. Mixed-mode fracture toughness of APC-2 as a function of crystallinity. The error bars represent the standard deviation of the data.

REFERENCES

1) Springer, G. S. "A Model of the Curing Process of Epoxy Matrix Composites," in *Progress in Science and Engineering of Composites,* (T. Hayashi, K. Kawaka, and S. Umekawa, eds.), Japan Society for Composite Materials, 1982, pp. 23–35.

2) Loos, A. C. and G. S. Springer. "Curing of Epoxy Matrix Composites," *Journal of Composite Materials, Vol. 17* (1983), pp. 135–169.

3) Campbell, F. C., A. L. Mallow, F. R. Muncaster, B. L. Boman, G. A. Blase. "Computer Aided Curing of Composites," Air Force Materials Laboratory Report, AFWAL-TR-86-4060, Wright Patterson Air Force Base, Ohio, 1986.

4) Calius, E. P. and G. S. Springer. "Modeling the Filament Winding of Composites," Proceedings of the Fifth International Conference on Composite Materials (W. C. Harrigan, Jr., J. Strife, and A. K. Dhingra, eds.), The Metallurigical Society, 1985, pp. 1071–1088.

5) Streeter, V. L. and E. B. Wylie. *Fluid Mechanics,* McGraw-Hill, New York, 1975.

6) Happel, J. "Viscous Flow Relative to Arrays of Cylinders," *AICHE Journal, Vol. 5* (1959), pp. 174–177.

7) Dara, P. H. and A. C. Loos. "Thermoplastic Matrix Composite Processing Model," Center for Composite Materials and Structures, Report CCMS-85-10, VPI-E-85-21, Virginia Polytechnic Institute and State University, Blacksburg, Virginia, 1985.

8) Wool, R. P. and K. M. O'Connor. "Theory of Crack Healing in Polymers," *Journal of Applied Physics, Vol. 52* (1981), pp. 5953–5963.

9) Wool, R. P. "Relations for Healing, Fracture, Self-Diffusion and Fatigue of Random Cool Polymers," *ACS Polymer Preprints, Vol. 23, No. 2* (1982), p. 62.

10) Jud, K., H. H. Kausch, and J. G. Williams. "Fracture Mechanics Studies of Crack Healing and Welding of Polymers," *Journal of Material Science, Vol. 16* (1981), pp. 204–210.

11) Eckert E.R.G. and R. M. Drake. *Heat and Mass Transfer,* McGraw-Hill, New York, 1975.

12) Springer, G. S. and S. W. Tsai. "Thermal Conductivities of Unidirectional Materials," *Journal of Composite Materials, Vol. 1* (1967), pp. 166–173.

13) Loos, A. C. and G. S. Springer. "Curing of Graphite Epoxy Composites," Air Force Materials Laboratory Report AFWAL-TR-83-4040, Wright Patterson Air Force Base, Ohio, 1983.

14) Lee, W. I., M. F. Talbott, G. S. Springer, and L. A. Berglund. "Effect of Cooling Rate on the Crystallinity and Mechanical Properties of Thermoplastic Composites," *Journal of Reinforced Plastics and Composites, Vol. 6* (1987), pp. 2–12.

15) Talbott, M. F., G. S. Springer, and L. A. Berglund. "The Effects of Crystallinity on the Mechanical Properties of PEEK Polymer and Graphite Fiber Reinforced PEEK," *Journal of Composite Materails, Vol. 21* (1987), pp.

16) Downs, R. J. and L. A. Berglund. "Apparatus for Preparing Thermoplastic Composites," *Journal of Reinforced Plastics and Composites, Vol. 6* (1987), pp. 89–99.

17) Nguyen, H. X. and H. Ishida. "Molecular Analysis of the Melting Behavior of Poly(aryl-ether-ether-ketone)," *Polymer, 27* (1986), pp. 1400–1405.

18) Blundell, D. J. and B. N. Osborn. "The Morphology of Poly(aryl-ether-ether-ketone)," *Polymer, 24* (1983), pp. 953–958.

19) Downs, R. J. and L. A. Berglund. "Apparatus for Preparing Thermoplastic Composites," *Journal of Reinforced Plastics and Composites, 6* (1987).

20) Lee, Y. and R. Porter. "Crystallization of Poly(etheretherketone) (PEEK) in Carbon Fiber Composites," *Polymer Engineering and Science, 26* (1986), pp. 633–639.

21) Ma, C.C.M., J. T. Hu, W. L. Lin, H. C. Hsia, B. Y. Shieh, and R. H. Lin. "The Thermal, Rheological, and Morphological Properties of Polyphenylene Sulfide and Polyetheretherketone Resins and Composites," in *Materials Science for the Future,* eds. J. L. Bauer and R. Dunaetz, Society for the Advancement of Materials and Processing Engineering, 1986, pp. 420–433.

22) Blundell, D. J., D. R. Beckett, and P. H. Willcocks. "Routine Crystallinity Measurements of Polymers by DSC," *Polymer, 22* (1981), pp. 704–707.

23) Ostberg, G.M.K. and J. C. Seferis. "Annealing Effects on the Crystallinity of Polyetheretherketone (PEEK) and Its Carbon Fiber Composite," *Journal of Applied Polymer Science, 33* (1987), pp. 29–39.

24) Velisaris, C. N. and J. C. Seferis. "Crystallization Kinetics of Polyetheretherketone (PEEK) Matrices," *Polymer Engineering and Science, 26* (1986), pp. 1574–1581.

25) Young, R. J. *Introduction to Polymers,* Chapman and Hall, 1981.

26) Lee, W. I., M. F. Talbott, G. S. Springer, and L. A. Berglund. "Effects of Cooling Rate on the Crystallinity and Mechanical Properties of Thermoplastic Composites," *Journal of Reinforced Plastics and Composites, 6* (1987).

27) Jones, D. P., D. C. Leach, and D. R. Moore. "Mechanical Properties of Poly(ether-ether-ketone) for Engineering Applications," *Polymer, 26* (1985), pp. 1385–1393.

28) Walrath, D. E. and D. F. Adams. "The Iosipescu Shear Test as Applied to Composite Materials," *Experimental Mechanics, 23* (1983), pp. 105–110.

29) Bassett, D. C. *Principles of Polymer Morphology,* Cambridge University Press, 1981.

30) Kinloch, A. J. and R. J. Young. *Fracture Behavior of Polymers,* Applied Science, 1983.

31) Young, R. J. "Deformation and Fracture of Polymer Crystals," in *Developments in Polymer Fracture–1,* ed. E. H. Andrews, Applied Science, 1979, p. 248.

32) Karger-Kocsis, J. and K. Friedrich. "Temperature and Strain-Rate Effects on the Fracture Toughness of Poly(etheretherketone) and Its Short Glass-Fiber Reinforced Composites," *Polymer, 27* (1986), pp. 1753–1760.

33) Klei, H. E. "Studies on Thermoplastic Resin Systems: Polyetheretherketone (PEEK)," Report number 83:4, Air Force Wright Aeronautical Laboratories, Materials Laboratory, Wright-Patterson Air Force Base, 1983.

34) Berglund, L. A. and T. Johanneson. "Mixed-Mode Fracture of PEEK/Carbon Fiber Composites," *Proceedings of the First European Conference on Composite Materials, ECCM-1,* Bordeaux, France, 1985, pp. 259–264.

35) Brown, W. F., Jr. and J. E. Srawley. *Plane Strain Crack Toughness Testing of High Strength Materials,* ASTM STP 410, American Society for Testing and Materials, 1966, p. 11.

36) Sih, G. C., P. C. Paris, and G. R. Irwin. "On Cracks in Rectilinearly Anisotropic Bodies," *International Journal of Fracture Mechanics, 1* (1965), pp. 189–203.

37) Tsai, S. W. *Composites Design 1986,* Think Composites, 1986, pp. 11.3–11.11 and B-2.

38) Tsai, S. W. and H. T. Hahn. *Introduction to Composite Materials,* Technomic, 1980, pp. 388–401.

39) Lakshminarayana, H. V. "A Symmetric Rail Shear Test for Mode II Fracture Toughness (G_{IIC}) fo Composite Materials—Finite Element Analysis," *Journal of Composite Materials, Vol. 18* (1984), pp. 227–238.

40) Russell, A. J. and K. N. Street. "Factors Affecting the Interlaminar Fracture Energy of Graphite/Epoxy Laminates," in *Progress in Science and Engineering of Composites, Vol. 1.* Eds. T. Hayashi, K. Kawata, and S. Umekawa. Japan Society for Composite Materials, 1982, pp. 279–286.

41) Donaldson, S. L. "Fracture Toughness Testing of Graphite/Epoxy and Graphite/PEEK Composites," *Composites, 16* (1985), pp. 103–112.

42) Russell, A. J. and K. N. Street. "The Effect of Matrix Toughness on Delamination Static and Fatigue Fracture Under Mode II Shear Loading of Graphite Fiber Composites," *ASTM STP...*, ed. N. J. Johnston, American Society for Testing and Materials, 1987.

43) Smiley, A. J. and R. B. Pipes. "Rate Effects on Mode I Interlaminar Fracture Toughness in Composite Materials," *Journal of Composite Materials,* 1987 (in print).

44) Leach, D. C., D. C. Curtis, and D. R. Tamblin. "Delamination Behavior of Aromatic Polymer Composite APC-2," *ASTM STP* ..., ed. N. J. Johnson, American Society for Testing and Materials, 1987.

45) Carlsson, L. A., J. W. Gillespie, and B. R. Tretheway. "Mode II Interlaminar Fracture of Graphite/Epoxy and Graphite/PEEK," *Journal of Reinforced Plastics and Composites, 5* (1986), pp. 170–187.

46) Wu, E. M. and R. C. Reuter, Jr. "Crack Extension in Fiberglass Reinforced Plastics," *TA&M Report No. 275,* University of Illinois, 1965.

47) Johnson, W. S. and P. D. Mangalgiri. "Influence of the Resin on Interlaminar Mixed-Mode Fracture," *NASA Technical Memorandum 87571,* July 1985.

48) Blundell, D. J. and B. N. Osborn. "The Morphology of Poly(aryl-ether-etherketone),"

Polymer, Vol. 24 (1983), pp. 953–958.

49) Ozawa, T. "Kinetics of Nonisothermal Crystallization," *Polymer, Vol. 12* (1971), pp. 150–158.

50) Seferis, J. C. and C. N. Velisaris. "Modeling-Processing-Structure Relationships of Polyetheretherketone (PEEK) Based Composites," in *Materials for the Future*, Society for the Advancement of Material and Process Engineering, 1986, pp. 1236–1252.

51) Velisaris, C. N. and J. C. Seferis. "Crystallization Kinetics of Polyetheretherketone (PEEK) Matrices," *Polymer Engineering and Science, Vol. 26* (1986), pp. 1574–1581.

52) Blundell, D. J., J. M. Chalmers, M. W. MacKenzie, and W. F. Gaskin. "Crystalline Morphology of the Matrix of PEEK-Carbon Fiber Aromatic Polymer Composites. I. Assessment of Crystallinity," *SAMPE Quarterly, Vol. 16* (1985), pp. 22–30.

53) Blundell, D. J. and B. N. Osborn. "Crystalline Morphology of the Matrix of PEEK-Carbon Fiber Aromatic Polymer Composites. II. Crystallization Behavior," *SAMPE Quarterly, Vol. 17* (1985), pp. 1–6.

54) Cebe, P. and S. D. Hong. "Crystallization Behaviour of Poly(ether-ether-ketone)," *Polymer, Vol. 27* (1986), pp. 1183–1192.

APPENDIX A

Material Properties Used in the Thermoplastic Processing Model

In this appendix the material properties pertaining to the processing of PEEK 150P polymer, T300/PEEK 150P and APC-2 composites are listed. Additional information on the crystallinity of PEEK 150P polymer is provided in Appendix B.

Table A-1

VALUES OF THE PARAMETERS IN THE IMPREGNATION CONSOLIDATION AND CRYSTALLINITY SUBMODELS

Impregnation—T300 Fiber

Initial tow radius	$r_o = 380\ \mu m$
Fiber diameter	$d = 6\ \mu m$
Average distance between two fibers (channel height)	$h = 2\ \mu m$
Average channel length	$L = 150\ \mu m$
Permeability of the tow	$K_p = 0.7\ (\mu m)^2$
Surface tension (T300/PEEK 150P at 698°F)	$\sigma^* = 0.026\ Nm^{-1} (= 0.0018$ lbf/ft)

Viscosity (PEEK 150P)

$$\mu = 1.13 \times 10^{-10} \left[\exp \frac{19100}{T(^\circ K)}\right] \qquad Pa \cdot s$$

Intimate Contact

Geometric ratio	$w_o/b_o = 1.0$
Geometric ratio	$a_o/b_o = 0.3$

Matrix-fiber viscosity

$$\mu_{mf} = 1.14 \times 10^{-12} \left[\exp \frac{26300}{T(^\circ K)}\right] \qquad Pa \cdot s$$

Autohesion

Proportionality constant

$$\kappa = 44.1\ \exp \frac{3810}{T(^\circ K)} \qquad s^{-1/4}$$

Crystallinity

PEEK density	$\rho_m = 1300$ kg/m^3 (81.1 lbm/ft^3)
PEEK specific heat	$C_m = 1340$ J/kg/°C (0.32 BTU/lbm/°F)
PEEK thermal conductivity	$k_m = 0.25$ J/s/m/°C (0.145 BTU/hr/ft/°F)
PEEK ultimate heat of crystallization	$H_u = 130$ J/g (56 BTU/lbm)
APC-2 matrix mass fraction	$m_m = 0.31$
APC-2 ply thickness	$s_o = 0.125$ mm (0.005 in)

Table A-2

MECHANICAL PROPERTIES OF PEEK 150P POLYMER AND UNIDIRECTIONAL APC-2 COMPOSITE AS FUNCTIONS OF CRYSTALLINITY [15]

PEEK 150P

Tensile strength:	$S_t = 8.2 + 0.17\ c$ (ksi)
Tensile modulus:	$E_t = 404 + 4.0\ c + 0.075\ c^2$ (ksi)
Shear strength:	$S_s = 4.9 + 0.10\ c + 0.0015\ c^2$ (ksi)
Shear modulus:	$E_s = 140 + 1.59\ c$ (ksi)
Compression strength:	$S_c = 18 + 0.22\ c$ (ksi)
Fracture toughness:	$K = 27.6 * 10^{-0.027\ c}$ (ksi) $\sqrt{\text{in}}$

APC-2

Mode I and Mode II fracture toughnesses (K_{IC} and K_{IIC}) and fracture energies (G_{IC} and G_{IIC})

$$K_{IC} = 4.3 - 0.007\ c - 0.001\ c^2 \quad (\text{ksi})\sqrt{\text{in}}$$
$$K_{IIC} = 9.2 - 0.005\ c - 0.002\ c^2 \quad (\text{ksi})\sqrt{\text{in}}$$
$$G_{IC} = 12.01 - 0.022\ c - 0.006\ c^2 \quad (\text{lbf/in})$$
$$G_{IIC} = 12.78 - 0.024\ c - 0.004\ c^2 \quad (\text{lbf/in})$$

APPENDIX B

Crystallinity of PEEK 150P Polymer

Several empirical expressions have been proposed in the past for correlating the measured rate of crystallization with temperature [48–54]. We adopted the simple expression proposed by Ozawa [49], which is convenient and adequate for the purpose of engineering analysis. Ozawa's expression can be written as

$$\log[-\ln(1-c_r)] = \log\phi + n\log\left(\frac{dT}{dt}\right) \tag{B.1}$$

or in differential form

$$\frac{dc_r}{dt} = -(1-c_r)\frac{(d\phi/dT)}{(dT/dt)^{n-1}} \tag{B.2}$$

c_r is the relative crystallinity and is related to the crystallinity by

$$c_r = \frac{H_u}{H_T}c \tag{B.3}$$

c_r can be determined from measurements performed in a differential scanning calorimeter. H_u is the theoretical ultimate heat of crystallization of the polymer. H_T is the total heat of crystallization at the given cooling rate (Figure 47). ϕ is a parameter which depends on the temperature only and n is a constant. The parameters ϕ and n were obtained by fitting the above expression to the data obtained by DSC measurements. This procedure yielded the following ϕ and n values

$$\begin{aligned} \phi &= \exp[-0.037\ T + 11.3] \\ n &= 0.8 \end{aligned} \tag{B.4}$$

In addition, a best fit to the data yielded the following expression for H_T/H_u

$$\frac{H_T}{H_u} = -0.03\ln\left(\frac{dT}{dt}\right) + 0.42 \tag{B.5}$$

where dT/dt is the cooling rate in °C/min, and H_u is [48]

$$H_u = 130\ J/g \tag{B.6}$$

Crystallinities as a function of cooling rate measured by different investigators for PEEK 150P polymer and APC-2 composite are given in Figure 48. The volume percent crystallinity data of Velisaris and Seferis [7, 51] and Blundell et al. [52] were converted to weight percent, using the densities given in Reference [51]. In Figure 48 crystallinities computed by the above expressions are also shown (solid line). As can be seen these expressions approximate the data reasonably well.

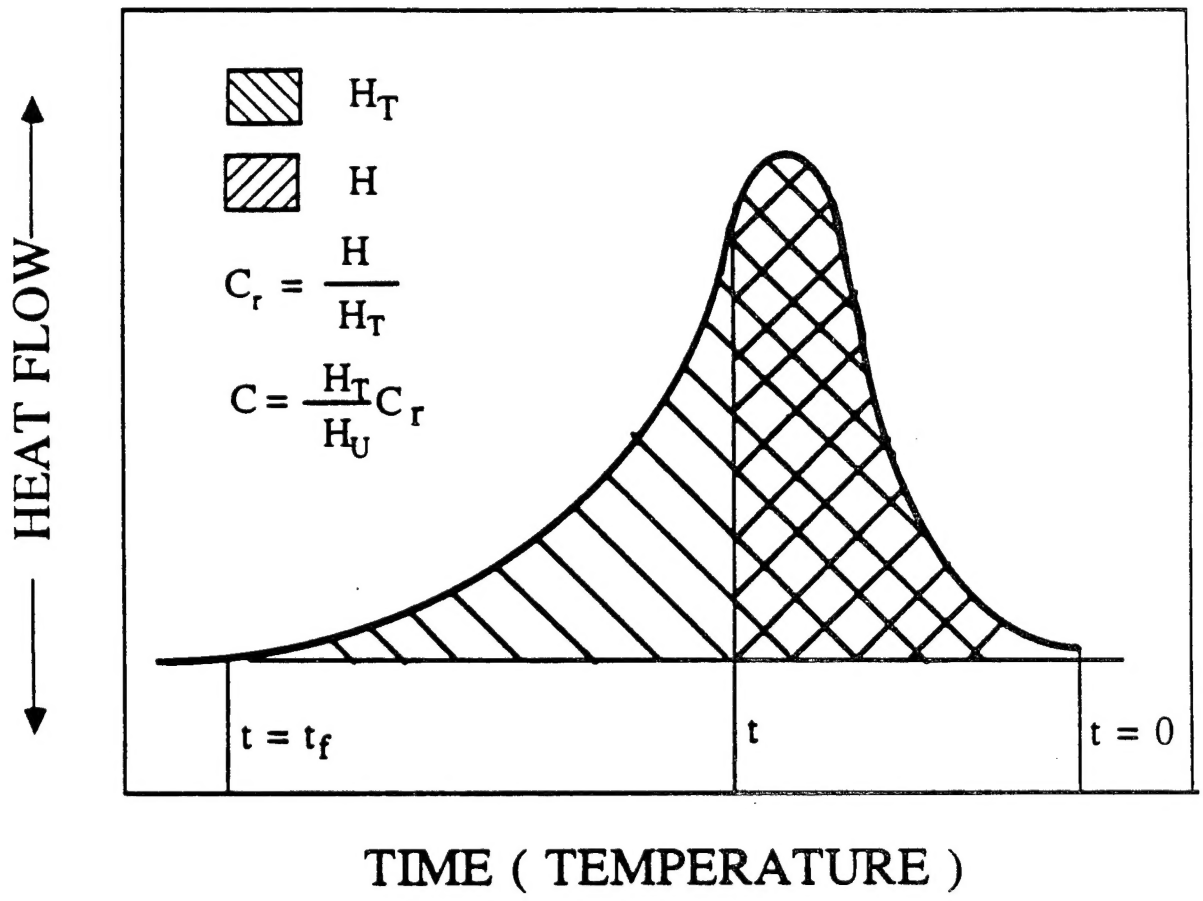

Figure 47. Illustration of the results obtained on cooling a PEEK 150P polymer sample in the DSC.

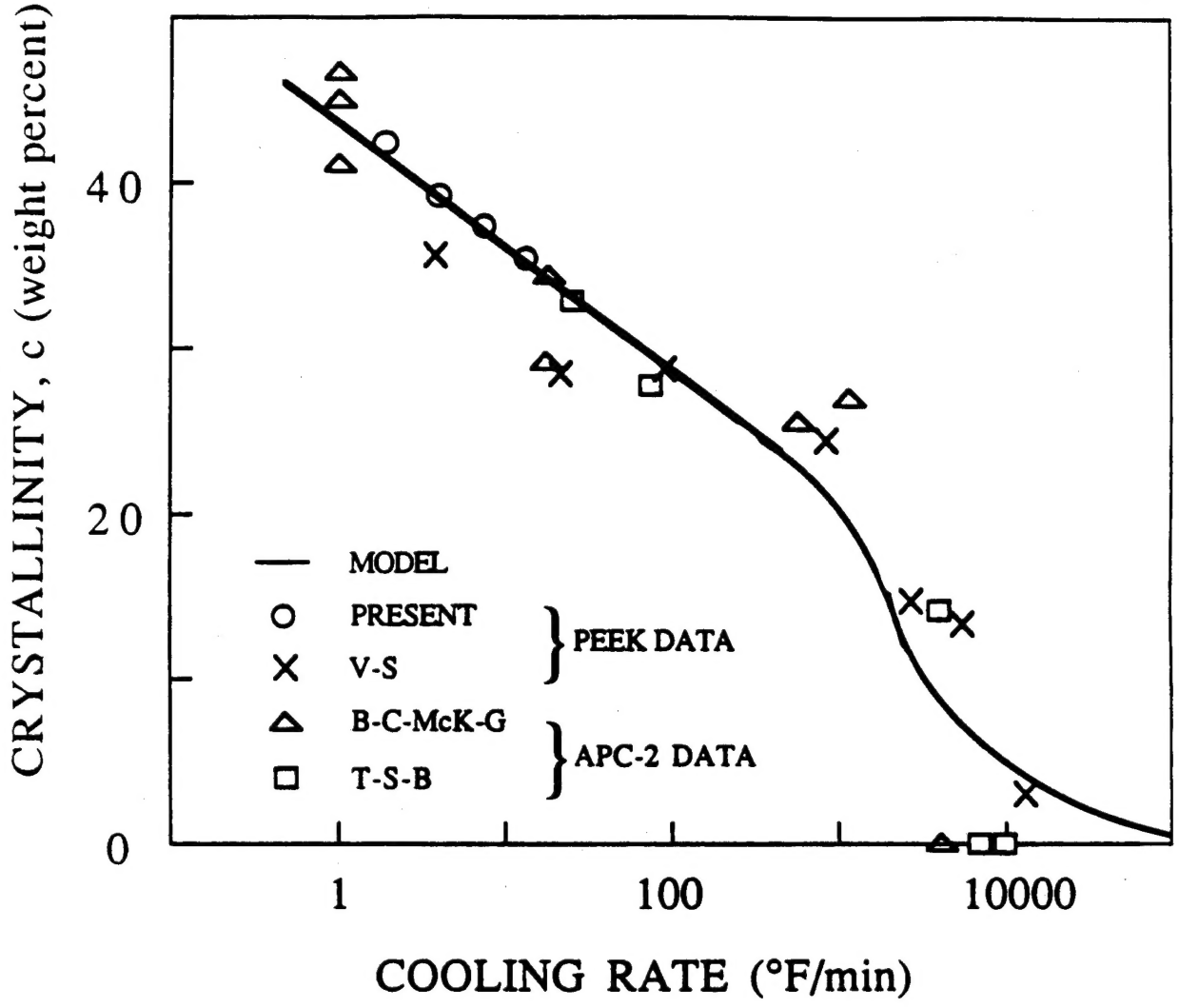

Figure 48. Crystallinity of PEEK 150P polymer and APC-2 composite as a function of cooling rate comparisons between data of Velisaris and Seferis [7, 51], Blundell and Osborne [53], Blundell et al. [52], Talbott et al. [15], and the model described in Appendix B.